PNNL-26265
EMSP-RPT-035 Rev 0.0


*Proudly Operated by Battelle Since 1965*

# Characterization of Non-Pertechnetate Species Relevant to the Hanford Tank Waste

SD Chatterjee
A Andersen
Y Du
MH Engelhard
GB Hall
TG Levitskaia
WW Lukens
V Shutthanandan
ED Walter
NM Washton

**February 2017**

U.S. DEPARTMENT OF ENERGY

Prepared for the U.S. Department of Energy
under Contract DE-AC05-76RL01830

**DISCLAIMER**



PACIFIC NORTHWEST NATIONAL LABORATORY
*operated by*
BATTELLE
*for the*
UNITED STATES DEPARTMENT OF ENERGY
*under Contract DE-AC05-76RL01830*

**Printed in the United States of America**

**Available to DOE and DOE contractors from the**
**Office of Scientific and Technical Information,**
**P.O. Box 62, Oak Ridge, TN 37831-0062;**
**ph: (865) 576-8401**
**fax: (865) 576-5728**
**email: reports@adonis.osti.gov**

**Available to the public from the National Technical Information Service**
**5301 Shawnee Rd., Alexandria, VA 22312**
**ph: (800) 553-NTIS (6847)**
**email: orders@ntis.gov <http://www.ntis.gov/about/form.aspx>**
**Online ordering: http://www.ntis.gov**

This document was printed on recycled paper.
(8/2010)

PNNL-26265
EMSP-RPT-035 Rev 0.0

# Characterization of Non-Pertechnetate Species Relevant to the Hanford Tank Waste

SD Chatterjee
A Andersen
Y Du
MH Engelhard
GB Hall
TG Levitskaia
WW Lukens
V Shutthanandan
ED Walter
NM Washton

February 2017

Prepared for
the U.S. Department of Energy
under Contract DE-AC05-76RL01830

Pacific Northwest National Laboratory
Richland, Washington 99352

# Summary

Among radioactive constituents present in the tank waste stored at the U.S. DOE Hanford Site, technetium-99 (Tc), which is generated from the fission of $^{235}U$ and $^{239}Pu$ in high yields, presents a unique challenge in that it has a long half-life ($\beta$ = 292 keV; $T_{1/2} = 2.11\times10^5$ y) and exists predominately in soluble forms in the liquid supernatant and salt cake fractions of the waste. In the strongly alkaline environments prevalent in most of the tank waste, its dominant chemical form is pertechnetate ($TcO_4^-$, oxidation state +7). However, attempts to remove Tc from the Hanford tank waste using ion-exchange processes specific to $TcO_4^-$ only met with limited success, particularly when processing tank waste samples containing elevated concentrations of organic complexants. This suggests that a significant fraction of the soluble Tc can be present as low-valent Tc (oxidation state < +7) (non-pertechnetate). The chemical identities of these non-pertechnetate species are poorly understood. Previous analysis of the SY-101 and SY-103 tank waste samples provided strong evidence that non-pertechnetate can be comprised of $[fac\text{-}Tc(CO)_3]^+$ complexes containing Tc in oxidation state +1 (Lukens et al. 2004). During the last three years, our team has expanded this work and demonstrated that high-ionic-strength solutions typifying tank waste supernatants promote oxidative stability of the $[fac\text{-}Tc(CO)_3]^+$ species (Rapko et al. 2013a; 2013b; Levitskaia et al. 2014; Chatterjee et al. 2015). Results also suggest possible stabilization of Tc(VI) and potentially Tc(IV) oxidation states in the high-ionic-strength alkaline matrices particularly in the presence of organic chelators, so that Tc(IV, VI) can serve as important redox intermediates facilitating the reduction of Tc(VII) to Tc(I). Designing strategies for effective Tc management, including separation and immobilization, necessitates understanding the molecular structure of the non-pertechnetate species and their identification in the actual tank waste samples, which would facilitate development of new treatment technologies effective for dissimilar Tc species. The key FY 2016 results are summarized below.

1. **Spectroscopic $^{99}Tc$ library of the model non-pertechnetate compounds in various oxidation states was developed and validated using multicomponent tank waste supernatant simulant. It will be used for identification of non-pertechnetate species in the actual AN-102 tank waste sample in Fiscal Year (FY) 2017.**

One of the main objectives of this project is to identify the oxidation state and chemical forms of non-pertechnetate species in Hanford tank waste. This is a challenging task considering the complicated redox behavior of Tc, which can adopt multiple oxidation states in solution from I to VII and form dissimilar compounds. In addition, Tc is only a minor chemical component present at micromolar to low millimolar concentrations in the brine-like liquid fractions of the tank waste, which is comprised mostly of highly concentrated sodium, aluminum, and other salts. Identification of the non-pertechnetate species relies on availability of a spectral library of reference compounds that can be compared against experimental signatures observed for samples of the actual waste. In FY 2014 – 2015, a spectroscopic library of the Tc(I) $[fac\text{-}Tc(CO)_3]^+$ and Tc(IV, VI) compounds was generated using a range of techniques, including $^{99}Tc$ nuclear magnetic resonance (NMR), infrared (IR) and electron paramagnetic resonance (EPR) spectroscopies. In FY 2016 this work was continued, and the spectroscopic library of the Tc compounds in I through VII oxidation states, using x-ray photoelectron spectroscopy (XPS) and x-ray absorption spectroscopy (XAS), was developed. Table S1 summarizes Tc compounds comprising the developed library.

**Table S1**. Spectroscopic library of Tc compounds developed for identification of the non-pertechnetate species in the Hanford tank waste.[a] N/A = not applicable for the analysis by this technique.

| Compound | Tc oxidation state | XPS Tc $3d_{5/2}$ electron binding energy (eV) | XAS Tc K-edge (eV) | $^{99}$Tc NMR chemical shift (ppm) | EPR chemical shift (G) |
|---|---|---|---|---|---|
| $(Et_4N)_2[Tc(CO)_3Cl_3]$[b] | I | 254.2 | 21036.5 | -1117, -1140 | N/A |
| $[Tc(CO)_3(OH)]_4$ | | 255.4 | | -585 | |
| $[Tc(CO)_3(H_2O)_3]^+$ | | 255.2 | | -868 | |
| $[Tc(CO)_3(H_2O)_2(OH)]$ | | 255.0 | | -1056 | |
| $[Tc(CO)_3(H_2O)(OH)_2]^-$ | | Not measured | | -1139 | |
| $[Tc(CO)_3]^+$•IDA | | 255.1, 256.3 | | -850, -998 | |
| $[Tc(CO)_3]^+$•gluconate | | Not measured | | -1110, -1232, -1253 | |
| $[Tc(CO)_3]^+$•EDTA | | | | -916 | |
| $[Tc(CO)_3]^+$•NTA | | | | -918 | |
| $[Tc(CO)_3]^+$•pyridine | | | | -1000 | |
| $[Tc(CO)_3]^+$•glycine | | | | -1000 | |
| $[Tc(CO)_2(NO)]^{n+}$ | II | Not measured | 21037.9 | N/A | 3050 |
| Tc(IV) from reduction of $(n\text{-}Bu_4N)[TcOCl_4]$[c] | IV | 256.7 | Not measured | N/A | 3300 |
| Tc(IV) from electrochemical reduction of $TcO_4^-$ | | 256.1 | 21039.5 | | 3300 |
| $(n\text{-}Bu_4N)[TcOCl_4]$[c] | V | 258.3 | 21042 | 4695 | N/A |
| Tc(VI) from electrochemical reduction of $TcO_4^-$ | VI | 258 | Not measured | N/A | 3000 |
| $NH_4TcO_4$ | VII | 259.5 | 21044 | 0 | N/A |

[a]All measurements are taken in 5 M $NaNO_3$, 0 – 6 M NaOH, unless otherwise mentioned.
[b] Measured in acetonitrile
[c] Measured in methylene chloride

Based on the obtained results it was concluded that a combination of NMR, EPR, XAS, and XPS techniques should provide sufficient information regarding Tc oxidation state and coordination environment in the tank waste, as summarized below.

- $^{99}$Tc NMR is highly effective for the identification and quantification of diamagnetic nuclei, namely Tc(VII) and Tc(I) species, and is suitable for identification of both the oxidation state

and the coordination environment of these species simultaneously present in the Hanford tank waste;

- EPR is demonstrated to be a reliable technique for identification of paramagnetic Tc(VI) species with an electronic spin of ½ and is suitable for identification of oxidation state of the Tc(VI) in the Hanford tank waste;
- XAS is observed to be suitable for identification of both the oxidation state and the coordination environment of Tc(I), Tc(IV) and Tc(VII) simultaneously present in the multi-component tank waste simulant matrix. Reference Tc(VI) compounds are needed to enable its identification by XAS. It should be noted that XAS measurements are complicated by the availability of the required synchrotron beamline, which is not readily available.
- XPS is demonstrated to be a powerful tool to probe Tc in co-existing oxidation states from I through VII and is applicable for the analysis of the tank waste samples. However its application can be in part hindered by the lack of adequate XPS spectral data for the reference compounds. For instance, the NIST XPS database contains only 20 entries for Tc, including two for Tc(I), one for Tc(V) standards and none for Tc(II) and Tc(VI). This work significantly expanded the XPS spectral database by collecting spectra for pure Tc(I) complexes with a $[Tc(CO)_3]^+$ framework and Tc(IV) compounds. A similar XPS database is needed for Tc in other oxidation states, most notably Tc(II) and Tc(VI).
- Our spectroscopic library was validated using tank waste supernatant simulant containing Tc in various co-existing oxidation states generated by *in situ* reduction of $TcO_4^-$. The samples were characterized by $^{99}$Tc NMR, EPR, XAS, and XPS, and Tc(I, IV, VI, and VII) species were observed. This work demonstrated that the combination of the aforementioned techniques is sufficient to identify oxidation state as well as coordination environment of non-pertechnetate species in the AN-102 tank waste planned in FY 2017.

2. **A computational Density Functional Theory (DFT) framework for interpretation of the experimental $^{99}$Tc NMR signature of the [*fac*-$Tc(CO)_3]^+$ compounds was developed.**

The DFT computation tool is being developed to enable identification of unknown Tc species, which may be present in the Hanford tank waste but not yet included in the currently built library of non-pertechnetate compounds. DFT enables correlation of the experimental spectroscopic signature of the unknown Tc species with their oxidation state and chemical structure. The developed DFT approach was validated via assignment of an experimentally observed $^{99}$Tc NMR peak at − 1204 ppm to the new [*fac*-$Tc(CO)_3(OH)_3]^{2-}$ species, for which characterization is lacking (Hall et al. 2016). This DFT tool is currently being expanded for the interpretation of XAS and XPS experimental spectra.

- The DFT tool will assist in identification of non-pertechnetate species in the AN-102 tank waste sample.

3. **High oxidative stability of non-pertechnetate species in pseudo-Hanford tank supernatant simulant was demonstrated**.

This task evaluates oxidative stability of model non-pertechnetate species to identify structural motifs of the Tc(I) [*fac*-$Tc(CO)_3]^+$ and Tc(IV, VI) complexes viable under the aggressive tank waste conditions. Testing was in part initiated in FY 2014 – 2015 when a series of samples containing non-pertechnetate Tc generated *ex situ* or *in situ* in pseudo-Hanford tank supernatant simulant solutions was prepared,

characterized, and monitored for oxidation to Tc(VII) (Levitskaia et al. 2014; Chatterjee et al. 2015). This work was continued and expanded in FY 2016 and showed that the generated samples contain significant fractions of Tc(I, IV, VI) even after 2.5 years when stored unprotected to exposure to air and light.

- A non-pertechnetate Tc(I) [*fac*-$Tc(CO)_3]^+$•IDA complex (where IDA is iminodiacetate) that was generated *ex situ* by a laboratory synthetic route in FY 2015 shows remarkable stability in simulant solutions. About 50% and 28% of this Tc(I) complex remains after 500 days of monitoring in 5 M $NaNO_3$/0.1 M NaOH and in pseudo-Hanford tank supernatant simulant at 0.5 M NaOH, respectively. The [*fac*-$Tc(CO)_3]^+$•IDA complex is a viable candidate species potentially present in the high-organics tanks wastes such as AN-102.

- Formation of stable Tc (I, IV, VI) non-pertechnetate species generated *in situ* by chemical reduction of $TcO_4^-$ using $CO/H_2$ as a reductant at elevated pressure and temperature in pseudo-Hanford tank supernatant in the presence of gluconate chelator and catalytic noble metals was observed. Major fractions of [*fac*-$Tc(CO)_3]^+$•gluconate and Tc(VI)•gluconate species persist in the simulant after about 2.5 years while stored exposed to ambient air and light. This work demonstrates potential mechanistic pathways for generation and stabilization of [*fac*-$Tc(CO)_3]^+$•gluconate and Tc(VI) non-pertechenetate species in the high-organics tanks wastes such as AN-102. Presence of catalytic noble metals facilitates reduction of Tc(VII) to Tc(I) and stabilization of [*fac*-$Tc(CO)_3]^+$ in presence of small organic chelators (e.g., iminodiacetate or gluconate) for prolonged times. In the absence of catalytic noble metals, Tc(VII) is reduced to Tc(VI), and ongoing experimentation shows that the Tc(VI)•gluconate complex is stable for at least 2.5 years. This is a significant finding because Tc in an oxidation state of VI is widely regarded as highly unstable. Additional experimentation is needed to explain this result.

- While multiple viable pathways for generation of non-pertechnetate species (depending on several factors such as waste composition, radiolysis, etc.) are anticipated, the results of this work strongly suggest that the tank waste environment can support the presence of non-pertechnetate species for the long term. One intriguing observation is that stability of non-pertechnetate species present in the liquid phase of the simulant subjected to the reducing conditions is significantly greater (30% fraction of non-pertechnetate after 2.5 years of unprotected storage) when it remains in equilibrium with the solid reaction product. When the liquid phase is removed from the contact with solids, the non-pertechnetate species oxidize to Tc(VII) much faster so that only less than 7% non-pertechnetate fraction was found in these samples after the same time of storage. This resembles behavior of non-pertechnetate in the actual tank waste samples in which it rapidly oxidizes to Tc(VII) when separated from the waste matrix while remains stable in the tank waste environment.

Results of this work emphasize that a combination of NMR, EPR, XAS, and XPS techniques should provide sufficient information regarding Tc redox speciation in the tank waste. Once non-pertechnetate species in actual tank waste are identified, the work can be directed towards achieving control over Tc redox behavior in the alkaline tank waste, and to develop methods for the separation of non-pertechnetate species from low-activity waste (LAW) by either their conversion to pertechnetate or direct removal. Examination of Tc speciation in actual waste samples collected from the Hanford tanks with confirmed high non-pertechnetate and evaluating the feasibility of treatment of total Tc is integral for the development of successful waste processing strategies.

# Acknowledgements

This work was completed as part of the Technetium Management Hanford Site project. Support for this project came from the U.S. Department of Energy's Office of Environmental Management. We would like to especially acknowledge the support of Dr. NP Machara.

The authors would like to thank Mr. RJ Serne for his technical review and Dr. CI Pearce for helpful discussions in the interpretation of XAS/XFS results.

# Acronyms and Abbreviations

| | |
|---|---|
| BASi | BioAnalytical Systems inc. |
| BE | binding energy |
| DFT | density functional theory |
| DTPA | diethylenetriamine pentaacetic acid |
| EDTA | ethylenediaminetetraacetic acid |
| EMSL | Environmental & Molecular Sciences Laboratory |
| EXAFS | Extended X-ray absorption fine structure |
| EPR | electron paramagnetic resonance |
| FY | fiscal year |
| IDA | iminodiacetic acid |
| IR | Infrared |
| LAW | low-activity waste |
| LSC | liquid scintillation counting |
| NMR | nuclear magnetic resonance |
| NTA | nitrilotriacetic acid |
| PEP | Pretreatment Engineering Platform |
| PNNL | Pacific Northwest National Laboratory |
| QA | Quality Assurance |
| RPL | Radiochemical Processing Laboratory |
| UV-Vis | ultraviolet-visible |
| XAS | X-ray absorption spectroscopy |
| XPS | X-ray photoelectron spectroscopy |

# Contents

# Figures

# Tables

# 1.0 Introduction

Technetium (Tc) is a major contaminant found in nuclear tank waste stored at the U.S. DOE Hanford Site. Existing predominately in the liquid supernatant and salt cake fractions Tc is one of the most difficult contaminants to dispose of and/or remediate. In strongly alkaline environments, Tc exists as pertechnetate ($TcO_4^-$) (oxidation state VII) and in reduced forms (oxidation state < VII) collectively known as non-pertechnetate species. Pertechnetate is a well-characterized, anionic Tc species that can be removed from LAW by anion exchange or other methods (Duncan et al. 2011). There is no definitive information on the origin or comprehensive description of the non-$TcO_4^-$ species in Hanford tanks. This project is focused on characterization of the composition of non-$TcO_4^-$ species to gain better understanding and control over their redox behavior. The objective of this work is to understand the chemical and redox speciation of non-pertechnetate in the tank waste supernatant matrices, to investigate interconversion among $TcO_4^-$ and soluble non-$TcO_4^-$ species and to elucidate the mechanistic pathways for the separation of non-pertechnetate species from LAW. This work is also focused on building a spectroscopic library of the various non-pertechnetate species that can be used for their identification and quantification in actual tank waste supernatants.

In fiscal year 2012 (FY 2012), a study by Rapko *et al* reviewed prior work on the nature and extent of this non-pertechnetate, alkaline-soluble technetium in the Hanford waste tanks (Rapko et al. 2013a), and tentatively identified a Tc(I) carbonyl type compound of the form $[Tc(CO)_3]^+$ as a predominant component of the non-pertechnetate species present in tank waste.[1] In FY 2013, research was initiated to investigate the chemistry of the Tc(I) carbonyl compound noted above. Initial research was focused on synthesizing pure forms of the $[Tc(CO)_3]^+$ on a laboratory scale. Based on consolidation of multiple synthesis approaches from literature, a modified synthesis method was adapted that, albeit time-consuming, was shown to provide a Tc-tricarbonyl compound pure with respect to Tc. A range of characterization methods was also explored for analyzing this species, and were summarized along with the synthesis route in a report (Rapko et al. 2013b). Subsequent research in FY 2014 – 2015 emphasized the optimization of the synthesis and purification of $[Tc(CO)_3]^+$ species. Generating a chemically pure form of the $[Tc(CO)_3]^+$ precursor served as the necessary first step (Levitskaia et al. 2014). Subsequent experimental work focused on understanding various aspects of the reactivities and stability of various Tc-tricarbonyl aqua species under various aqueous matrices. Three sets of solution matrices were chosen: (a) simple alkaline conditions with and without a chelating agent (eg: gluconate), (b) high-ionic-strength alkaline conditions with and without a gluconate, and (c) alkaline Hanford tank supernatant simulants. These three solution matrices provided a representative set of solvent matrices with gradual progression of the solvent conditions from simple aqueous systems to the complex multi-component systems typifying tank waste supernatants. It was found that high ionic strength solutions typifying Hanford tank waste supernatants promote oxidative stability of the $[Tc(CO)_3]^+$ . It was also observed that the presence of gluconate enhances the stability of the $[Tc(CO)_3]^+$ species.

Based on the observation of the enhanced stability of $[Tc(CO)_3]^+$ in presence of chelator such as gluconate, and the fact that several other chelators can be found in abundance in several Hanford tanks (representative examples being iminodiacetic acid (IDA), nitrilotriacetic acid (NTA),

1 All Tc(I) carbonyl compounds described in this report have *facial* octahedral geometry, and in the following text the notation "*fac*-" is omitted for clarity.

ethylenediaminetetraacetic acid **(**EDTA), and diethylenetriamine-N,N,N,N'',N''-pentaacetic acid (DTPA)), the potential impact of these chelators on the chemistry of $[Tc(CO)_3]^+$ in tank waste supernatants was recognized. Therefore, research in FY 2015 involved a systematic investigation of the binding affinity of these chelators towards $[Tc(CO)_3]^+$ species. As these complexes have not been chemically isolated previously, a companion effort was to develop a spectroscopic library of $[Tc(CO)_3]^+$•chelator complexes. These synthesis and characterization efforts were summarized in a report (Levitskaia et al. 2015).

Another companion effort in FY 2015 involved the studies on isoelectronic $[Tc(CO)_2(NO)]^{2+}$ species. It had been proposed that similar to the presence of $[Tc(CO)_3]^+$ species in the tank waste, $[Tc(CO)_2(NO)]^{2+}$ can also be formed due to the radiolysis of nitrite that is common in tank waste.

In FY 2015-2016, experimental work continued towards the development of the spectroscopic library of the $[Tc(CO)_3]^+$ species. Significant progress was made toward this goal in FY 2015 for the techniques of $^{99}$Tc NMR, EPR, IR and UV-vis spectroscopies. In the chemically simple systems, IR spectroscopy is particularly useful for metal carbonyls, and gives information about the energy at which bonds stretch, and bend, providing a useful fingerprint for a given molecule. UV-Visible spectroscopy directly probes the electronic state of the metal complex. However, UV-visible and IR spectroscopies suffer from interferences due to the presence of other chemical species and could not be effectively used for identification of $[Tc(CO)_3]^+$ species in the multicomponent mixtures. On the other hand $^{99}$Tc NMR is only applicable to diamagnetic Tc species in VII, V, III and I oxidation states, while EPR is applicable only to paramagnetic Tc species in VI, IV and II oxidation states. In FY 2015 it was demonstrated that the combination of these two techniques allows characterization of the Tc species in multiple oxidation states simultaneously present in complex solutions. The work this year was focused on expanding the Tc spectroscopic library to include X-ray phototelectron (XPS) and X-ray absorbance/fluorescence (XAS) spectroscopies, with an objective to expand the range of techniques that can identify the complete picture of oxidation state and chemical structure of Tc in multi-component systems. XPS probes the core orbitals of the Tc center, and is used to determine the oxidation state of the Tc. XAS is also somewhat sensitive to the Tc oxidation state but provides additional information about the ligand character in the coordination sphere. Unfortunately XAS requires the use of highly specialized equipment that is rare outside of synchrotron facilities.

A companion effort in FY 2016 involved studies to gain mechanistic information on the reductive conversion of pertechnetate to Tc-tricarbonyl and other non-pertechnetate species in the simulant solutions. The initial proof-of-principle tests were conducted to evaluate the concept of *in situ* reductive conversion of pertechnetate to Tc(I) tricarbonyl in simulant solutions (Levitskaia et al. 2014) and continued in FY 2015. The initial studies showed that during the attempted *in situ* chemical reduction of $TcO_4^-$ under environments typifying tank waste, formation of several non-pertechnetate species, such as Tc(VI) and Tc(IV), is observed depending upon the reaction conditions. The work in FY 2016 involved further variations in the reaction conditions to gain a more detailed understanding. In order to gain insight into these processes, the focus of FY 2016 studies was three-fold: (a) to expand the spectroscopic library for non-pertechnetate species other than $[Tc(CO)_3]^+$, (b) to elucidate the applicability of this library for identification of the various $TcO_4^-$ and non-pertechnetate species in multicomponent matrices, and (c) based on this identification, to design further $TcO_4^-$ reduction experiments under modified conditions which would allow further mechanistic insight on the reductive conversion of $TcO_4^-$ to non-pertechnetate species. With this aim in mind, the Tc XPS and XAS libraries were significantly expanded to include Tc(I) species in the form $[Tc(CO)_3]^+$; and Tc(IV), Tc(V) and Tc(VI) species scarcely available in the

literature. The generated spectra were effectively used to distinguish and identify the various Tc species generated during the chemical reduction of $TcO_4^-$, allowing us to gain valuable insight into the reduction mechanism.

Another companion effort involved continued evaluation of the oxidative stability of non-pertechnetate species relevant to Hanford tank waste was in part initiated in FY 2014 and FY 2015, where a series of non-pertechnetate samples generated *in situ* in presence of pseudo-Hanford tank supernatant simulant solutions as described above, or a series of samples generated *ex situ*,[2] monitored for re-oxidation to Tc(VII). This work was continued in FY 2016. In addition, new studies were initiated in simulant solutions consisting of an added oxidant $CrO_4^{2-}$ that is common in Hanford tank supernatants.

2 In the context of this work, *ex situ* and *in situ* generation of the non-pertechnetate species is referred to their preparation by reduction of Tc(VII) using reducing agents of choice followed by addition of the reduced Tc species to the test solution (*ex situ*) as opposed to the Tc(VII) reduction directly in the test solution (*in situ*).

# 2.0 Quality Assurance

This work was conducted as part of Pacific Northwest National Laboratory (PNNL) Project 54042 under the Technetium Management Program, with funding from the U.S. Department of Energy Office of Environmental Management.

All research and development (R&D) work at PNNL is performed in accordance with PNNL's laboratory-level Quality Management Program, which is based on a graded application of NQA-1-2000, *Quality Assurance Requirements for Nuclear Facility Applications*, to R&D activities. In addition to the PNNL-wide quality assurance (QA) controls, the QA controls of the WRPS Waste Form Testing Program (WWFTP) QA program were also implemented for the work. The WWFTP QA program consists of the WWFTP Quality Assurance Plan (QA-WWFTP-001) and associated QA-NSLW-numbered procedures that provide detailed instructions for implementing NQA-1 requirements for R&D work. The WWFTP QA program is based on the requirements of NQA-1-2008, *Quality Assurance Requirements for Nuclear Facility Applications*, and NQA-1a-2009, *Addenda to ASME NQA-1-2008 Quality Assurance Requirements for Nuclear Facility Applications*, graded on the approach presented in NQA-1-2008, Part IV, Subpart 4.2, "Guidance on Graded Application of Quality Assurance (QA) for Nuclear-Related Research and Development". Preparation of this report and performance of the associated experimental work were assigned the technology level "Applied Research" and were conducted in accordance with procedure QA-NSLW-1102, *Scientific Investigation for Applied Research*. All staff members contributing to the work have technical expertise in the subject matter and received QA training prior to performing quality-affecting work. The "Applied Research" technology level provides adequate controls to ensure that the activities were performed correctly. Use of both the PNNL-wide and WWFTP QA controls ensured that all client QA expectations were addressed in performing the work.

# 3.0 Experimental

## 3.1 Materials

$NH_4TcO_4$ stock available in-house at the Radiochemical Processing Laboratory (RPL) at PNNL was used. Diglyme, acetonitrile, diethyl ether, dichloromethane, and borane-tetrahydrofuran $BH_3$/THF complex were obtained from Sigma-Aldrich and used without further purification. Gaseous CO used in the diglyme synthesis of $(Et_4N)_2[Tc(CO)_3Cl_3]$ was obtained from Matheson Tri-Gas. Argon gas also was obtained from Matheson. All inorganic sodium salts (including carbonate, oxalate, gluconate, nitrilotriacetate (NTA), iminodiacetate (IDA) nitrate, nitrite, hydroxide, and sulfate) and aluminum nitrate were obtained from Sigma-Aldrich and were reagent grade. All aqueous solutions were prepared using distilled water deionized to ≥15 MΩ cm with a Barnstead Nanopure water purification system.

Caustic solution simulating Hanford tank waste supernatants was prepared following a procedure previously developed for the Pretreatment Engineering Platform (PEP) testing (Scheele et al. 2009), albeit with a reduced NaOH concentration. The composition of the Hanford tank supernatant simulant used in FY 2014 – 2015 studies is given in (Levitskaia et al. 2014). Table 1 shows composition of the simulant prepared in FY 2016.

**Table 1.** Composition of the Hanford supernatant simulants prepared in FY 2014 and used in FY 2014 – 2015 and prepared in FY 2016.

| Constituent | Concentration (FY 2014) | | Concentration (FY 2016) | |
|---|---|---|---|---|
| | µg/mL | M | µg/mL | M |
| $Al^{3+}$ | 5,900 | 0.219 | 5,100 | 0.19 |
| $Na^{+}$ | 108,700 | 4.73 | 105,200 | 4.57 |
| $C_2O_4^{2-}$ | <450 | <0.005 | <450 | <0.005 |
| $NO_2^{-}$ | 25,300 | 0.55 | 22,800 | 0.50 |
| $NO_3^{-}$ | 104,800 | 1.69 | 95,600 | 1.54 |
| $PO_4^{3-}$ | 15,100 | 0.158 | 5,900 | 0.062 |
| $SO_4^{2-}$ | 19,200 | 0.20 | 16,500 | 0.17 |
| $CO_3^{2-}$ | 7,360 | 0.61 | 6,640 | 0.55 |
| Total $OH^{-}$ | 18,800 | 1.11 | 22,400 | 1.32 |
| Free $OH^{-}$ | | 0.47 | | 0.56 |

## 3.2 Synthesis of Tc(I) carbonyl compounds

The starting Tc carbonyl complex, $(Et_4N)_2[Tc(CO)_3Cl_3]$, was prepared by a two-step reduction procedure starting from $NH_4TcO_4$ as described in our previous reports (Levitskaia et al. 2014; Levitskaia et al. 2015). The tetrameric Tc carbonyl compound, $[Tc(CO)_3(OH)]_4$, was prepared according to a modified literature procedure (Alberto et al. 1998) by dissolution of $(Et_4N)_2[Tc(CO)_3Cl_3]$ in NaOH solution followed by extraction into diethyl ether, and crystallization from dichloromethane. $(Et_4N)_2[Tc(CO)_3Cl_3]$ and $[Tc(CO)_3(OH)]_4$ were used to generate other Tc(I) tricarbonyl complexes for use in subsequent studies.

$[Tc(CO)_3]^+$ aqua species of the general formula $[Tc(CO)_3(H_2O)_{3-n}(OH)_n]^{1-n}$ (n = 0 – 3) were generated by dissolving $(Et_4N)_2[Tc(CO)_3Cl_3]$ or $[Tc(CO)_3(OH)]_4$ in 5M $NaNO_3$ containing variable NaOH concentrations or the tank supernatant simulant solution.

To prepare polyaminocarboxylate-coordinated $[Tc(CO)_3]^+$ complexes, $[Tc(CO)_3(OH)]_4$ was first converted to $[Tc(CO)_3(H_2O)_3]^+$ by dissolution in 1 M triflic acid, extraction into diethyl ether, and crystallization. Solid $[Tc(CO)_3(H_2O)_3]^+$ as the triflate salt was dissolved in 5 M $NaNO_3$ / 0.1 M NaOH or in the tank supernatant simulant and mixed with the 0.2 M chelator solution in the same matrix in a 1:1 ratio so that the resulting solution contained 2.5 – 3.2 mM Tc(I) and 0.1 M chelator. The tested chelators included iminodiacetic acid (IDA), nitrilotriacetic acid (NTA), ethylenediaminetetraacetic acid **(**EDTA), and diethylenetriamine-N,N,N,N'',N''-pentaacetic acid (DTPA). The molecular structures of these chelators are shown in Figure 1.

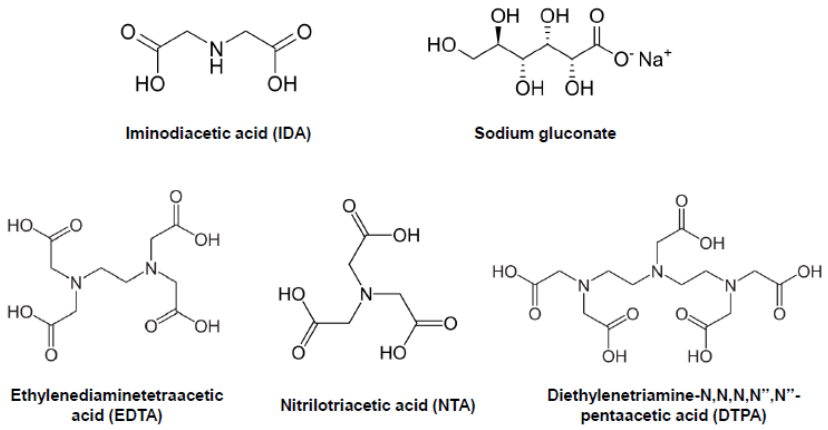


**Figure 1.** Molecular structure of the small organic chelators used in this study.

The $[Tc(CO)_2(NO)]^{2+}$ complex species were generated by substitution of CO with $NO^+$ ligands in the $[Tc(CO)_3]^+$ core using either $[Et_4N]_2[Tc(CO)_3Cl_3]$ or $[Tc(CO)_3(OH)]_4$ as precursor, as described in our FY 2015 report (Hall et. al 2015). These species will be referred to as the $[Tc(CO)_2(NO)]^{2+}$ species. While the NMR and EPR analyses on these species were reported previously (Hall et al. 2015), this year they were subjected to XAS and XPS measurements.

## 3.3 Preparation of low-valent Tc species by *in situ* reduction of pertechnetate

### 3.3.1 Electrochemical reduction of pertechnetate to generate Tc(VI) and Tc(IV) species

Electrochemical methods were used to generate Tc(IV) and Tc(VI) compounds, so we could expand the non-pertechnetate spectroscopic library. Controlled potential electrolysis methods were used for the electrochemical reduction of $TcO_4^-$ using a standard three-electrode cell stand and an Epsilon Potentiostat from Bioanalytical Systems (BASi), Indiana, USA. Reduction was conducted in a BASi thin layer absorbance cell (1mm pathlength). All reported potentials were referenced versus a Ag/AgCl micro-electrode and a platinum wire was used at the auxiliary electrode. For the reduction of $TcO_4^-$ to Tc(VI), a platinum 100 mesh electrode from Sigma-Aldrich (99.9%) was used as the working electrode. For the reduction to Tc(IV), a platinum coil electrode was used as the working electrode, onto which the Tc(IV) was electrodeposited by application of the appropriate reduction potential.

Reduction of Tc(VII) to Tc(VI) was confirmed by a spectroelectrochemical technique employing absorption based double potential step chronoabsorptometry (Kissinger et al. 1996; DeAngelis et al. 1976). In a typical experiment, the initial potential was set to −0.1 V to ensure that the entire Tc mass in the sample was in the fully oxidized $TcO_4^-$ state, while absorption spectra were concurrently recorded. Subsequently, the working potential was set to a given value ($E_{app}$), and the solution was allowed to reach equilibrium, which was inferred when the UV-visible absorption spectrum no longer changed over a 3–4 min period. For spectroelectrochemistry measurements, a platinum 100 mesh electrode from Sigma-Aldrich (99.9%) was used as the working electrode. UV absorption spectra were recorded with a deuterium light source (Mikropack, model# DH 2000) and an Ocean Optics USB2000 detector (188-880 nm) using Spectra Suite Software for spectral data acquisitions. Spectroelectrochemical titration data thus obtained was analyzed according to the Nernstian expression (see equation 1) for a multi-electron transfer reaction:

$$E_{app} = E^{0\prime} - \frac{0.0591}{n} log \frac{a_{red}}{a_{ox}} \qquad (1)$$

where $E^{0\prime}$ is the formal electrode potential, n is the number of electrons transferred, $a_{red}$ and $a_{ox}$ are the respective activities of the fully reduced and fully oxidized species. First step reduction of $TcO_4^-$ was demonstrated to be a one electron process, and the reduction product was assumed to be $TcO_4^{2-}$. It is reasonable to assume such under conditions of the constant ionic strength and low concentration of these electroanalytes, the activity coefficients of the reactant and product are similar, and the $\frac{a_{red}}{a_{ox}}$ term can be replaced by [Red]/[Ox] where [Red] and [Ox] are the respective concentrations of the fully reduced and fully oxidized species. The ratio [Red]/[Ox] at applied potential $E_{app}$ was estimated from $(A_{ox}\text{-}A)/(A\text{-}A_{red})$, where $A$ is the absorbance at a given wavelength. $A_{ox}$ is the absorbance of the fully oxidized species, which was estimated from the absorbance at the most positive value of $E_{app}$ ($E_{app}$ = -0.1 V; where [Ox]/[Red] > 1000); $A_{red}$ is the absorbance of the fully reduced sample, which was estimated from the absorbance at the most negative value of $E_{app}$ ($E_{app}$ = -0.8 V; where [Ox]/[Red] < 0.001 (Schroll et al. 2013).

Tc reduction and generation of Tc(IV) species was monitored by characterization of the isolated product using Electron Paramagnetic Resonance (EPR) and X-ray photoelectron spectroscopies (XPS).

### 3.3.2 Synthesis of non-pertechnetate species through chemical reduction of pertechnetate

Studies to evaluate nature and time stability of the non-petechnetate species generated via chemical reduction studies of $TcO_4^-$ in Hanford tank supernatant simulant (see Table 1) have been ongoing for last 2.5 years. Experimental conditions and preliminary results are discussed in the FY 2014 and 2015 reports (Levitskaia et al. 2015; Chatterjee et al. 2015). In brief, the reduction was carried out under four different reaction conditions corresponding to **Parr Reactions 1 – 4** (Table 2). In all tests, CO gas that contained approximately 75 ppm $H_2$ served as a reductant. The effect of gluconate (100 mM) and catalytic noble metals (0.13 mM Pt, 0.57 mM Pd, 0.014 mM Rh, and 1.04 mM Ru) simulating fission products on reduction of $TcO_4^-$ (10 mM) was investigated. Small aliquots of the liquid fractions of the reaction mixtures were withdrawn and analyzed by LSC, $^{99}$Tc NMR and EPR. Samples were periodically monitored by $^{99}$Tc NMR for about 2.5 years. During this time, all Tc samples were stored in polyethylene containers under ambient laboratory conditions and were not protected from exposure to light. In FY 2016, monitoring of these samples continued and was supplemented with XPS and XAS measurements to gain more insight into the structure of the Tc species present in the reaction mixtures.

In FY 2016, in order to examine effects of such parameters as reaction temperature, pressure, time and presence of redox active species, e.g. chromate, on the $TcO_4^-$ reduction, several new studies were conducted. The employed reaction conditions are summarized in Table 2 (**Parr Reactions 5 – 9**).

**Table 2.** Reaction conditions of the *in situ* $TcO_4^-$ reduction in Hanford supernatant simulant using gaseous CO/75 ppm $H_2$ reductant. Initial $TcO_4^-$ concentration is 9.8 – 10.2 mM.

| Parr reaction # | Year simulant made | P(psi) | T(°C) | Added ligand | Cr(VI) added | Noble metals | Reaction time (days) |
|---|---|---|---|---|---|---|---|
| 1 | FY 2014 | 1300 | 80 | 100 mM gluconate | No | Yes | 10 |
| 2 | FY 2014 | 1300 | 80 | none | No | Yes | 10 |
| 3 | FY 2014 | 1300 | 80 | 100 mM gluconate | No | No | 10 |
| 4 | FY 2014 | 1300 | 80 | none | No | No | 7 |
| 5 | FY 2016 | 250 | 80 | 100 mM gluconate | No | Yes | 21 |
| 6 | FY 2016 | 250 | 25 | 100 mM gluconate | No | Yes | 14 |
| 7 | FY 2016 | ambient | 80 | 100 mM gluconate | No | Yes | 21 |
| 8 | FY 2016 | 250 | 80 | 100 mM gluconate | Yes | Yes | 21 |
| 9 | FY 2016 | 250 | 80 | 100 mM IDA | No | Yes | 14 |

Upon conclusion of each test, the reaction mixture was returned to room temperature and atmospheric pressure, unsealed, and sampled soon after exposure to atmospheric conditions. If the sample contained precipitate, it was centrifuged, and small aliquots of the liquid fractions of the reaction mixtures were withdrawn and analyzed by LSC, $^{99}$Tc NMR, EPR and XPS; the major portion of the supernate was left in the contact with precipitate during storage. Samples were periodically monitored by $^{99}$Tc NMR to test their kinetic stability.

## 3.4 Characterization Techniques

### 3.4.1 Technetium-99 nuclear magnetic resonance (NMR) spectroscopy

The solution aliquots used for $^{99}$Tc- NMR analyses were placed in capped polytetrafluoroethylene (PTFE)/fluorinated ethylene propylene (FEP) copolymer sleeves (Wilmad Lab Glass, Vineland, NJ), which were then inserted into 5- or 10-mm glass NMR tubes to provide secondary containment for the radioactive liquid. $^{99}$Tc NMR data were routinely collected at 67.565 MHz on a Tecmag Discovery spectrometer equipped with a 10-mm broadband Nalorac probe as described previously (Cho et al. 2004). A solution containing 10 mM $TcO_4^-$ was used as a $^{99}$Tc chemical shift reference, and all chemical shift data are quoted relative to $TcO_4^-$ (Franklin et al. 1982).

### 3.4.2 Technetium-99 electron paramagnetic resonance (EPR) spectroscopy

EPR spectra were acquired on a Bruker EMX Spectrometer equipped with an ER4102ST resonator (spectra at room temperature and 120 K) or an ER4116DM Dual Mode resonator (spectra at 5 K) and an Oxford ESR910 cryostat. Samples were doubly contained by employing unbreakable FEP tube liners (Wilmad Lab Glass, Vineland, NJ) inside traditional quartz EPR tubes. Liquid samples employed 1.5 mm inner diameter (ID) liners and 4 mm outer diameter (OD) quartz tubes while frozen solution and powder samples used 3.15 mm ID liners and 5 mm OD tubes.

### 3.4.3 X-ray photoelectron spectroscopy (XPS)

X-ray photoelectron spectroscopy (XPS) spectra were recorded using a Kratos AXIS Ultra DLD system equipped with a monochromatic Al Kα x-ray source (1486.7 eV) and a hemispherical analyzer. Solid samples were mounted either as a powder form or as a wet slurry using double-sided Scotch brand tape attached to a silicon substrate. In case of slurries, the liquid was completely evaporated either under air or under vacuum, before the samples were ran. The instrument work function was calibrated to give a binding energy (BE) of 83.96 ± 0.1 eV for the Au $4f_{7/2}$ line for metallic gold and the spectrometer dispersion was adjusted to give a BE of 932.62 ± 0.1 eV for the Cu $2p_{3/2}$ line of metallic copper. High resolution analyses were carried out with an analysis area of 300 x 700 microns using a pass energy of 40 eV with a step size of 0.1 eV. Surface charge was eliminated with a charge neutralizer and data were corrected through referencing the 285.0 eV C 1s peak. The percentages of individual elements detected were determined from the relative composition analysis of the peak areas of the bands on the basis of the relative peak areas and their corresponding sensitivity factors to provide relative compositions. XPS peak fitting was performed using the software CasaXPS under an agreement with Casa Software Ltd. (Levitskaia et al. 2016).

### 3.4.4 X-ray absorption near edge structure (XANES) spectroscopy

XANES data were obtained either at SSRL BL 11-2 or at APS BL-12 BM in fluorescence mode. XANES data were obtained from 200 eV below the Tc edge to 1000 eV above the edge; the data from 75 eV below the edge to 200 eV above the edge was obtained with 0.5 eV spacing. The rest of the data points are widely spaced (50 eV) and were used for the pre- and post-edge correction. The monochromator was detuned 50% to reduce the harmonic content of the beam. Transmission data was obtained using Ar filled ion chambers. Fluorescence data was obtained using a 100 element Ge detector and were corrected for detector dead time. Data were converted from raw data to spectra using SixPack (Rehr et al, 1992). Spectra were normalized using Artemis, to process raw data (Lukens et al. 2002). Normalized XANES spectra were fit using standard spectra in the locally written program "fites." XANES standard spectra were carefully energy calibrated using $TcO_4^-$ adsorbed on Reillex-HPQ as the energy reference. The XANES spectra of the "unknown" samples were allowed to vary in energy during fitting. The XANES spectral resolution is 7 eV based on the width of the $TcO_4^-$ pre-edge peak, so each spectrum possesses 14 independent data points (range of the spectrum/resolution). XANES spectra for the samples were convolved with a 1.7 eV Gaussian to match to the energy resolution of the $TcO_2$ and $TcO_4^-$ "reference standards" spectra, and the XANES spectrum of $[Tc(CO)_3(H_2O)_2(OH)]$ was convolved with a 1.5 eV Gaussian for the same reason.

### 3.4.5 Liquid Scintillation Counting (LSC)

The concentration of Tc in liquid samples was measured by a LSC technique. Typically, 10 mL of Ultima Gold XR liquid scintillation cocktail (Packard BioScience, Meriden, CT) was used for $^{99}$Tc beta counting. The relative beta activity of the samples was determined using a Packard Tri-Carb Model 2500TR Liquid Scintillation Analyzer (Packard Instrument Company, Meriden, CT 06450) with a 0.98 counting efficiency. In a typical measurement, beta counts were integrated over a 10 min collection time; all counts were corrected for background and then converted to activity (or mass) by dividing by the stated efficiency.

## 3.5 Computational Methods-DFT

All Density Functional Theory (DFT)[3] computations were performed on either Cascade or Constance which are high performance computers available through Environmental & Molecular Sciences Laboratory (EMSL) at PNNL, and the PNNL institutional computing respectively. The ORCA software program version 3.0.3 (Neese 2012) was chosen due to the emphasis on magnetic spectroscopies during software development. Further details about the computational methodology have already been published (Hall et al. 2016).

[3] **Density functional theory** (**DFT**) is a computational quantum mechanical modeling method used in physics, chemistry and materials science to investigate the electronic structure (principally the ground state) of many-body systems, in particular atoms, molecules, and the condensed phases.

# 4.0 Results and Discussion

## 4.1 Spectroscopic library of Tc(I – VII) species

### 4.1.1 X-ray photoelectron spectroscopy

XPS is a powerful tool to probe Tc oxidation state and can provide quantitative information on the relative abundance of co-existing Tc species in different oxidation states. As evident from Table 3, binding energies of Tc(0) and Tc(VII) $3d_{5/2}$ electron differ by at least 5.5 eV providing sufficient energy window to simultaneously identify and quantify relevant abundance of the co-existing Tc(I through VII) species. It was also of our interest to evaluate if XPS can differentiate among the various $[Tc(CO)_3]^+$ species containing dissimilar auxiliary ligands coordinated to the Tc center. To date, XPS measurements of Tc compounds are scarce, and application is hindered by the lack of adequate XPS data for low-valent Tc reference or known standards. For instance, the NIST XPS database contains only 21 entries predominantly for Tc(III, IV, and VII) (Thompson et al. 1986; Wester et al. 1987). Even more scarce are XPS measurements of Tc(I) complexes, with only two Tc(I) species being reported in literature as shown in Table 3, none of which belong to the class of $[Tc(CO)_3]^+$ compounds. Therefore, one objective of this work is to create an XPS spectroscopic database for the various $[Tc(CO)_3]^+$ and $[Tc(CO)_2(NO)]^{n+}$ species that may be present in certain Hanford tanks and further expand the available to-date XPS spectroscopic library in general. To do this, XPS spectra of the Tc(I), Tc(II), Tc(IV), Tc(V) and Tc(VI) compounds prepared chemically or electrochemically were collected to provide a reference library that can be used to identify the oxidation states and chemical nature of the Tc species present in real tank waste samples.

**Table 3.** Technetium $3d_{5/2}$ electron binding energies reported in literature referenced with respect to the hydrocarbon signal for C 1s electron of 285 eV (Wester et al. 1987).

| Compound | Tc oxidation state | Tc $3d_{5/2}$ electron binding energy (eV) |
|---|---|---|
| Tc | 0 | 254.0 |
| $Tc(tmp)_6BPh_4$ | I | 253.6 |
| $Tc(dmmp)_6BPh_4$ | I | 253.8 |
| $[Tc(dmpe)_2Br_2]Br$ | III | 255.3 |
| $[Tc(dmpe)_2Cl_2]Cl$ | III | 255.5 |
| $TcBr[(dmg)_3bub]$ | III | 255.6 |
| $TcCl[(dmg)_3bub]$ | III | 255.6 |
| $[Tc(diars)_2Br_2]Br$ | III | 255.6 |
| $TcCl[(cdo)_3mb]$ | III | 255.7 |
| $[Tc(dppe)_2Cl_2]Cl$ | III | 255.7 |
| $(NH_4)_2TcCl_6$ | IV | 256.6 |
| *trans*-$TcCl_4(PO_3)_2$ | IV | 256.8 |
| $(NH_4)_2TcBr_6$ | IV | 256.8 |
| $TcO_2$ | IV | 257.0 |
| $[(CH_3)_4N]_2TcCl_6$ | IV | 257.6 |

| Compound | Tc oxidation state | Tc $3d_{5/2}$ electron binding energy (eV) |
|---|---|---|
| $[(n\text{-}C_4H_9)_4N]TcOCl_4$ | V | 258.2 |
| $NH_4TcO_4$ | VII | 259.5 |
| $KTcO_4$ | VII | 259.7 |
| $NH_4TcO_4$ | VII | 259.8 |
| $NaTcO_4$ | VII | 259.9 |

#### 4.1.1.1 Tc(I): $[Tc(CO)_3]^+$ species

XPS spectra of Tc(I) complexes are rare in literature with only two complexes being reported in the NIST database. Among these, none are $[Tc(CO)_3]^+$ complexes. In order to obtain the XPS spectra of the various $[Tc(CO)_3]^+$ species, the samples were prepared by either gluing solid powders onto a carbon tape, or by depositing drops of freshly prepared solutions onto the tape and evaporating to a solid under normal atmospheric conditions. The various $[Tc(CO)_3(H_2O)_{3-n}(OH)_n]^{1-n}$ species were prepared by dissolving specified amounts of $[Tc(CO)_3(OH)]_4$ in water and changing the pH of the solution to 1 to generate $[Tc(CO)_3(H_2O)_3]^+$ or 14 to form $[Tc(CO)_3(H_2O)_2(OH)]$. Alternatively, the same species were generated using $(Et_4N)_2[Tc(CO)_3Cl_3]$ as a starting material and dissolving in water under slightly acidic or neutral pH to generate $[Tc(CO)_3(H_2O)_3]^+$ or in a solution of 1 M NaOH to generate $[Tc(CO)_3(H_2O)_2(OH)]$. The XPS spectra of the solid $(Et_4N)_2[Tc(CO)_3Cl_3]$ and $[Tc(CO)_3(OH)]_4$ showed a single set of doublets respectively, with $3d_{5/2}$ electron binding energies of 254.2 eV and 255.4 eV (Figures 2 and 5), suggesting a unique Tc coordination and electronic environment. The differences in binding energies are consistent with the different nature and electron withdrawing character of the $Cl^-$ vs. O binding groups. $Cl^-$ is less electronegative and being a stronger π-donating group, results in a higher electron density on the metal center compared to the σ-donating, more electronegative O, and therefore results in a lower binding energy. This binding energy trend is continued for additional Tc carbonyl hydrolysis species where the XPS spectra show that the binding energies of $[Tc(CO)_3(H_2O)_2(OH)]$ and $[Tc(CO)_3(H_2O)_3]^+$ are 255.0 and 255.2 respectively. The binding energy of $(Et_4N)_2[Tc(CO)_3Cl_3]$ is closer to the two literature reported Tc(I) species (253.6 – 253.8 eV, Table 3), while the $[Tc(CO)_3]^+$ species binding energies are significantly greater and are closer to that reported for Tc(III) (255.3 – 255.7 eV, Table 3). This demonstrates the value of expanding this library to better understand how the electronic environment affects the binding energies of $[Tc(CO)_3]^+$ species and highlights the need for creating an XPS spectral library with a diverse range of Tc electronic structures that can demonstrate the effect of ligand binding on the electronic structure and the oxidation states. Fitting of the spectrum of $(Et_4N)_2[Tc(CO)_3Cl_3]$ suggests that in addition to Tc(I) it contains two minor components with the $3d_{5/2}$ electron binding energy positioned at 255.5 eV and another at 258.4 eV (Figure 2). While the former can be tentatively assigned to at Tc(IV) species arising out of the $TcCl_6^{2-}$ side product, its binding energy is slightly lower than that reported in the literature. Similarly, the peak with lower binding energy is slightly lower than that expected for a Tc(VII) species, and its origin is under further investigation. Similarly, small Tc(IV) and Tc(VII) components are observed for $[Tc(CO)_3(H_2O)_2(OH)]$ (Figure 3).

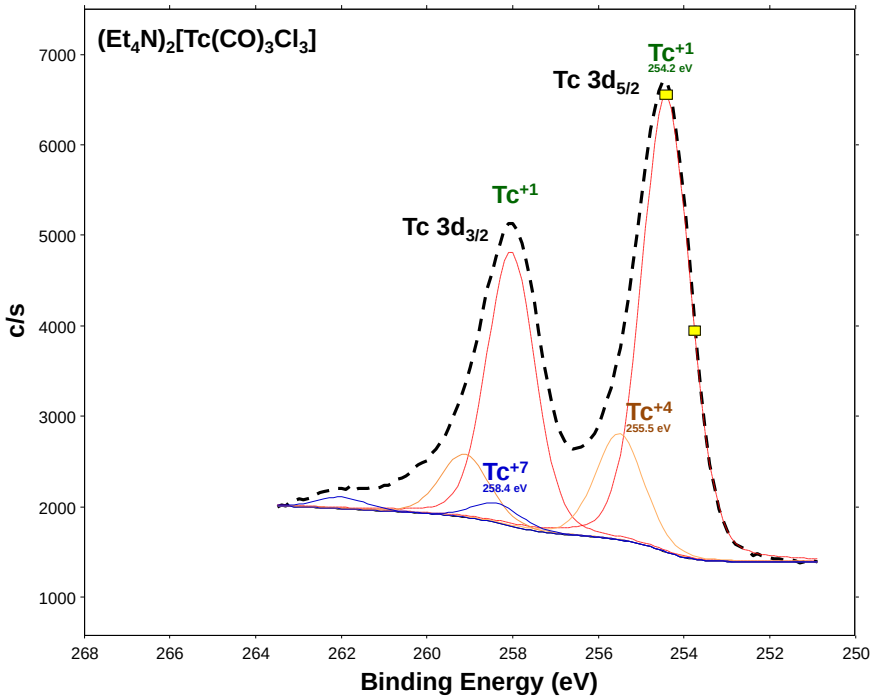


**Figure 2.** X-ray photoelectron spectrum of Tc $3d_{5/2}$ and $3d_{3/2}$ regions for $(Et_4N)_2[Tc(CO)_3Cl_3]$. Black trace: experimental spectrum, red trace: Tc(I) fit, orange trace: Tc(IV) fit, blue trace: Tc(VII) fit.

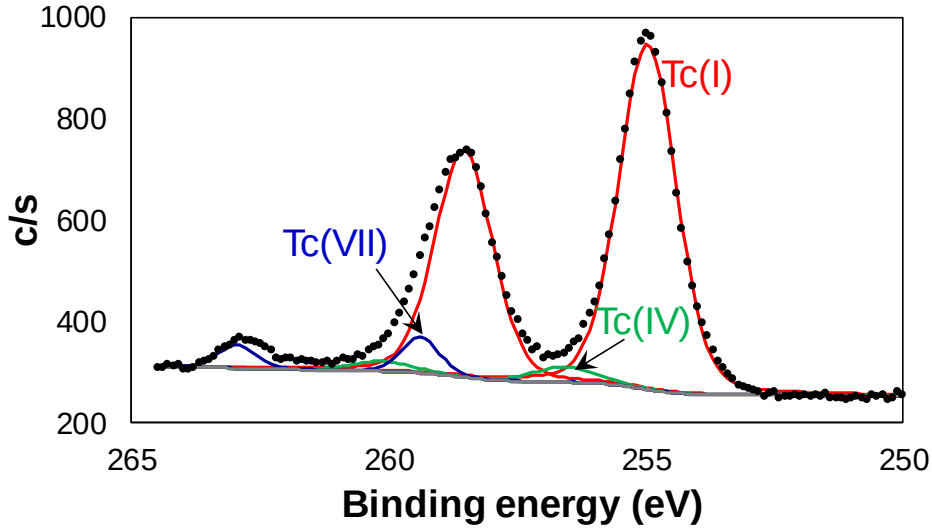


**Figure 3.** X-ray photoelectron spectrum of Tc $3d_{5/2}$ and $3d_{3/2}$ regions for $[Tc(CO)_3(H_2O)_2(OH)]$. Black circles: experimental spectrum, red trace: Tc(I) fit, green trace: Tc(IV) fit, blue trace: Tc(VII) fit.

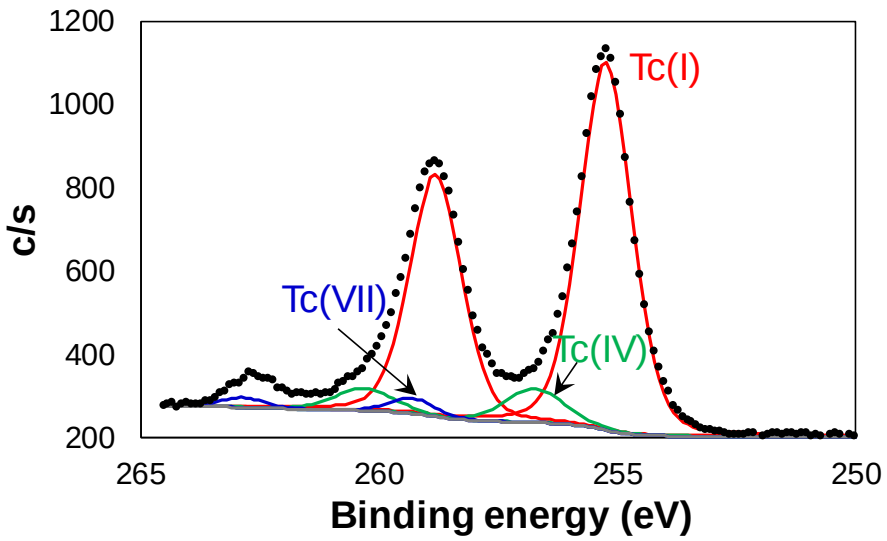


**Figure 4.** X-ray photoelectron spectrum of Tc $3d_{5/2}$ and $3d_{3/2}$ regions for $[Tc(CO)_3(H_2O)_3]^+$. Black circles: experimental spectrum, red trace: Tc(I) fit, green trace: Tc(IV) fit, blue trace: Tc(VII) fit.

The XPS spectrum of the $[Tc(CO)_3]^+$•IDA complex in 5 M $NaNO_3$/0.1 M NaOH shows a doublet of $3d_{5/2}$ and $3d_{3/2}$ broad peaks which can be fit to two Tc(I) species with lower binding energies of 255.1 and 256.3 eV (Figure 5). The photoelectron spectrum also shows a small fraction of Tc(VII) characterized by a component with lower binding energy of 259.5 eV, which is attributed to partial oxidation of Tc(I) to Tc(VII). These results are consistent with the NMR analysis of the $[Tc(CO)_3]^+$•IDA complex exhibiting two resonances due to dissimilar $[Tc(CO)_3]^+$ centers and a small $TcO_4^-$ resonance due to oxidation of a small portion of $[Tc(CO)_3]^+$ during its preparation (Chatterjee et al. 2015).

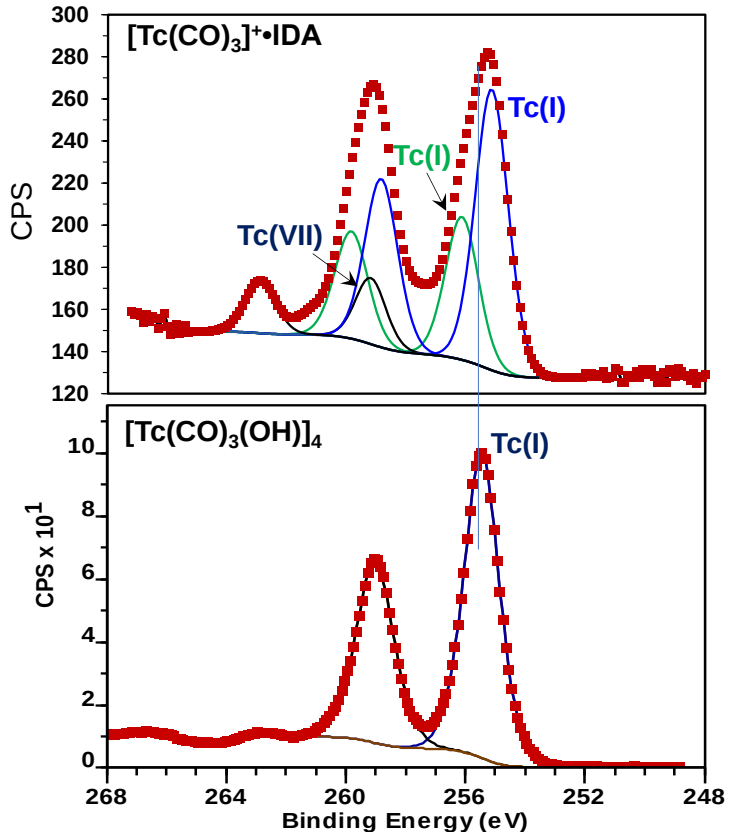


**Figure 5.** X-ray photoelectron spectrum of Tc $3d_{5/2}$ and $3d_{3/2}$ regions for $[Tc(CO)_3]^+$•IDA (top) and $[Tc(CO)_3(OH)]_4$ (bottom). Red squares: experimental spectrum; blue trace, bottom plot: Tc(I) fit; green trace, top plot: Tc(I) fit; black trace: Tc(VII) fit.

### 4.1.1.2 Tc(V): (n-$Bu_4N$)[$TcOCl_4$] species

The intermediate oxidation states of Tc are unstable due to disproportionation and the resulting dynamic equilibrium between the Tc(IV)↔Tc(V)↔Tc(VI) oxidation states and air-induced oxidation. Therefore, these species are usually generated in unison. (n-$Bu_4N$)[$TcOCl_4$] served as the model Tc(V) compound in our studies.

While the XPS spectrum of (n-$Bu_4N$)[$TcOCl_4$], where n-Bu = n-$C_4H_9$, had been reported previously (Thompson et al. 1986), it is the only Tc(V) complex reported in the NIST database. Evaluation of the redox stability of this complex in vacuum is important in order to obtain the correct values of binding energy. The spectrum of this complex monitored over time is shown in Figure 6. It is observed that the initial phototelectron spectrum of the complex can be resolved into two bands with the dominating species having a lower binding energy of 256.7 eV and a minor component with a binding energy of 258.3 eV, respectively. The binding energy of 256.7 eV is attributed to the Tc(V) species, while the lower value of 258.3 eV is attributed to a reduced Tc(IV) product. It is observed that in vacuum, the Tc(V) is gradually reduced to the Tc(IV) product in 4 days.

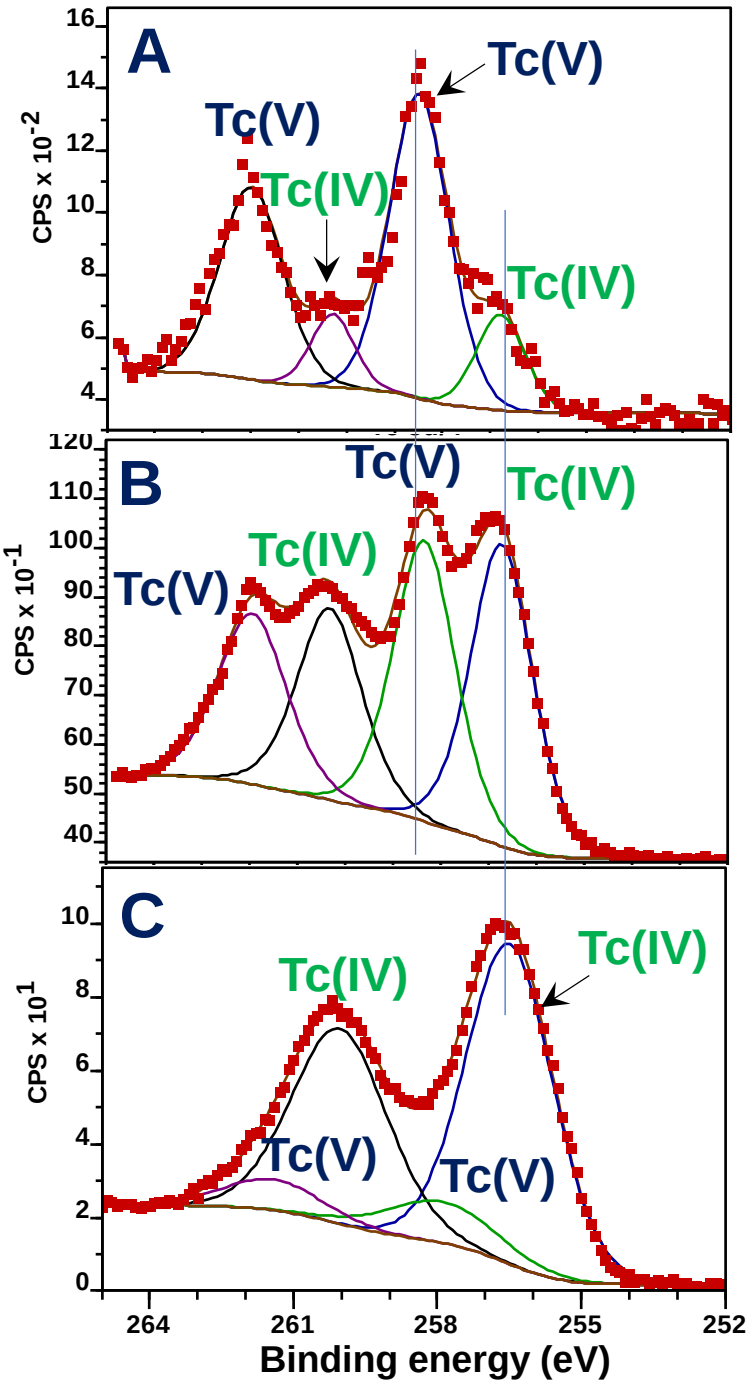


**Figure 6.** X-ray photoelectron spectrum of Tc $3d_{5/2}$ and $3d_{3/2}$ regions for (n-$Bu_4N$)[$TcOCl_4$] (A) immediately after subjecting to vacuum, (B) one day in vacuum and (C) 4 days in vacuum. Brown trace: baseline for fit. The fits for Tc(IV) and Tc(V) $3d_{5/2}$ fits are labeled on the panels.

### 4.1.1.3 Tc(IV, VI): electrochemically generated solid $TcO_2 \cdot nH_2O$ and solution Tc(VI) (tentatively assigned to $TcO_4^{2-}$) species

Tc(VI) and Tc(IV) species were electrochemically generated by sequential electrochemical reduction of $NH_4TcO_4$ in 5 M $NaNO_3$/2 M NaOH under controlled potential environments. The initial electrochemical reduction of $NH_4TcO_4$ resulted in a $1e^-$ reduction to Tc(VI), which was followed by another 2 e- reduction at more reducing potentials to form Tc(IV).

#### 4.1.1.3.1 Electrochemical reduction of $TcO_4^-$ and characterization of the Tc(IV, VI) products

**Tc(VI) product.** The redox potential of the first $1e^-$ reduction process was determined through spectroelectrochemistry followed by Nernstian analyses, and was determined to be -0.82 V vs. Ag/AgCl. In a typical spectroelectrochemical experiment, the initial potential was set to 0.0 V to ensure that the entire Tc concentration in the sample was in the fully oxidized $TcO_4^-$ state as monitored at 429 wavelength, while absorption spectra were concurrently recorded. Subsequently, the working potential was set to a given value ($E_{app}$), and the solution was allowed to reach equilibrium, which was inferred when the UV-visible absorption spectrum no longer changed over a 3–4 min period. Shown in Figure 7 are the absorption spectra at each potential as $E_{app}$ was decreased in a stepwise fashion from the most positive to the most negative value. This allowed for measurements on the fully oxidized ($TcO_4^-$) and finally fully reduced forms, as well as intermediate oxidation state species mixtures. The initial spectrum of fully oxidized $TcO_4^-$ in 5.0 M $NaNO_3$, 2 M NaOH measured at 0 mV was only recorded from wavelengths of 340 nm and higher due to strong absorbance of the $NO_3^-$ anion at shorter wavelengths. At 0 V, the spectrum of $TcO_4^-$ only shows a shoulder at 429 nm. Figure 7A shows an overall increase in the intensities of the entire spectral region from 340-800 nm, highlighted by a progressive growth of a band centered at ~ 445 nm, along with a simultaneous build-up of the intensity of a shoulder at ~650 nm. Reversing the step direction or varying the step size gave spectral changes that are consistent with the observed data. The spectroelectrochemical titration data resembled an [A]→[B] process, which motivated the analysis of the process according to the Nernst equation, [1]. A plot of $E_{app}$ versus log([Ox]/[Red]) at 429 nm, shown in Figure 7B, exhibits a linear correlation with the equation: $E_{app}$(mV)={65.8 log([Ox]/[Red])-819}. The slope of 66(±1) mV gives electron stoichiometry (n) value of 1.1(±0.1), suggesting an electron transfer stoichiometry of 1, that suggests the generation of a Tc(VI) species. The formal potential for the redox process of 0.82 V is obtained from the y-intercept.

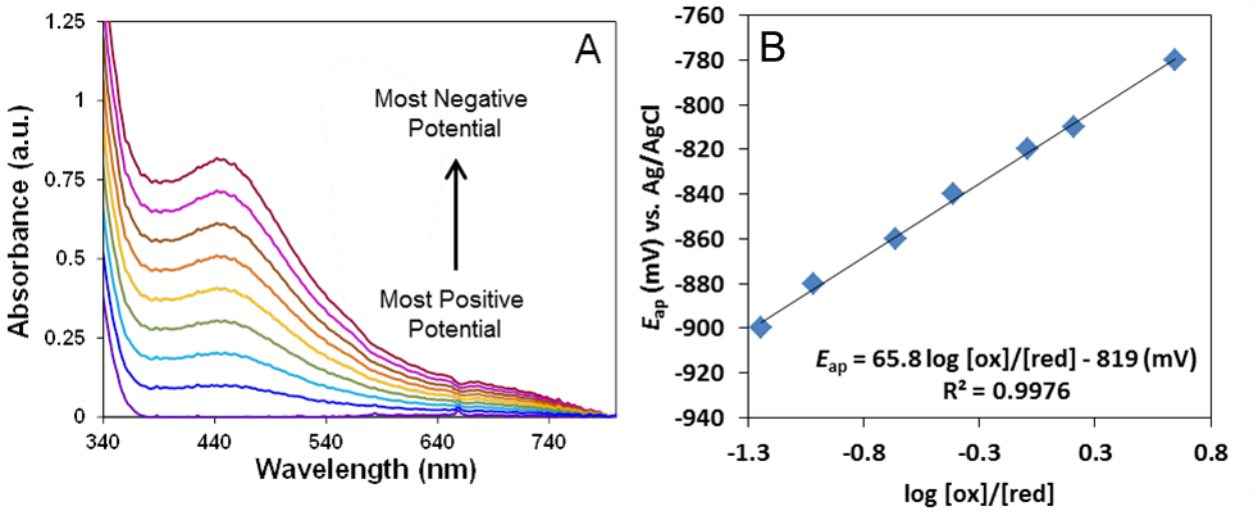


**Figure 7.** (A) Absorption spectra of 10.0 mM $NH_4TcO_4$ in an aqueous solution of 5.0 M $NaNO_3$/2.0 M NaOH recorded as a function of decreasing potential. The applied potentials (vs. Ag/AgCl) are (from bottom to top): 0 mV, -780 mV, -800 mV, -820 mV, -840 mV, -860 mV, -880 mV, -900 mV and -950 mV. (B) Nernst plot of log([Ox]/[Red]) vs. *E* (mV) vs. Ag/AgCl at 445 nm. The equation: $E_{app}$ (mV) vs. Ag/AgCl = -819 mV + 65.8 log([Ox]/[Red]).

Subsequent electrochemical generation and isolation of Tc(VI) was done by subjecting a stock solution of $NH_4TcO_4$ in 5 M $NaNO_3$/2 M NaOH to a reducing potential of -1000 mV under controlled potential environments, and isolation of the purple-red solution that surrounded the working electrode.

The electrochemically generated product (solution) was characterized by $^{99}$Tc NMR and EPR spectroscopies. NMR can be effectively used for probing diamagnetic odd numbered Tc oxidation states Tc(V) and Tc(VII). On the other hand, the even-numbered Tc(IV) and Tc(VI) oxidation states with unpaired electrons do not have a characteristic NMR signature, but can be probed using EPR spectroscopy as their monomeric forms are expected to have paramagnetic ground states. $^{99}$Tc NMR on a solution of 10 mM $TcO_4^-$ in 5.0 M $NaNO_3$, 2 M NaOH before electrolysis showed a single sharp resonance at 0 ppm (peak width = 10 Hz), characteristic of $TcO_4^-$. The NMR spectrum of the isolated working electrode solution after bulk electrolysis at -950 mV showed a reduction in the intensity of the $TcO_4^-$ resonance, with no appearance of any other resonances to compensate for the reduction in $TcO_4^-$ intensity. This is suggestive of partial conversion of pertechnetate to a paramagnetic species, which is no longer observed by NMR spectroscopy.

Complimentary EPR spectroscopy on the isolated working electrode solution displayed a spectrum when cooled to a temperature of 125 K, showing a signal split into 10 lines, which can be attributed to hyperfine splitting due to the $^{99}$Tc nucleus with a nuclear spin of 9/2 (Figure 8). The fact that the signal is observed even at temperatures well above that of liquid helium, suggests a s=½ technetium species, which is consistent with the formation of Tc(VI) species during the electroreduction process. The spectrum at 125 K resembles the spectra of other Tc(VI) complexes reported in literature (Abram et al. 1993). The spectrum increased in intensity as the temperature decreased and reached a maximum at approximately 40 K, whereupon the spectrum showed signs of power saturation. Fitting the spectrum yielded parameters

typical for Tc(VI) compounds – axial values for both Zeeman and hyperfine (allowing rhombicity yielded small deviations from axiality and concordantly small improvements in fit).

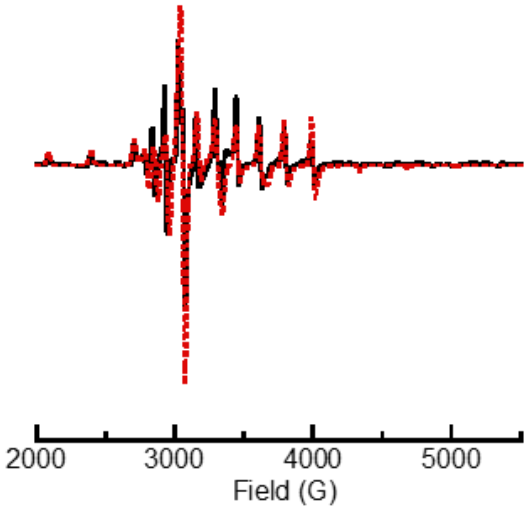


**Figure 8.** $^{99}$Tc EPR spectrum of working electrode solution obtained by electrochemical reduction of 10 mM $TcO_4^-$ in 5.0 M $NaNO_3$, 2 M NaOH solution (T = 125 K). The dashed red line represents the experimentally obtained spectrum, while the solid black line represents the fit.

**Tc(IV) product.** Electrochemical reduction of the $TcO_4^-$ beyond -1000 mV resulted in an irreversible 2e- reduction of the Tc(VI) to a Tc(IV) product--- a black precipitate on the electrode surface. The irreversible nature of this redox process prevented its electron transfer stoichiometry from being determined by spectroelectrochemistry followed by Nernstian analysis. Therefore, other modes of characterization such as EPR analysis were used.

For the generation of the Tc(IV) product, a bulk electrolysis was conducted at -1000 mV for 40 minutes, which resulted in the electrodeposition of a black precipitate on the working electrode surface. The platinum working electrode, along with the precipitate, was carefully removed from the electrolysis apparatus after the reduction experiment, and inserted in an EPR tube. Variable temperature EPR was then acquired; however no spectrum became evident until the temperature was below 10 K. At 3.7 K, a broad signal was observed centered at ~3300 G, split again into approximately 10 lines (Figure 9). This spectrum matches closely to that previously reported for $TcO_2$ prepared in a variety of ways (Lukens et al. 2002). It should be noted that while this previous work reported spin Hamiltonian parameters from a simulation, our parameters are the results of least squares data-fitting.

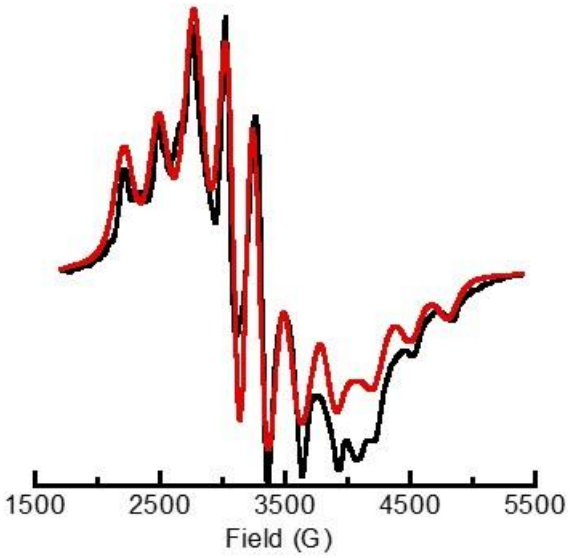


**Figure 9.** $^{99}$Tc EPR spectrum of black precipitate deposited on the working electrode (T = 3.7 K). The dashed red line represents the experimentally obtained spectrum, while the solid black line represents obtained fit.

### 4.1.1.3.2 XPS of Tc(IV, VI)

In order to obtain the photoelectron spectrum of the electro-reduced Tc(VI) species in solution, a drop of the isolated electrolyzed solution was placed on a carbon platform and allowed to evaporate under normal atmospheric conditions. The photoelectron spectrum of the solid residue left after evaporation exhibits three doublets whose lower binding energies are 259.9 eV, 258.0 eV and 256.1 eV respectively, as shown in Figure 10. The binding energies of 259.9 eV and 256.1 eV can be assigned to the $3d_{3/2}$ lines for Tc(VII) and Tc(IV) oxidation states, respectively. In addition to these, a peak is observed that corresponds to an intermediate Tc oxidation state. To our knowledge, the binding energy of Tc(VI) has not been reported in literature thus far. The observed peak at 258.0 eV is consistent with either a Tc(V) or Tc(VI) oxidation state.

The XPS spectrum for the electrodeposited black precipitate shown in Figure 10 (blue squares), shows the dominance of the Tc(IV) oxidation state characterized by the peak with the lower binding energy of 256.1 eV. However, small fractions of the intermediate Tc oxidation state are also observed. A small portion of Tc(VII) is also observed presumably due to air oxidation of one or more of the reduced products, or due to left over residual solution from the incomplete $TcO_4^-$ reduction.

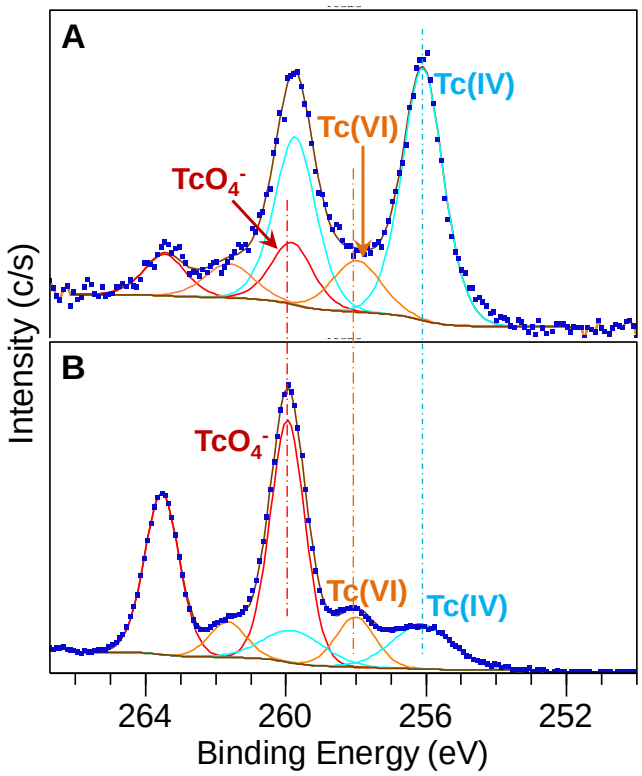


**Figure 10.** Tc photoelectron spectra of (A) electrodeposited black precipitate and (B) one-electron electroreduction product. Dark blue square: experimental spectra, light blue trace: Tc(IV) fit, orange trace: Tc(VI) fit, red trace: $TcO_4^-$ fit.

### 4.1.2 X-ray Absorption and X-ray fluorescence spectroscopies

A combination of x-ray absorption (XAS) and x-ray fluorescence (XFS) spectroscopies can unequivocally determine the oxidation state of a metal center, and possibly be useful in the identification of the coordination and binding environment around the metal center. In the organics-containing tank wastes, Tc can adopt multiple oxidation states in part due to the presence of small organic chelating agents such as nitrilotriacetate (NTA), ethylenediaminetetraacetate (EDTA), citrate, iminodiacetate, and gluconate. One objective of this project was to establish XAS/XFS signatures of the Tc(I) $[Tc(CO)_3]^+$ compounds that can serve for the reference purposes and for the identification of the relevant species in the tank waste and differentiate them from Tc in other oxidation states. To achieve this objective, an XAS/XFS library of Tc(I) for a set of model $[Tc(CO)_3]^+$ compounds as well Tc(II – VII) compounds was built.

The XAS spectra of the Tc compounds in various oxidation states are shown in Figure 11. It is evident that the XANES spectra of each lower oxidation state of Tc is distinctly different from $TcO_4^-$ as well as from each other, reinforcing the fact that XANES can be used to determine Tc oxidation state without ambiguity. The XANES of the model Tc(V) compound, $(Bu_4N)[TcOCl_4]$ and the model Tc(IV) compound, $TcO_2 \cdot nH_2O$, are 2 and 4.5 eV lower than that of $TcO_4^-$ respectively, while the model Tc(II) compound from the $[Tc(CO)_2(NO)]^{n+}$ species and the model Tc(I) compound, $[Tc(CO)_3(OH)]_4$, are further lower by 6.1 and 7.5 eV, respectively.

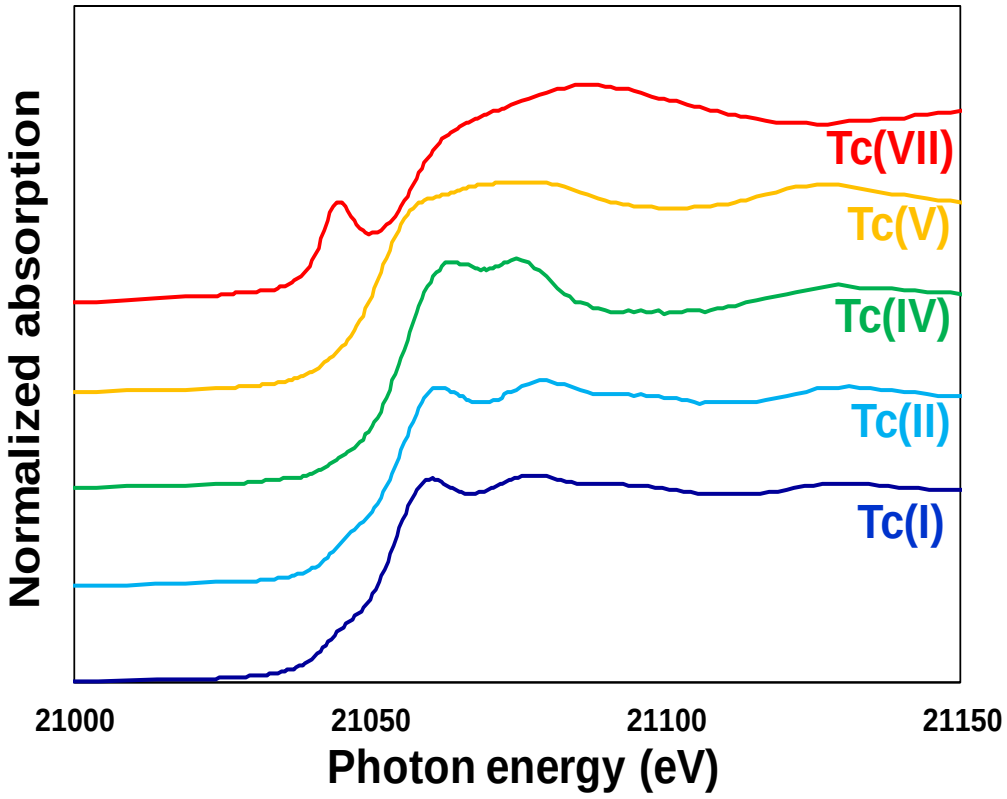


**Figure 11.** Tc K-edge XANES spectra for the various model Tc complexes. Red trace: $NH_4TcO_4$ aqueous solution, yellow trace: $(n\text{-}C_4H_9)_4N[TcOCl_4]$ solution in $CH_2Cl_2$, green trace: $TcO_2 \bullet nH_2O$ generated electrochemically, light blue trace: $[Tc(CO)_2(NO)]^{n+}$ in water, dark blue trace: $[Tc(CO)_3(OH)]_4$ in water.

While the above results demonstrate that Tc in different oxidation states can be differentiated by XAS, it is of interest to expand the library of Tc compounds in each oxidation state. To date, the XAS spectroscopic data of the pure Tc(I) complexes belonging to the $[Tc(CO)_3]^+$ family, are limited to $[Tc(CO)_3(H_2O)_3]^+$, $[Tc(CO)_3(H_2O)_2(OH)]$ and $[Tc(CO)_3]^+ \bullet$gluconate. This project further expanded this database to evaluate sensitivity of the Tc K-edge to the nature of auxiliary non-CO ligands. While subtle differences are discernible in the EXAFS spectra of the various $[Tc(CO)_3]^+$ species, as evident from Figure 12, more prominent changes become obvious in the Fourier transforms of the spectra in R space. It is of particular importance to note the differences between the aqua species $[Tc(CO)_3(H_2O)_2(OH)]$ with $[Tc(CO)_3]^+ \bullet$gluconate and polyaminocarboxylate complexes $[Tc(CO)_3]^+ \bullet$NTA, $[Tc(CO)_3]^+ \bullet$EDTA and $[Tc(CO)_3]^+ \bullet$IDA. Under conditions of 5 M $NaNO_3$ and 0 – 1 M NaOH, in the presence of ~10-100 fold excess of these ligands, we observed weak complexations by NTA and EDTA onto the $[Tc(CO)_3]^+$ center, and strong complexation by IDA using NMR measurements (Chatterjee et al. 2015). The XAS data support these NMR observations, and suggest that polyaminocarboxylate chelators may affect $[Tc(CO)_3]^+$ chemistry in the tank waste.

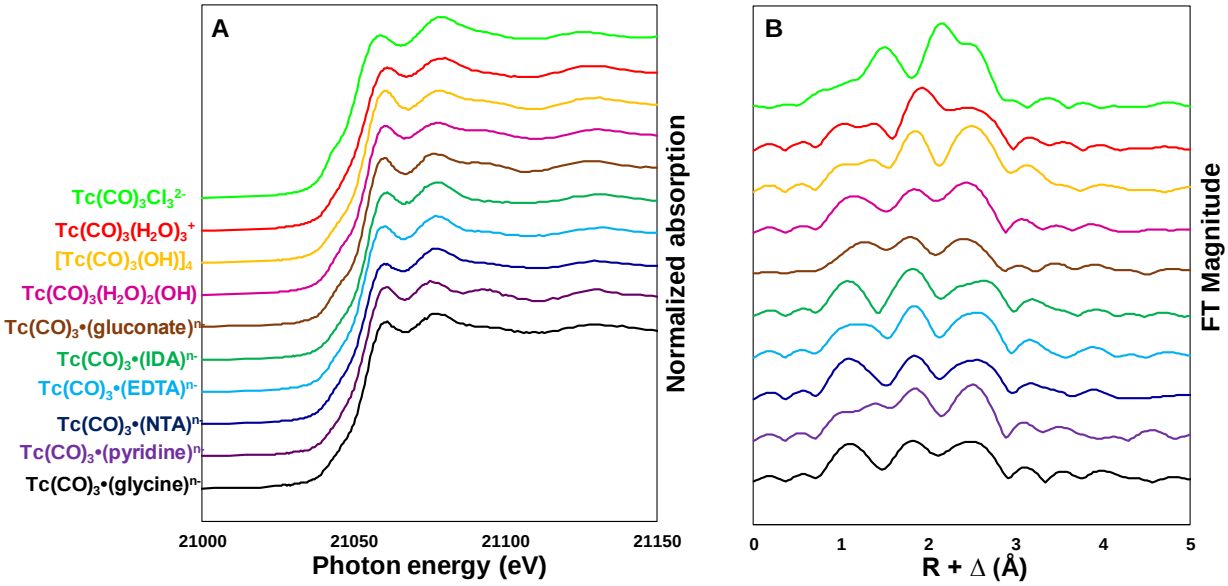


**Figure 12.** Tc K-edge XANES spectra (left) and their Fourier transforms (right) for various $[Tc(CO)_3]^+$ species.

This work is focused on evaluating of the $[Tc(CO)_3]^+$ chemical environment, and representative examples are shown below.

### 4.1.2.1 $(Et_4N)_2[Tc(CO)_3Cl_3]$

As the XAS of $[Tc(CO)_3Cl_3]^{2-}$ has not been reported before, attempts were made to fit the EXAFS data for this complex. EXAFS data were fit using theoretical scattering factors calculated for a model $[Tc(CO)_3Cl_3]^{2-}$ compound based on the distances recorded by Alberto et al. (1995). The value of $S_0^2$ for this and other fittings was determined to be 1.0 by modeling several EXAFS spectra of $TcO_4^-$, for which the coordination number is 4. The fitting results are given in Table 4 and shown in Figure 13. The EXAFS are consistent with the presence of only $[Tc(CO)_3Cl_3]^{2-}$. There was no $TcO_4^-$ in this sample, suggesting that $[Tc(CO)_3Cl_3]^{2-}$ is an appropriate reference standard for XANES analyses.

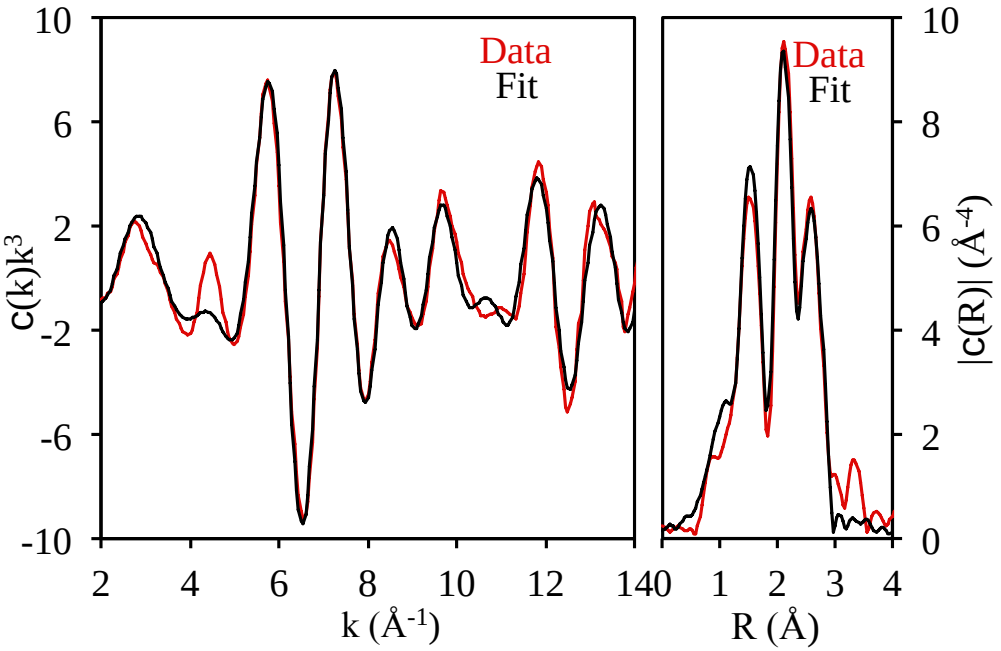


**Figure 13.** Tc K-edge EXAFS spectrum of $[Tc(CO)_3Cl_3]^{2-}$ (red) and fit (black) (left panel) and its Fourier transform (right panel).

**Table 4.** EXAFS fit parameters for $[Tc(CO)_3Cl_3]^{2-}$.[a]

| Neighbor | # of Neighbors[b] | Distance (Å) | $\sigma^2$ (Å$^2$) | π |
|---|---|---|---|---|
| *C* | 3 | 1.909(7) | 0.0026(6) | <0.001 |
| *Cl* | 3 | 2.511(8) | 0.0038(5) | <0.001 |
| *O* | 3 | 3.21(2) | 0.0015(7) | 0.006 |
| *O-C-Tc-C-O (MS)* | 3 | 2.991(9) | 0.0015(7)[c] | <0.001 |

a) $S_0^2$=1 (fixed), ΔE=0(2) eV; fit range 2<k<14; 1.1<R<3; # of independent points: 16.2; # of parameters: 8, r_factor 0.016; standard deviations are given in parentheses and are in the same units as the last digit.
b) Parameter fixed
c) Parameter constrained to equal that of the previous shell.

### 4.1.2.2 $[Tc(CO)_3]^+$•IDA

For the $[Tc(CO)_3]^+$•IDA complex, theoretical scattering factors were calculated using Feff6 and an idealized model for $[Tc(CO)_3O_2Cl]^{2-}$ based on the distances recorded by Alberto et al (1995). The "O" atoms are 2.05 Å from the Tc atom in the ideal model. The fitting results are given in Table 5 and shown in Figure 14. The sample contains ~15% $TcO_4^-$ as determined by the number of O neighbors at 1.78 Å. The coordination numbers of the other atoms are proportional to the amount of sample that is not $TcO_4^-$ (85% of their usual values). The fit results are consistent with the presence of $[Tc(CO)_3]^+$ coordinated by

oxygen or nitrogen atoms (it is difficult to impossible to distinguish between O and N neighbors by EXAFS).

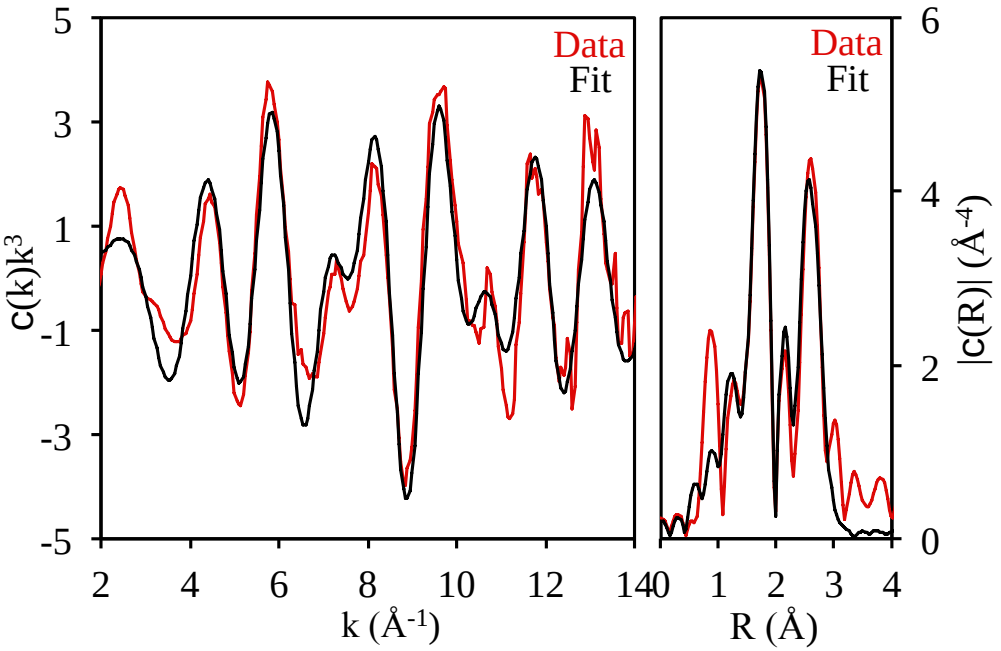


**Figure 14.** Tc K-edge EXAFS spectrum of $[Tc(CO)_3]^+$•IDA (red) and fit (black) (left panel) and its Fourier transform (right panel).

**Table 5.** EXAFS fit parameters for $[Tc(CO)_3]^+$•IDA.[a]

| Neighbor | # of Neighbors | Distance (Å) | $\sigma^2$ (Å$^2$) | π |
|---|---|---|---|---|
| *O* | 0.6(2) | 1.78(1) | 0.001[b] | 0.007 |
| *C* | 2.5(2)[c] | 2.00(3) | 0.006(3) | 0.004 |
| *O/N* | 2.5(2)[c] | 2.144(9) | 0.0013(7) | <0.001 |
| *O/N* | 2.5(2)[c] | 3.07(1) | 0.0050(6) | 0.026 |
| *O-C-Tc-C-O (MS)* | 2.5(2)[c] | 3.07(1)[d] | 0.0050(6)[d] | 0.317 |
| *O-C-Tc-O/N (MS)* | 5.0(4)[e] | 3.07(1)[d] | 0.0050(6)[d] | 0.001 |

a) $S_0^2$=1 (fixed), ΔE=-7(2) eV; fit range 2<k<14; 1.1<R<3; # of independent points: 16.2; # of parameters: 9, r_factor 0.021; standard deviations are given in parentheses and are in the same units as the last digit.
b) Parameter fixed at a typical value for $TcO_4^-$
c) Parameter constrained by the number of O neighbors in closest shell N=3×(1-$N_1$/4), where $N_1$ is the number of nearest oxygen neighbors (corresponds to $TcO_4^-$)
d) Parameter constrained to be equal that of the previous shell.
e) Parameter constrained by the number of O neighbors in closest shell N=6×(1-$N_1$/4), where $N_1$ is the number of nearest oxygen neighbors (corresponds to $TcO_4^-$)

### 4.1.2.3 $[Tc(CO)_3]^+$•gluconate

For the $[Tc(CO)_3]^+$•gluconate complex, data was obtained at Stanford Synchrotron Lightsource beam line 11-2, counting times varied from 1 s to 15 s, and are weighted by $k^3$. X-rays were monochromatized using a Si (220) $\phi$ = 90 monochromator with the second crystal detuned by 60 % to reduce the harmonic content of the beam. Intensity of the incident radiation was determined using an Ar-filled ion chamber. Data was recorded in fluorescence mode using a 100 element Ge detector and was corrected for detector dead time and background signal. EXAFS data was fit and theoretical scattering curves calculated based on the structure of $\{(C_5H_5)Co[PO(OR)_2]_3\}Tc(CO)_3$ where R is an alkyl group (Kramer et al. 2001). Each Debye-Waller parameter was allowed to vary. In no case did allowing the Debye-Waller parameter to vary improve the fit, but the fit was improved by setting the *trans* multiple scattering path to twice the Debye-Waller parameter.

The significance of the contribution of each shell to the total fit was determined using the F-test, which yields the p-value for each shell. The p value is the probability that the improvement due to adding the scattering atoms is due to random noise. A p-value less than 0.05 means that adding the scattering shell improves the fit by greater than two standard deviations.

**Table 6.** EXAFS fitting parameters for $[Tc(CO)_3]^+$•gluconate.[a]

| Neighbor | # of Neighbors | Distance (Å) | $\sigma^2$ (Å$^2$) | p | Distance (Å) reported by Lukens et al. 2004 |
|---|---|---|---|---|---|
| *C* | 3 | 1.909(6) | 0.0032(3) | <0.001 | 1.911(2) |
| *O* | 3 | 2.169(6) | 0.0032(3)[b] | <0.001 | 2.137(2) |
| *O*[c] | 3 | 3.061(6) | 0.0032(3)[b] | <0.001 | 3.09(3) |
| *C* | 3 | 3.12(2) | 0.0032(3)[b] | 0.185 | 3.44 |
| *Trans-MS* | 6 | 3.98(4) | 0.0064(6)[b] | 0.440 | 3.96(1) |

a) $S_0^2$=0.9 (fixed), $\Delta E$= 9(1)

b) Parameter set equal to parameter of previous shell

c) This path includes two multiple scattering path to the carbonyl oxygen atom.

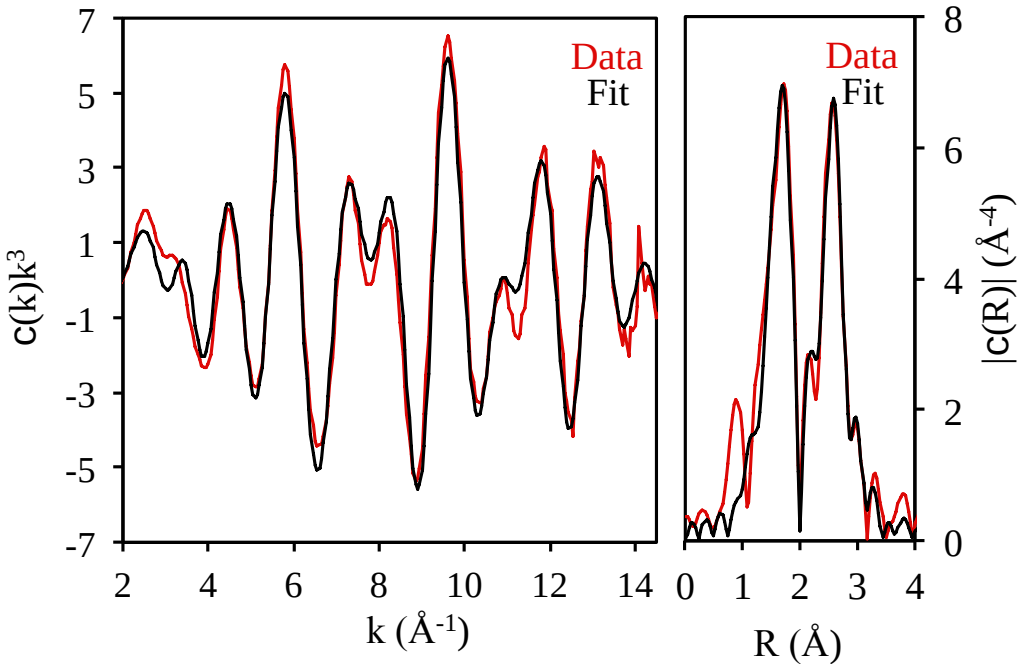


**Figure 15.** EXAFS spectrum of $[Tc(CO)_3]^+$•gluconate (red) and fit (black) (left panel) and its Fourier Transform (right panel)

Only the carbonyl groups and the oxygen atoms coordinated to Tc contribute significantly to the fit. Although including the C atoms at 3.12 Å improves the fit, the improvement is only between one and two standard deviations and cannot be considered significant. Likewise, including the *trans* multiple scattering path between the carbonyl carbon atoms and the oxygen atoms directly coordinated to the Tc improves the fit, but the improvement is not significant. The CO distance of the carbonyl is 1.15(1) Å. The only difference between the EXAFS parameters determined here and those previously determined at pH 14 (Lukens et al. 2004) is the Tc-C distance that corresponds to the gluconate backbone.

These individual spectra of the model compounds are highly useful in the resolution of the chemical components present in the tank waste. As a representative example, XAS of various Parr reaction products were generated, and the obtained spectra were fit on a combination of the spectra of the pure compounds.

## 4.2 Oxidative stability of generated *ex situ* $[Tc(CO)_3]^+$ species

### 4.2.1 Aqua $[Tc(CO)_3]^+$ species

In our previous studies, evaluation of the oxidative stabilities of $[Tc(CO)_3(H_2O)_{3-n}(OH)_n]^{1-n}$ species in $NaNO_3$/NaOH solutions were initiated in FY 2014 as described previously (Levitskaia et al. 2014) and continued in FY 2015 (Chatterjee et al. 2015). In these tests, $(Et_4N)_2[Tc(CO)_3Cl_3]$ was used to generate $[Tc(CO)_3(H_2O)_{3-n}(OH)_n]^{1-n}$ species. The stability of aqueous Tc(I) coordination compounds over time with respect to their re-oxidation back to the stable $TcO_4^-$ species was monitored by $^{99}Tc$ NMR

spectroscopy. This monitoring was continued in FY 2016 and is currently in progress for the stable Tc(I)-tricarbonyl solutions. The long-term monitoring results are shown in Table 7.

Previously reported $^{99}$Tc NMR measurements indicated that the $[Tc(CO)_3(H_2O)_{3-n}(OH)_n]^{1-n}$ species in near-neutral solutions containing 2, 5, or 5.7 M $NaNO_3$, had shown minimal re-oxidation back to $TcO_4^-$ within the time period of monitoring as evident from the absence of the corresponding Tc resonance around 0 ppm (Table 2). In the 2 M $NaNO_3$ solution, slow conversion of $[Tc(CO)_3(H_2O)_3]^+$ to the tetrameric $[Tc(CO)_3(OH)]_4$ species is observed over time. The dynamic equilibrium corresponds to about 60% of $[Tc(CO)_3(H_2O)_3]^+$ and 40% of $[Tc(CO)_3(OH)]_4$. Only small amounts of decomposition of these compounds back to $TcO_4^-$ was observed with $TcO_4^-$ appearing on the 931$^{st}$ day of monitoring and amounting to <0.01% of total Tc concentration in the sample.

Dissolution of $[Tc(CO)_3Cl_3]^{2-}$ in 5 or 5.7 M $NaNO_3$ solution resulted in a mixture of both the $[Tc(CO)_3(H_2O)_3]^+$ and $[Tc(CO)_3(OH)]_4$ species, with $[Tc(CO)_3(H_2O)_3]^+$ converting completely to $[Tc(CO)_3(OH)]_4$ in 75 – 80 days. This is consistent with the observation that at near-neutral pH, the $[Tc(CO)_3(H_2O)_3]^+$ complex undergoes partial hydrolysis and oligomerization to generate a tetrameric hydrolysis product $[Tc(CO)_3(OH)]_4$ (see Alberto et al. 1998; Gorshkov et al. 2000). The formation of the $[Tc(CO)_3(OH)]_4$ tetramer primarily depends on the solution pH and Tc(I) concentration. In 5 and 5.7 M $NaNO_3$ solutions, the concentration of Tc(I) was about 7 times greater than in 2 M $NaNO_3$ solution, which undoubtedly led to the enhanced formation of the $[Tc(CO)_3(OH)]_4$ species. In 5 and 5.7 M $NaNO_3$ solutions, less than 0.5% of $TcO_4^-$ was observed after 154 and 132 days of monitoring respectively. However, there was no further increase in $TcO_4^-$ even after 919 and 918 days of monitoring, respectively.

**Table 7.** Time stability of $[Tc(CO)_3]^+$ species in $NaNO_3$ solutions monitored by $^{99}$Tc NMR spectroscopy. Relative quantities of the Tc(I) species $[Tc(CO)_3(H_2O)_3]^+$ and $[Tc(CO)_3(OH)]_4$ were determined by the integration of the respective resonances at about -868 and -585 ppm.

| **Time elapsed** | **Fraction of total Tc in each species** | | | |
|---|---|---|---|---|
| | **$[Tc(CO)_3(H_2O)_3]^+$** | **$[Tc(CO)_3(OH)]_4$** | **Total $[Tc(CO)_3]^+$** | **$TcO_4^-$** |
| **2 M $NaNO_3$ / 0.028 mM Tc** | | | | |
| Start Day | 1 | 0 | 1 | 0 |
| 3 days | 0.95 | 0.05 | 1 | 0 |
| 18 days | 0.73 | 0.27 | 1 | 0 |
| 45 days | 0.62 | 0.38 | 1 | 0 |
| 125 days | 0.63 | 0.37 | 1 | 0 |
| 296 days | 0.68 | 0.32 | 1 | 0 |
| 576 days | 0.70 | 0.30 | >0.995 | <0.005 |
| 931 days | 0.64 | 0.36 | >0.990 | <0.010 |
| **5 M $NaNO_3$ / 0.19 mM Tc** | | | | |
| Start Day | 0.51 | 0.49 | 1 | 0 |
| 3 days | 0.28 | 0.72 | 1 | 0 |

| Time elapsed | Fraction of total Tc in each species | | | |
|---|---|---|---|---|
| | **$[Tc(CO)_3(H_2O)_3]^+$** | **$[Tc(CO)_3(OH)]_4$** | **Total $[Tc(CO)_3]^+$** | **$TcO_4^-$** |
| 18 days | 0.07 | 0.93 | 1 | 0 |
| 38 days | 0.05 | 0.95 | 1 | 0 |
| 81 days | 0.05 | 0.95 | 1 | 0 |
| 154 days | 0.04 | >0.95 | >0.99 | <0.01 |
| 193 days | 0.04 | >0.95 | >0.99 | <0.01 |
| 564 days | 0.04 | 0.96 | >0.99 | <0.01 |
| 919 days | 0.02 | 0.96 | >0.99 | <0.01 |
| **5.7 M $NaNO_3$ / 0.21 mM Tc** | | | | |
| Start Day | 0.58 | 0.42 | 1 | 0 |
| 2 days | 0.08 | 0.92 | 1 | 0 |
| 9 days | 0 | 1 | 1 | 0 |
| 132 days | 0 | >0.99 | >0.99 | <0.01 |
| 194 days | 0 | >0.99 | >0.99 | <0.01 |
| 563 days | 0 | >0.99 | >0.99 | <0.01 |
| 918 days | 0 | >0.99 | >0.99 | <0.01 |

Among alkaline solutions (0.01 – 2 M NaOH) with high nitrate concentrations (5 M $NaNO_3$) prepared in FY 2014, Tc(I) had fully oxidized to Tc(VII) by the end of FY 2014 in all solutions but the 5 M $NaNO_3$/0.01 M NaOH (Levitskaia et al. 2014). Monitoring of this sample was continued in FY 2015, where the sample was initially in the mono-deprotonated $[Tc(CO)_3(H_2O)_2(OH)]$ monomeric species due to the high pH (~13) of the solution. Over the course of FY 2015, the sample exhibited a combination of two gradual processes, an oligomerization of the monomer, $[Tc(CO)_3(H_2O)_2(OH)]$, to the tetramer, $[Tc(CO)_3(OH)]_4$, and an oxidative decomposition of $[Tc(CO)_3]^+$ species to $TcO_4^-$. This was consistent with the previous reports (Alberto et al. 1998 and references therein) showing that formation of tetrameric species depends of the Tc concentration and solution pH (Rapko et al. 2013b). Monitoring of this sample continued in FY 2016, and the sample still shows a considerable fraction of $[Tc(CO)_3]^+$ present as $[Tc(CO)_3(OH)]_4$ even after 2.5 years as shown in Table 8, suggesting the high stability of this oligomeric species towards re-oxidative decomposition.

**Table 8.** Time stability of $[Tc(CO)_3]^+$ species in 5 M $NaNO_3$ / 0.01 M NaOH / 0.19 mM Tc monitored by $^{99}Tc$ NMR spectroscopy. Relative quantities of $[Tc(CO)_3(H_2O)_2(OH)]$, $[Tc(CO)_3(OH)]_4$ and $TcO_4^-$ were determined by the integration of the respective resonances at -1070, -585, and near 0 ppm.

| Time elapsed | Fraction of total Tc in each species | | | |
|---|---|---|---|---|
| | **$[Tc(CO)_3(H_2O)_3(OH)]$** | **$[Tc(CO)_3(OH)]_4$** | **Total $[Tc(CO)_3]^+$** | **$TcO_4^-$** |
| Start Day | 1 | 0 | 1 | 0 |
| 10 days | 1 | 0 | 1 | 0 |
| 16 days | 0.95 | 0 | 0.95 | 0.05 |
| 78 days | 0.90 | 0 | 0.90 | 0.1 |
| 117 days | 0.79 | 0.06 | 0.85 | 0.15 |
| 196 days | 0.60 | 0.15 | 0.61 | 0.39 |
| 563 days | 0.03 | 0.42 | 0.45 | 0.55 |
| 918 days | 0.01 | 0.35 | 0.36 | 0.64 |

Studies initiated in FY 2016 involved monitoring the oxidative stabilities of $[Tc(CO)_3]^+$ species in NaOH (0.01 – 2 M NaOH) and high nitrate concentrations (5 M $NaNO_3$) in the presence of the chromate oxidant commonly found in tank waste supernatants (30 mM $CrO_4^{2-}$) (Table 9). It was observed that in presence of $CrO_4^{2-}$, the kinetics of oxidative decomposition of $[Tc(CO)_3]^+$ to $TcO_4^-$ were significantly enhanced compared to in absence of $CrO_4^{2-}$. In 0.01 M, 0.1 M and 0.5 M NaOH, the decomposition rates are enhanced 48, 9 and 1.8 times, respectively, in presence of a constant $CrO_4^{2-}$ concentration of 30 mM. It is interesting to note that at low $OH^-$ concentrations, significant enhancement of the decomposition rate is observed. Also, while the mechanism of oxidation is still under investigation, it is found that the increase in $TcO_4^-$ concentration over time can be reasonably fit to a linear equation (Figure 16). A similar linear increase of $TcO_4^-$ concentration with time was also observed for the studies in the absence of $CrO_4^2$. Further, the magnitudes of the calculated linear regression slopes quantifying the rate of $[Tc(CO)_3]^+$ oxidation with time (fraction per day) exhibit a nearly linear dependence on $OH^-$ concentration in solution consistent with an oxidation rate that is first-order in hydroxide (Figure 17). This result is also similar to that observed in the absence of $CrO_4^{2-}$ though the slope is significantly lower in tests not containing $CrO_4^{2-}$, suggesting that in the presence of $CrO_4^{2-}$, $OH^-$ concentration has less influence on the rate of $[Tc(CO)_3]^+$ oxidation. It is also worth mentioning that for solutions containing only 0.01 M $OH^-$, no formation of tetrameric species is observed in presence of $CrO_4^{2-}$. This result is not too surprising as the decomposition of the $[Tc(CO)_3(H_2O)_2(OH)]$ species to $TcO_4^-$ is completed within 15 days, which is significantly faster than the time it took for the tetramer to form under the given Tc concentrations.

**Table 9.** Time stability of $[Tc(CO)_3]^+$ species in $NaNO_3$/NaOH solutions in presence of 30 mM $CrO_4^{2-}$ monitored by $^{99}Tc$ NMR spectroscopy. Relative quantities of the Tc(I) species $[Tc(CO)_3(H_2O)_3]^+$ and $[Tc(CO)_3(OH)]_4$ were determined by the integration of the respective resonances at about -868 and -585 ppm.

| Time elapsed | Fraction of total Tc in each species | | | |
|---|---|---|---|---|
| | $[Tc(CO)_3(H_2O)_2(OH)]$ | $[Tc(CO)_3(OH)]_4$ | Total $[Tc(CO)_3]^+$ | $TcO_4^-$ |
| **5 M $NaNO_3$ / 0.01 M NaOH / 30 mM $CrO_4^{2-}$ / 0.18 mM Tc** | | | | |
| Start Day | 0.95 | 0 | 0.95 | 0.05 |
| 1 day | 0.89 | 0 | 0.89 | 0.11 |
| 2 days | 0.77 | 0 | 0.77 | 0.23 |
| 3 days | 0.69 | 0 | 0.69 | 0.31 |
| 5 days | 0.56 | 0 | 0.56 | 0.44 |
| 7 days | 0.39 | 0 | 0.39 | 0.61 |
| 10 days | 0.21 | 0 | 0.21 | 0.79 |
| 12 days | 0.04 | 0 | 0.04 | 0.96 |
| 15 days | 0 | 0 | 0 | 1 |
| **5 M $NaNO_3$ / 0.1 M NaOH / 30 mM $CrO_4^{2-}$ / 0.18 mM Tc** | | | | |
| Start Day | 0.9 | 0 | 0.9 | 0.1 |
| 1 day | 0.81 | 0 | 0.81 | 0.19 |
| 2 days | 0.69 | 0 | 0.69 | 0.31 |
| 3 days | 0.56 | 0 | 0.56 | 0.44 |
| 4 days | 0.43 | 0 | 0.43 | 0.57 |
| 5 days | 0.29 | 0 | 0.29 | 0.71 |
| 6 days | 0.15 | 0 | 0.15 | 0.85 |
| 7 days | 0.07 | 0 | 0.07 | 0.93 |
| 8 days | 0 | 0 | 0 | 1 |
| **5 M $NaNO_3$ / 0.5 M NaOH / 30 mM $CrO_4^{2-}$ / 0.18 mM Tc** | | | | |
| Start Day | 0.89 | 0 | 0.89 | 0.11 |
| 1 day | 0.76 | 0 | 0.76 | 0.24 |
| 2 days | 0.61 | 0 | 0.61 | 0.39 |
| 3 days | 0.42 | 0 | 0.42 | 0.58 |
| 4 days | 0.21 | 0 | 0.21 | 0.79 |
| 5 days | 0 | 0 | 0 | 1 |
| **5 M $NaNO_3$ / 1 M NaOH / 30 mM $CrO_4^{2-}$ / 0.18 mM Tc** | | | | |
| Start Day | 1 | 0 | 1 | 0 |
| 1 day | 0.75 | 0 | 0.75 | 0.25 |
| 2 days | 0.5 | 0 | 0.5 | 0.5 |
| 10 days | 0 | 0 | 0 | 1 |

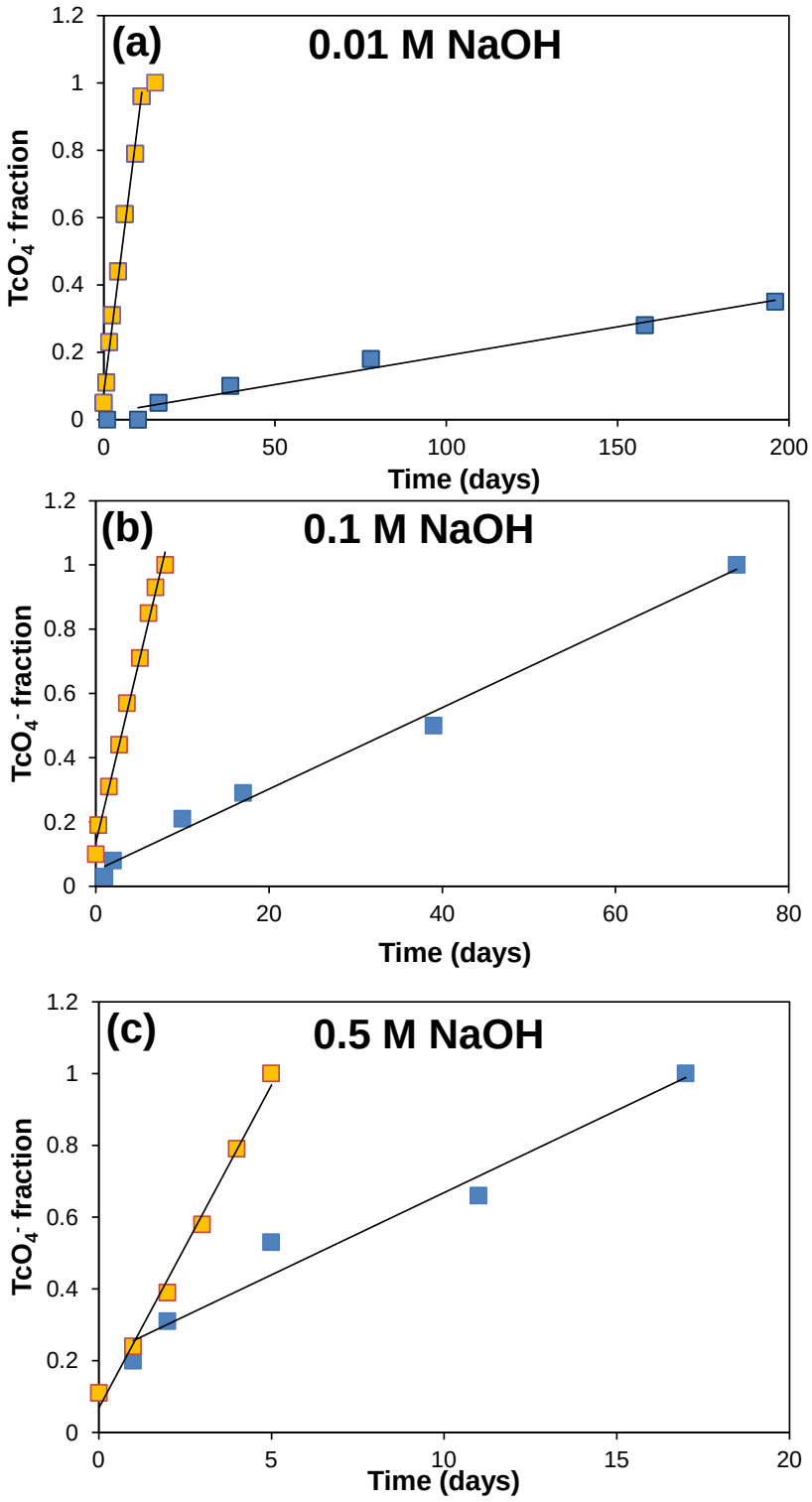


**Figure 16.** Time generation of $TcO_4^-$ due to the oxidative decomposition of $[Tc(CO)_3]^+$ species (data are given in Table 9) in 5 M $NaNO_3$ / variable hydroxide (blue squares) and 5 M $NaNO_3$ / variable hydroxide / 30 mM $CrO_4^{2-}$ (yellow squares): (a) 0.01 M NaOH, (b) 0.1 M NaOH, (c) 0.5 M NaOH.

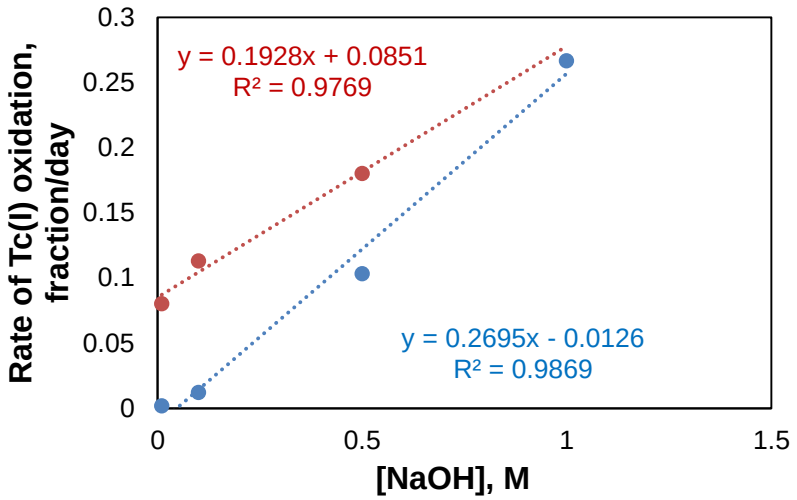


**Figure 17.** Dependence of kinetics of Tc(I) oxidation to $TcO_4^-$ on $OH^-$ concentration in 5 M $NaNO_3$. Blue symbols and line: in the absence of $CrO_4^{2-}$, red symbols and line: in presence of 30 mM $CrO_4^{2-}$.

Subsequent studies involved monitoring the oxidative stabilities of $[Tc(CO)_3]^+$ species in the tank supernatant simulant matrix spiked with 30 mM $CrO_4^{2-}$. For this work, a fresh pseudo-Hanford Tank supernatant simulant prepared in FY 2016 was used (composition in table 1). As in the previous cases, it was observed that in presence of $CrO_4^{2-}$, the kinetics of oxidative decomposition of $[Tc(CO)_3]^+$ to $TcO_4^-$ is enhanced by approximately an order of magnitude compared to the re-oxidation rate in absence of $CrO_4^{2-}$. The results are listed in Table 10 and the comparative kinetic dependence is shown in Figure 17.

**Table 10.** Time stability of $[Tc(CO)_3]^+$ species in the Hanford supernatant simulant prepared in FY 2016 containing 30 mM $CrO_4^{2-}$ monitored by $^{99}Tc$ NMR spectroscopy. Relative quantities of $[Tc(CO)_3(H_2O)_2(OH)]$ and $TcO_4^-$ were determined by the integration of the respective resonances at about -1070 and 0 ppm.

| **Time elapsed** | **Fraction of total Tc in each species** | |
|---|---|---|
| | **$[Tc(CO)_3(H_2O)_2(OH)]$** | **$TcO_4^-$** |
| **FY 2016 simulant / 30 mM $CrO_4^{2-}$ / 2.1 mM Tc** | | |
| Start Day | 0.86 | 0.14 |
| 1 day | 0.69 | 0.31 |
| 2 days | 0.35 | 0.65 |
| 3 days | 0.17 | 0.83 |
| 4 days | 0.03 | 0.97 |
| 5 days | 0 | 1 |

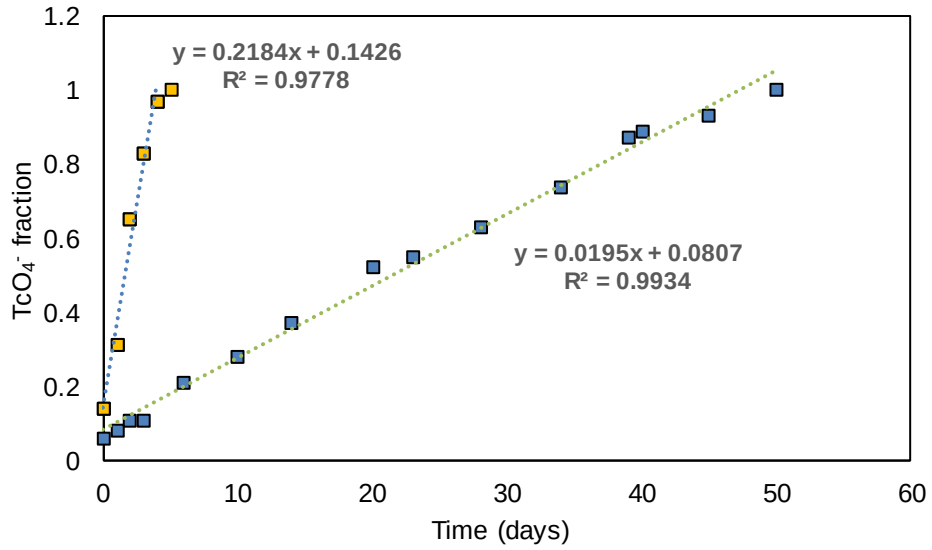


**Figure 18.** Time generation of $TcO_4^-$ due to the oxidative decomposition of $[Tc(CO)_3]^+$ species (data are given in Table 10) in Hanford supernatant simulant containing noble metals prepared in FY 2016 without (blue squares) and with 30 mM $CrO_4^{2-}$ (yellow squares).

### 4.2.2 $[Tc(CO)_3]^+$•Ligand Complexes

In FY 2015, Tc(I) complexes containing the $[Tc(CO)_3]^+$ moiety coordinated with IDA, gluconate, NTA, EDTA, or DTPA were prepared by dissolution of solid $[Tc(CO)_3(H_2O)_3]^+$ in either 5 M $NaNO_3$ / 0.1 M NaOH or the tank supernatant simulant and monitored by $^{99}$Tc NMR spectroscopy (Chatterjee et al. 2015). In all cases it was observed that $[Tc(CO)_3(H_2O)_2(OH)]$ initially formed upon dissolution of the $[Tc(CO)_3(H_2O)_3]^+$ material in the alkaline solutions, which slowly converted to the $[Tc(CO)_3]^+$•Ligand complex. For the NTA, EDTA and DTPA ligands, the oxidation of the $[Tc(CO)_3]^+$ species was completed with 25 – 40 days in 5 M $NaNO_3$, 0.1 M NaOH, and within 20 days in the tank supernatant simulant solution (simulant prepared in FY 2014 – 2015). The $[Tc(CO)_3]^+$•IDA complex was observed to exhibit a significant stability, only undergoing 25% decomposition within the first 132 days of monitoring in 5 M $NaNO_3$, 0.1 M NaOH while exhibiting slightly less stability in the tank supernatant simulant, which exhibited 30% decomposition after 120 days. The monitoring was continued in FY 2016 (Table 11, Figure 19), and the $[Tc(CO)_3]^+$•IDA complex continued to demonstrate remarkable stability towards decomposition, undergoing only ~49% decomposition in 5 M $NaNO_3$, 0.1 M NaOH after 510 days of monitoring. While the decomposition kinetics was comparatively faster in the tank supernatant simulant, 28% of the $[Tc(CO)_3]^+$•IDA complex remained in the tank supernatant after 498 days of monitoring.

**Table 11.** Formation kinetics and time stability of the $[Tc(CO)_3]^+$•IDA complex in 5 M $NaNO_3$ / 0.1 M NaOH and Hanford supernatant simulant prepared in FY 2014 – 2015 monitored by $^{99}Tc$ NMR spectroscopy. Relative quantities of $[Tc(CO)_3(H_2O)_2(OH)]$, $[Tc(CO)_3]^+$•IDA, and $TcO_4^-$ were determined by the integration of the respective resonances at -1065, -1000 and near 0 ppm.

| Time elapsed | Fraction of total Tc in each species | | |
|---|---|---|---|
| (days) | $[Tc(CO)_3(H_2O)_2(OH)]$ | $[Tc(CO)_3]^+$•IDA | $TcO_4^-$ |
| **5 M $NaNO_3$ / 0.1 M NaOH / 0.1 M IDA / 3.2 mM Tc** | | | |
| 0.01 day | 0.39 | 0.58 | 0.026 |
| 5 days | 0.021 | 0.94 | 0.037 |
| 10 days | 0.013 | 0.93 | 0.057 |
| 20 days | 0.004 | 0.92 | 0.081 |
| 40 days | 0 | 0.88 | 0.12 |
| 66 days | 0 | 0.85 | 0.15 |
| 81 days | 0 | 0.82 | 0.18 |
| 96 days | 0 | 0.80 | 0.20 |
| 114 days | 0 | 0.78 | 0.22 |
| 132 days | 0 | 0.75 | 0.25 |
| 144 days | 0 | 0.73 | 0.27 |
| 168 days | 0 | 0.71 | 0.29 |
| 192 days | 0 | 0.68 | 0.32 |
| 240 days | 0 | 0.66 | 0.343 |
| 288 days | 0 | 0.63 | 0.37 |
| 336 days | 0 | 0.61 | 0.391 |
| 384 days | 0 | 0.59 | 0.41 |
| 432 days | 0 | 0.56 | 0.44 |
| 480 days | 0 | 0.54 | 0.46 |
| 510 days | 0 | 0.52 | 0.48 |
| **FY 2014 simulant / 0.1 M IDA / 2.6 mM Tc** | | | |
| 0.05 days | 0.58 | 0.38 | 0.032 |
| 2 days | 0.038 | 0.92 | 0.039 |
| 6 days | 0.010 | 0.94 | 0.048 |
| 10 days | 0.005 | 0.94 | 0.056 |
| 14 days | 0.004 | 0.93 | 0.065 |
| 20 days | 0.002 | 0.92 | 0.076 |
| 26 days | 0 | 0.91 | 0.088 |
| 32 days | 0 | 0.90 | 0.10 |
| 40 days | 0 | 0.88 | 0.12 |
| 52 days | 0 | 0.86 | 0.14 |
| 66 days | 0 | 0.83 | 0.17 |

| Time elapsed | Fraction of total Tc in each species | | |
|---|---|---|---|
| (days) | $[Tc(CO)_3(H_2O)_2(OH)]$ | $[Tc(CO)_3]^+$•IDA | $TcO_4^-$ |
| 81 days | 0 | 0.80 | 0.20 |
| 96 days | 0 | 0.77 | 0.23 |
| 108 days | 0 | 0.73 | 0.27 |
| 120 days | 0 | 0.70 | 0.30 |
| 132 days | 0 | 0.68 | 0.32 |
| 156 days | 0 | 0.64 | 0.36 |
| 180 days | 0 | 0.61 | 0.39 |
| 228 days | 0 | 0.53 | 0.47 |
| 276 days | 0 | 0.48 | 0.52 |
| 324 days | 0 | 0.43 | 0.57 |
| 372 days | 0 | 0.39 | 0.61 |
| 420 days | 0 | 0.35 | 0.65 |
| 468 days | 0 | 0.30 | 0.70 |
| 498 days | 0 | 0.28 | 0.72 |

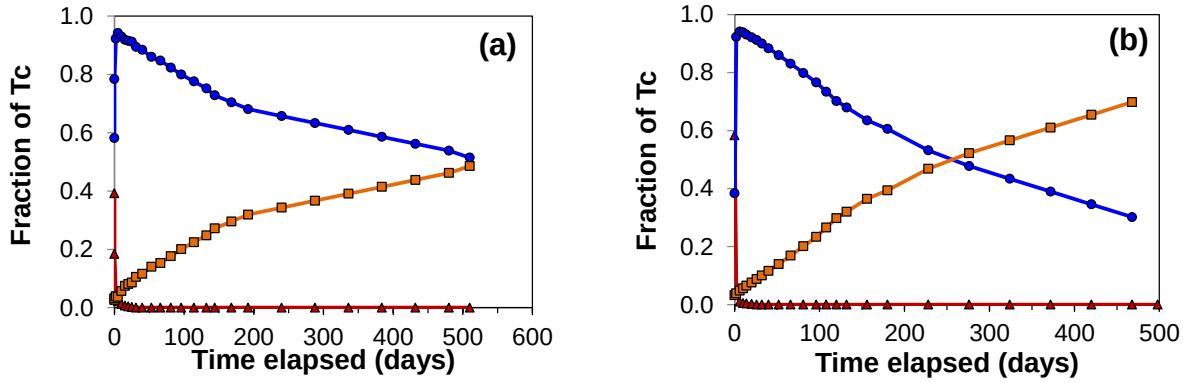


**Figure 19.** Tc speciation over time of the $[Tc(CO)_3(H_2O)_2(OH)]$ solution in 0.1 M IDA in (A) 5 M $NaNO_3$ / 0.1 M NaOH and (B) Tank supernatant simulant prepared in FY 2014. Blue circles: $[Tc(CO)_3]^+$•IDA. Red triangles: $[Tc(CO)_3(H_2O)_2(OH)]$. Orange squares: $TcO_4^-$.

Studies initiated in FY 2016 involved monitoring the oxidative stabilities of the $[Tc(CO)_3]^+$•IDA complex in 5 M $NaNO_3$ solution at variable 0.01 – 2 M NaOH in presence of 30 mM $CrO_4^{2-}$. As in the case of the aqua complexes, the presence of $CrO_4^{2-}$ was observed to accelerate the rate of oxidative decomposition of $[Tc(CO)_3]^+$•IDA to $TcO_4^-$ by at least an order of magnitude, with the complex undergoing complete oxidation to $TcO_4^-$ within 52 days in 5 M $NaNO_3$ / 0.1 M NaOH, and in half that time in the tank supernatant simulant solutions as shown in Table 12.

**Table 12.** Formation kinetics and time stability of the $[Tc(CO)_3]^+$•IDA complex in presence of 30 mM $CrO_4^{2-}$ in 5 M $NaNO_3$ / 0.1 M NaOH and in the supernatant simulant solutions prepared in FY 2016 monitored by $^{99}$Tc NMR spectroscopy. Relative quantities of $[Tc(CO)_3(H_2O)_2(OH)]$, $[Tc(CO)_3]^+$•IDA, and $TcO_4^-$ were determined by the integration of the respective resonances at about -1065, -1000 and 0 ppm.

| **Time elapsed** | **Fraction of total Tc in each species** | | |
|---|---|---|---|
| **(days)** | **$[Tc(CO)_3(H_2O)_2(OH)]$** | **$[Tc(CO)_3]^+$•IDA** | **$TcO_4^-$** |
| **5 M $NaNO_3$ / 0.1 M NaOH / 0.1 M IDA / 30 mM $CrO_4^{2-}$ / 2.2 mM Tc** | | | |
| 0.01 day | 0.58 | 0.41 | 0.011 |
| 0.125 day | 0.06 | 0.92 | 0.017 |
| 0.25 day | 0 | 0.98 | 0.022 |
| 1 day | 0 | 0.94 | 0.056 |
| 2 days | 0 | 0.93 | 0.073 |
| 3 days | 0 | 0.910 | 0.090 |
| 5 days | 0 | 0.85 | 0.15 |
| 7 days | 0 | 0.79 | 0.21 |
| 10 days | 0 | 0.70 | 0.30 |
| 14 days | 0 | 0.61 | 0.39 |
| 20 days | 0 | 0.51 | 0.49 |
| 25 days | 0 | 0.42 | 0.58 |
| 30 days | 0 | 0.33 | 0.67 |
| 37 days | 0 | 0.24 | 0.76 |
| 42 days | 0 | 0.15 | 0.85 |
| 47 days | 0 | 0.059 | 0.94 |
| 52 days | 0 | 0 | 1 |
| **FY 2016 simulant / 0.1 M IDA / 30 mM $CrO_4^{2-}$ / 3.1 mM Tc** | | | |
| 0.01 day | 0.60 | 0.384 | 0.015 |
| 0.125 day | 0.11 | 0.87 | 0.023 |
| 0.25 day | 0.025 | 0.95 | 0.025 |
| 1 day | 0.011 | 0.92 | 0.068 |
| 2 days | 0.001 | 0.91 | 0.089 |
| 3 days | 0 | 0.89 | 0.11 |
| 5 days | 0 | 0.82 | 0.18 |
| 7 days | 0 | 0.72 | 0.28 |
| 10 days | 0 | 0.61 | 0.39 |
| 13 days | 0 | 0.50 | 0.50 |
| 17 days | 0 | 0.39 | 0.61 |
| 20 days | 0 | 0.27 | 0.73 |
| 22 days | 0 | 0.16 | 0.84 |
| 25 days | 0 | 0.052 | 0.95 |
| 26 days | 0 | 0 | 1 |

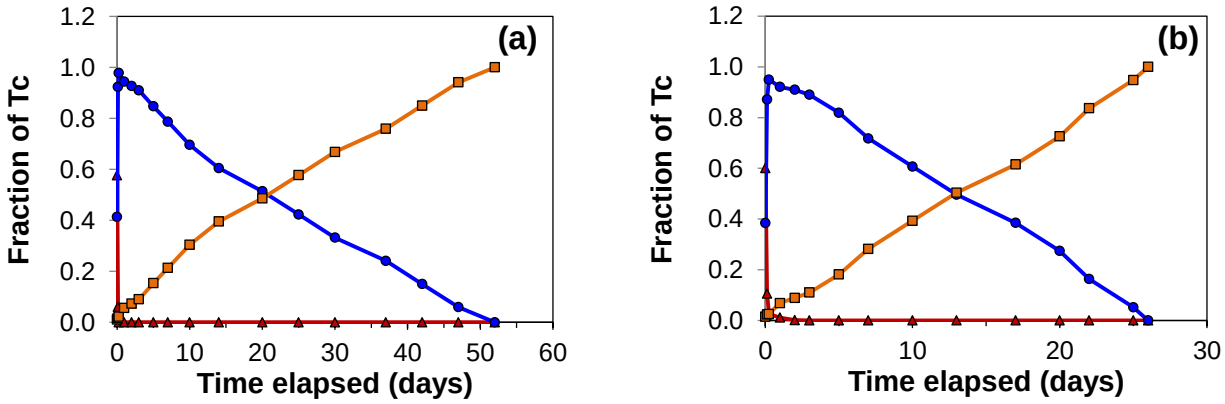


**Figure 20.** Tc speciation over time during reaction of $[Tc(CO)_3(H_2O)_2(OH)]$ with 0.1 M IDA in presence of 30 mM $CrO_4^{2-}$ in (a) 5 M $NaNO_3$ / 0.1 M NaOH and (b) simulant prepared in FY 2016. Blue circles: $[Tc(CO)_3]^+$•IDA, red triangles: $[Tc(CO)_3(H_2O)_2(OH)]$, orange squares: $TcO_4^-$.

The decomposition kinetics of the $[Tc(CO)_3]^+$•IDA species with time in various media is shown in Figure 21. In either 5 M $NaNO_3$ / 0.1 M NaOH or the tank supernatant simulant in the absence of $CrO_4^{2-}$, the decomposition rate is nearly linear with time up to ~200 days, before it levels off. On the other hand, in presence of $CrO_4^{2-}$, the decomposition rate follows linear kinetics throughout the entire duration.

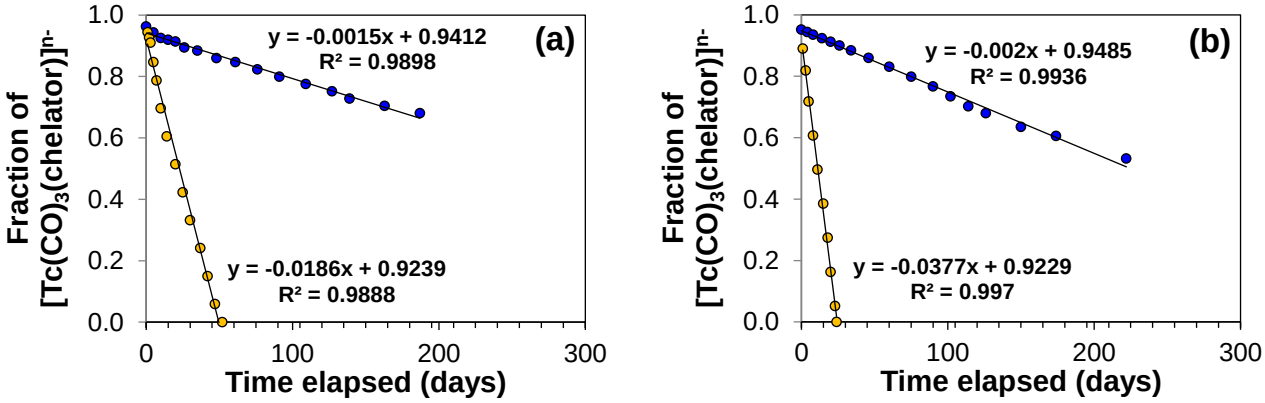


**Figure 21.** Kinetics of decomposition of the $[Tc(CO)_3]^+$•IDA complexes in (a) 5 M $NaNO_3$ / 0.1 M NaOH and (b) Tank supernatant simulant. Blue symbols: in the absence of $CrO_4^{2-}$, yellow symbols: in presence of 30 mM $CrO_4^{2-}$.

The observed oxidative stability of the $[Tc(CO)_3]^+$ compounds is summarized in Table 13.

**Table 13.** Summary of oxidative stability of the $[Tc(CO)_3]^+$ compounds.

| Solution matrix | Tc concentration mM | Tc(I) species | Half-life of Tc(I) species |
|---|---|---|---|
| 2 M $NaNO_3$ | 0.028 | $[Tc(CO)_3(H_2O)_3]^+$ $[Tc(CO)_3(OH)]_4$ | > 2.55 years |
| 5 M $NaNO_3$ | 0.19 | $[Tc(CO)_3(H_2O)_3]^+$ $[Tc(CO)_3(OH)]_4$ | > 2.52 years |
| 5.7 M $NaNO_3$ | 0.21 | $[Tc(CO)_3(H_2O)_3]^+$ $[Tc(CO)_3(OH)]_4$ | >2.52 years |
| 5 M $NaNO_3$ / 0.01 M NaOH | 0.19 | $[Tc(CO)_3(H_2O)_3(OH)]$ $[Tc(CO)_3(OH)]_4$ | ~1.5 years |
| 5 M $NaNO_3$ / 0.01 M NaOH / 30 mM $CrO_4^{2-}$ | 0.18 | $[Tc(CO)_3(H_2O)_3(OH)]$ | 6 days |
| 5 M $NaNO_3$ / 0.1 M NaOH | 0.19 | $[Tc(CO)_3(H_2O)_3(OH)]$ | 39 days |
| 5 M $NaNO_3$ / 0.1 M NaOH / 30 mM $CrO_4^{2-}$ | 0.18 | $[Tc(CO)_3(H_2O)_3(OH)]$ | 3.5 days |
| 5 M $NaNO_3$/0.5 M NaOH | 0.19 | $[Tc(CO)_3(H_2O)_3(OH)]$ | ~5 days |
| 5 M $NaNO_3$ / 0.5 M NaOH / 30 mM $CrO_4^{2-}$ | 0.18 | $[Tc(CO)_3(H_2O)_3(OH)]$ | 2.5 days |
| 5 M $NaNO_3$/1 M NaOH | 0.19 | $[Tc(CO)_3(H_2O)_3(OH)]$ | 2 days |
| 5 M $NaNO_3$ / 1 M NaOH / 30 mM $CrO_4^{2-}$ | 0.18 | $[Tc(CO)_3(H_2O)_3(OH)]$ | 2 days |
| FY 2014 simulant | 12.2 | $[Tc(CO)_3(H_2O)_3(OH)]$ | ~20 days |
| FY 2016 simulant | 2.1 | $[Tc(CO)_3(H_2O)_3(OH)]$ | ~18 days |
| FY 2016 simulant / 30 mM $CrO_4^{2-}$ | 2.1 | $[Tc(CO)_3(H_2O)_3(OH)]$ | 1.5 days |
| 5 M $NaNO_3$ / 0.1 M NaOH/0.1 M IDA | 3.2 | $[Tc(CO)_3]^+$•IDA | ~1.5 years |
| 5 M $NaNO_3$ / 0.1 M NaOH/0.1 M IDA/ 30 mM $CrO_4^{2-}$ | 2.2 | $[Tc(CO)_3]^+$•IDA | 22 days |
| FY 2014 simulant / 0.1 M IDA | 2.6 | $[Tc(CO)_3]^+$•IDA | ~0.8 years |
| FY 2016 simulant / 0.1 M IDA / 30 mM $CrO_4^{2-}$ | 3.1 | $[Tc(CO)_3]^+$•IDA | 13 days |

## 4.3 Non-pertechnetate species generated by *in situ* reduction of pertechnetate

Studies to evaluate in situ reduction of $TcO_4^-$ in the tank supernatant simulants using $CO/H_2$ as the reductant (**Parr Reactions 1 – 4**, Table 2) were initiated in FY 2014 and were continued in FY 2015. The observed results are described in detail previously (Levitskaia et al. 2014; Chatterjee et al. 2015), and only brief overview of the FY 2014/15 findings is given in this report. In FY 2016 these studies have continued, and additional reducting conditions were tested including variable pressure of the gaseous

$CO/H_2$ reducing agent, temperature, presence of polyaminocarboxylate chelator IDA and of the oxidant $CrO_4^{2-}$. These tests are referred to as **Parr Reactions 5 – 9** (Table 2). It is to be noted that the **Parr Reactions 1 – 4** were performed in simulant solutions prepared in FY 2014, having the compositions given in Table 1. On the other hand, **Parr Reactions 5 – 9** were performed in simulant solutions prepared in FY 2016 whose compositions are also given in Table 1.

The main objectives of these studies are three-fold:

1. Elucidation of possible mechanisms for *in situ* $TcO_4^-$ reduction and formation of low-valent Tc species that could exist in the current Hanford tank waste environments;

2. Evaluation of the stability of the non-pertechnetate species generated *in situ* to re-oxidation back to pertechnetate;

3. Proof-of-concept demonstration that the developed spectroscopic library ($^{99}$Tc NMR, EPR, XAS, and XPS) is sufficient for identification of the oxidation state and chemical nature of the non-pertechnetate species in the complex mixtures relevant to the Hanford tank wastes.

### 4.3.1 Characterization of the in situ generated non-pertechnetate species

The Tc reaction products generated by the *in situ* reduction of $TcO_4^-$ were characterized by various spectroscopic techniques (Table 13). The observed low-valent Tc species include Tc(I) as $[Tc(CO)_3]^+$, Tc(IV), and Tc(VI). These three Tc species were found to co-exist with residual $TcO_4^-$ in the product of the **Parr Reaction 1**, while other reaction products simultaneously contained Tc species in two or three oxidation states. Table 14 highlights general qualitative agreement among tested spectroscopic techniques with regard of the oxidation states of the co-existing Tc species. It is also evident that the combination of these techniques provides sufficient information to elucidate Tc in variable oxidation states in complex mixtures. It was observed that among non-pertechnetate species tested, Tc(I) tricarbonyl species are easily observable and quantifiable by $^{99}$Tc NMR, XAS, and XPS spectroscopic techniques, which provide complementary information. Tc(IV) species can be easily measured by XAS and XPS, while EPR does not provide definitive information regarding this oxidation state. On the other hand, Tc(VI) can be easily detected by EPR. Analysis of Tc(VI) by XAS requires generation of stable reference Tc(VI) compounds to expand XAS spectral library. Measurements of Tc(VI) by XPS can potentially be complicated by its decomposition or disproportionation in the X-ray beam, and additional experiments are needed to evaluate these phenomena.

**Table 14.** The various Tc-species observed after the completion of the various **Parr Reactions** and the techniques used to identify them.

| Parr reaction # | P(psi)/ T(ºC) | Product | Technique | $TcO_4^-$ | Tc(VI) | Tc(IV) | $Tc(CO)_3^+$ |
|---|---|---|---|---|---|---|---|
| 1 | 1300 / 80 | Brown solid + brown solution | NMR | Observed | N/A | N/A | Observed |
| | | | XAS | Observed | Not observed[a] | Observed | Observed |
| | | | XPS | Observed | Observed | Observed | Observed |
| | | | EPR | N/A | Observed | Inconclusive | N/A |
| 2 | 1300 / 80 | Greenish -brown solid + brown solution | NMR | Observed | N/A | N/A | Observed |
| | | | XAS | Observed | Not Observed | Observed | Observed |
| | | | XPS | Observed | Not Observed | Observed | Observed |
| | | | EPR | N/A | Not Observed | Inconclusive | N/A |
| 3 | 1300 / 80 | Wine red solution | NMR | Observed | N/A | N/A | Not Observed |
| | | | XAS | Observed | Not observed | Observed | N/A |
| | | | XPS | Observed | Observed | Observed | N/A |
| | | | EPR | N/A | Observed | Inconclusive | N/A |
| 4 | 1300 / 80 | Greenish -brown solid + brown solution | NMR | Observed | N/A | N/A | Observed |
| | | | XAS | Not performed | | | |
| | | | XPS | Observed | Not Observed | Observed | N/A |
| | | | EPR | N/A | Not Observed | Inconclusive | N/A |
| 5 | 250 / 80 | Brown solid + light brown solution | NMR | Observed | N/A | N/A | Observed |
| | | | XAS | Not performed | | | |
| | | | XPS | Not observed | Not observed[b] | Not Observed[b] | Observed |
| | | | EPR | N/A | Observed | Inconclusive | N/A |
| 6 | 250 / 25 | Pinkish red solution | NMR | Observed | N/A | N/A | Not Observed |
| | | | XAS | Not measured | | | |
| | | | XPS | Not measured | | | |
| | | | EPR | N/A | Observed | Inconclusive | N/A |

| Parr reaction # | P(psi)/ T(ºC) | Product | Technique | $TcO_4^-$ | Tc(VI) | Tc(IV) | $Tc(CO)_3^+$ |
|---|---|---|---|---|---|---|---|
| 7 | Ambient / 80 | Dirty-brown solid + brown solution | NMR | Observed | N/A | N/A | Not Observed |
| | | | XAS | Not measured | | | |
| | | | XPS | N/A | Not Observed | Observed | N/A |
| | | | EPR | N/A | Not Observed | Inconclusive | N/A |
| 8 | 250 / 80 | Greenish-brown solid + green solution | NMR | Observed | N/A | N/A | Observed |
| | | | XAS | Not measured | | | |
| | | | XPS | Not observed | N/A | Not observed[c] | N/A |
| | | | EPR | N/A | Not Observed | Observed | N/A |
| 9 | 250 / 80 | Brown black solid + straw colored solution | NMR | Observed | N/A | N/A | Observed |
| | | | XAS | Not measured | | | |
| | | | XPS | Not measured | | | |
| | | | EPR | Not measured | | | |

[a] The Tc(VI) not being observed may be a consequence of it undergoing significant decomposition or disproportionation
[b]XPS was performed on the liquid fraction.
[c]XPS was performed on the liquid fraction.
N/A = not applicable for the analysis by this technique

Sections below provide comprehensive spectroscopic analysis of the Tc products generated by the representative **Parr Reactions 1** and **5**. Detailed analysis of the Tc products corresponding to other Parr reactions is included in Appendix A.

#### 4.3.1.1 Parr reaction 1

*Reaction conditions: 10 mM $TcO_4^-$ in tank supernatant simulant containing 100 mM gluconate and noble metals pressurized to 1350 psi with CO containing 75 ppm $H_2$ at 80C for 10 days*.

The product from this reaction consisted of a molasses-like brown precipitate and a brown supernatant. The precipitate and the supernatant were separately studied after filtration. The detailed description of the $^{99}$Tc NMR and EPR analyses of the **Parr Reaction 1** products conducted in FY 2014-2015 can be found in our previous reports (Levitskaia et al. 2014; Chatterjee et al. 2015), and only a brief summary is given below.

**Liquid fraction:** The liquid fraction of the **Parr Reaction 1** product had been characterized extensively using complementary $^{99}$Tc NMR and EPR spectroscopies. The NMR spectrum demonstrated the formation of the $[Tc(CO)_3]^+$•gluconate species, characterized by the presence of three resonances at -

1094, -1232 and -1254 ppm, which gradually underwent partial oxidative decomposition to $TcO_4^-$. The EPR spectrum demonstrated a set of well resolved 10-line signal at 3100 Gauss, attributed to the hyperfine splitting of a $^{99}Tc$ nucleus of nuclear spin = 9/2. This signal was attributed to a Tc(VI) species based on the narrow line-width, g-values and the hyperfine splitting similar to the electrochemically generated Tc(VI) species described earlier. This species exhibited remarkable stability and the EPR intensity of the species was preserved even after two years as described in section 4.3.2 of this report.

**Solid fraction:** The solid fraction was analyzed by EPR spectroscopy. The spectrum showed a 10-line resonance at 3100 Gauss similar to the one observed for the liquid fraction, and was attributed to a similar Tc(VI) species being either present in the solid fraction, or in the form of some interstitial liquid fraction. In addition, another 10-line resonance was observed at ~1600 Gauss, and was attributed to a half-field transition in which the electron spin density associated with the $^{99}Tc$ nucleus is strongly coupled to another metal center with a total electron spin of ½. The analyzed solid fraction was stored in contact with a small amount of the solution fraction and was never allowed to dry out.

In the FY 2016, XAS and XPS measurements on the solid fraction containing a small amount of the supernatant were performed. A sample of the solid was separated from the supernatant by centrifugation. The separated solids were not further purified by rinsing, or otherwise, and allowed to dry out before recording the spectra.

The XAS spectrum, shown in Figure 22, can be resolved as a combination of $[Tc(CO)_3]^+$, Tc(IV) and Tc(VII) species. Thus the XAS spectrum of the resultant solid can be represented as a combination of the individual spectra of pure Tc(VII), Tc(IV) and Tc(I) compounds. It is observed that using $[Tc(CO)_3(H_2O)_3]^+$ as the Tc(I) compound, $TcO_2 \cdot xH_2O(s)$ as the Tc(IV) component and $TcO_4^-$ as the Tc(VII) component results in a reasonable fit with excellent matching in the XANES region and a close match in the EXAFS region. Substituting $[Tc(CO)_3(H_2O)_3]^+$ with $[Tc(CO)_3]^+$•gluconate as the Tc(I) component significantly improves the fit in the EXAFS region, while fit in the XANES region is still reasonably good. This is suggestive that the major Tc(I) component in the reaction mixture is presumably the chelated $[Tc(CO)_3]^+$•gluconate species. On the other hand, the fit is better using Tc(IV)•gluconate instead of $TcO_2 \cdot xH_2O$ as the Tc(IV) reference, but the results are the same within the measurement error. The fitting parameters are given in Table 15.

These results are consistent with the $^{99}Tc$ NMR and EPR measurements of the liquid fraction of the **Parr Reaction 1** product, which demonstrated presence of a combination of Tc(VII), Tc(VI) and $[Tc(CO)_3]^+$•gluconate species. It should be noted that the lack of a Tc(VI) XAS standard does not allow inclusion of this species in the fit and is presumably responsible for the deviation of the fitted spectrum from the experimental. However, this deviation is only minor suggesting that only a small amount Tc(VI) is present in the **Parr Reaction 1** sample.

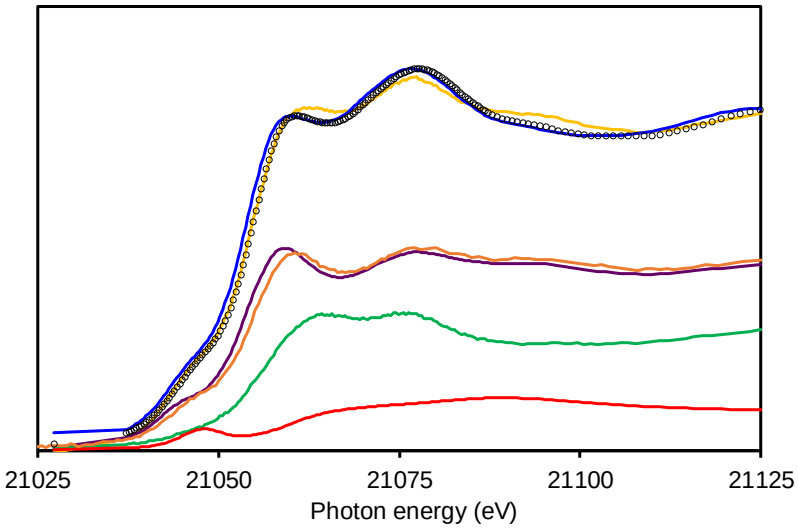


**Figure 22.** Tc K-edge XANES spectrum and corresponding fit for the solid fraction of **Parr Reaction 1** product. Circles: experimental data; blue trace: calculated fit obtained using $[Tc(CO)_3]^+$•gluconate as the Tc(I) species, $TcO_2$•$xH_2O$ as the Tc(IV) species, $TcO_4^-$ as the Tc(VII) species; yellow trace: calculated fit obtained using $[Tc(CO)_3(H_2O)_3]^+$ as the Tc(I) species, $TcO_2$•$xH_2O$ as the Tc(IV) species, $TcO_4^-$ as the Tc(VII) species; violet trace: contribution from $[Tc(CO)_3(H_2O)_3]^+$; orange trace: contribution from $[Tc(CO)_3]^+$•gluconate; green trace: contribution from $TcO_2$•$xH_2O$; red trace: contribution from $TcO_4^-$.

**Table 15.** Tc K-edge XANES results of the **Parr Reaction 1** product (fraction of each species in the best fit)[a].

| Tc(I) | σ | p | $TcO_2$•$xH_2O$ | σ | p | $TcO_4^-$ | σ | p |
|---|---|---|---|---|---|---|---|---|
| 0.57 | 0.09 | 0.0 | 0.37 | 0.07 | 0.0 | 0.14 | 0.05 | 0.001 |

a) Standard deviation of the fit is given as σ. The value of p is the probability that the improvement to the fit from including this spectrum is due to noise. Components with $p < 0.05$ are significant at the two-sigma level and those with $p < 0.01$ are significant at the 3 sigma level.

The XPS spectrum of the solid fraction was obtained using a sample that was deposited on carbon tape and allowed to dry out. The spectrum can be resolved into four different Tc chemical species with lower binding energies (assigned to Tc $3d_{3/2}$ lines) at 254.6 eV, 256.4 eV, 257.8 eV and 259.1 eV respectively, as shown in Figure 23. Based on the Tc $3d_{5/2}$ binding energies reported in literature and determined using the reference compounds as described in section 4.1.1 of this report, these are tentatively assigned to Tc(I), Tc(IV), Tc(VI) and Tc(VII) oxidation states respectively, with the contribution from the presumable Tc(VI) fraction being very small. The fact that the XAS and XPS results both point towards small to negligible quantities of Tc(VI) may not contradict the EPR measurements showing strong Tc(VI) signal. The intensity of the EPR signal depends on many factors most notably the structure, the electronic environment of the metal center, and the spin relaxation rate of the electron. Consequently, EPR intensity does not always correlate with the concentration of the EPR-active species (Pilbrow 1996). Another consideration is that the EPR measurements were obtained using

samples in constant contact with a liquid phase while XAS and XPS were recorded on dried samples, may also suggest disproportionation of Tc(VI) during sample preparation and drying.

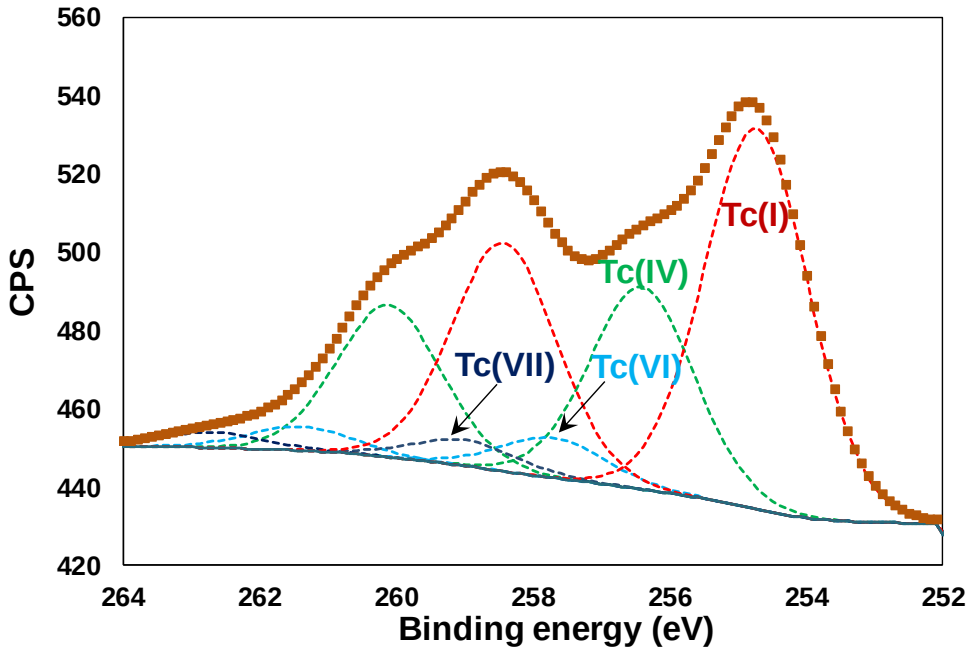


**Figure 23.** X-ray photoelectron spectrum of Tc $3d_{5/2}$ and $3d_{3/2}$ regions for the solid fraction of **Parr Reaction 1** product. Brown squares: experimental spectrum, red trace: Tc(I) fit, green trace: Tc(IV) fit, light blue trace: Tc(VI) fit, dark blue trace: Tc(VII) fit.

Both XAS and XPS measurements are in a good agreement with regard of relative abundance of Tc in different oxidation states (Table 14 and Figure 23). Surprisingly, both techniques indicate that a significant fraction of the total Tc present in the solid fraction is Tc(I). This is an unexpected result that highlights a need to test solubility of the $[Tc(CO)_3]^+$•gluconate species in the concentrated alkaline solutions typical for the Hanford tank waste. We also made the observation that some of the components of the tank supernatant simulant are responsible for stabilizing Tc in reduced oxidation states for long times. Therefore, a liquid fraction in contact with the solid reaction components retains about 30% of Tc(I) after ~750 days. On the other hand, for a liquid fraction of the **Parr Reaction 1** that has been separated from the solid fraction, the amount of Tc(I) reduces to <7% within the 750-day period (see section 4.2 of this report). The second most abundant Tc species in the solid fraction of the **Parr Reaction 1** is Tc(IV). This result is expected considering the low aqueous solubility of the $TcO_2$•$nH_2O$ species. As discussed above, only a small amount of Tc(VI) was observed by XPS. Both XAS and XPS also showed small amount of Tc(VII) in the sample presumably residual pertechnetate not reduced during the Parr reaction conditions (described in the first sentence in Section 4.3.1.2).

#### 4.3.1.2 Parr Reaction 5

*Reaction conditions: 10 mM $TcO_4^-$ in tank supernatant simulant containing 100 mM gluconate and noble metals pressurized to 250 psi with CO containing 75 ppm $H_2$ at 80°C for 21 days.*

It is of interest to compare Tc products generated by **Parr Reactions 5** and **1** conducted under different CO gas pressures of 250 and 1350 psi, respectively, while keeping other conditions (excepting total reaction time (21 vs. 10 days, respectively) the same. Similar to the **Parr Reaction 1**, the product of the **Parr Reaction 5** consisted of a brown precipitate and a light brown liquid. Liquid scintillation counting indicated that the solution accounts for 70% of the total starting Tc. Of the 70% present in solution, ~60% is converted into $[Tc(CO)_3]^+$•gluconate species, as indicated by the $^{99}$Tc NMR spectra of the liquid fraction showing three resonances at -1091, -1231 and -1253 ppm respectively (Figure 24). The NMR spectrum bears a strong resemblance with that of observed for the **Parr Reaction 1**. As in case of the **Parr Reaction 1**, reaction done at higher pressure, the NMR resonances for the **Parr Reaction 5** are significantly narrower than observed for the $[Tc(CO)_3]^+$•gluconate complex in simple 5 M NaNO3/0.1 M NaOH solution (Levitskaia et al. 2015). Only 5% $TcO_4^-$ is observed in the liquid fraction. The 5% unaccounted Tc in the liquid fraction and the narrow line widths are suggestive of some NMR silent paramagnetic species such as Tc(II/IV/VI), being generated in addition to Tc(I), as is the case for the reaction done at higher pressure **Parr Reaction 1** as well.

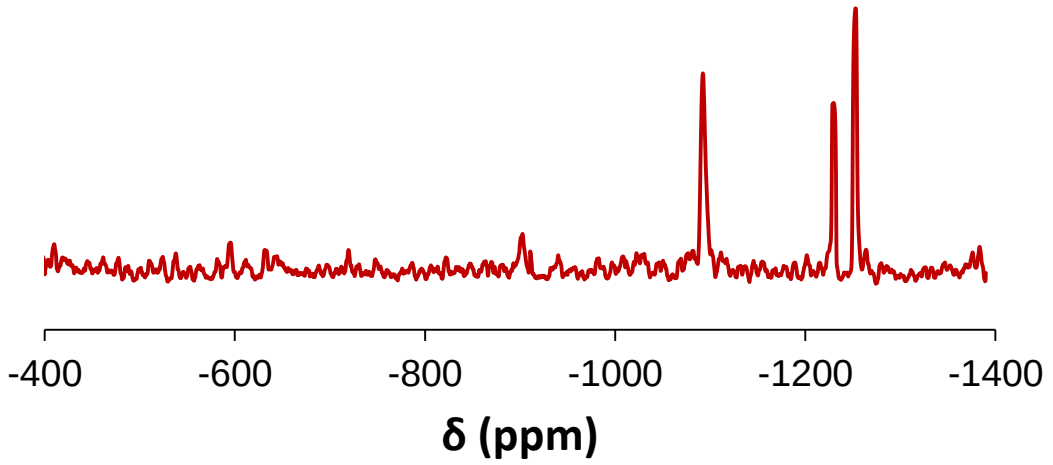


**Figure 24.** $^{99}$Tc NMR spectrum of the liquid fraction of **Parr Reaction 5** product, showing the resonances corresponding to $[Tc(CO)_3]^+$•gluconate species.

The EPR spectrum of the liquid fraction of **Parr Reaction 5** collected at 125 K exhibits at least three distinct regions (Figure 25). The low field part of the spectrum is dominated by a large single signal around 1,600 Gauss that is characterized by a g-value corresponding to Fe clusters. Iron clusters are commonly observed in EPR spectra due to external contamination on the instrument, specifically the sample holder. The high-field portion of the spectrum shows a single spectral signature at approximately 3100 Gauss, which displays a 10-line signal from a $^{99}$Tc nucleus in a relatively high symmetry chemical environment. This 10-line signal is very similar to the Tc EPR spectrum observed for **Parr Reaction 1**. The narrow line width, g-value, and hyperfine splitting constants suggest that this spectrum originates from a Tc(VI) product. An additional broad signal is observed at 6000 Gauss, which currently has not been identified. The EPR spectrum of the solid fraction (Figure 25) is similar to the liquid fraction with

appearance of the Fe cluster at 1600 Gauss, and the Tc(VI) species at 3100 Gauss. However, subtle variations are observed in the nature of the hyperfine splitting. Further, the broad resonance at 6000 Gauss is not observed in the **Parr Reaction 5** solid's EPR spectrum.

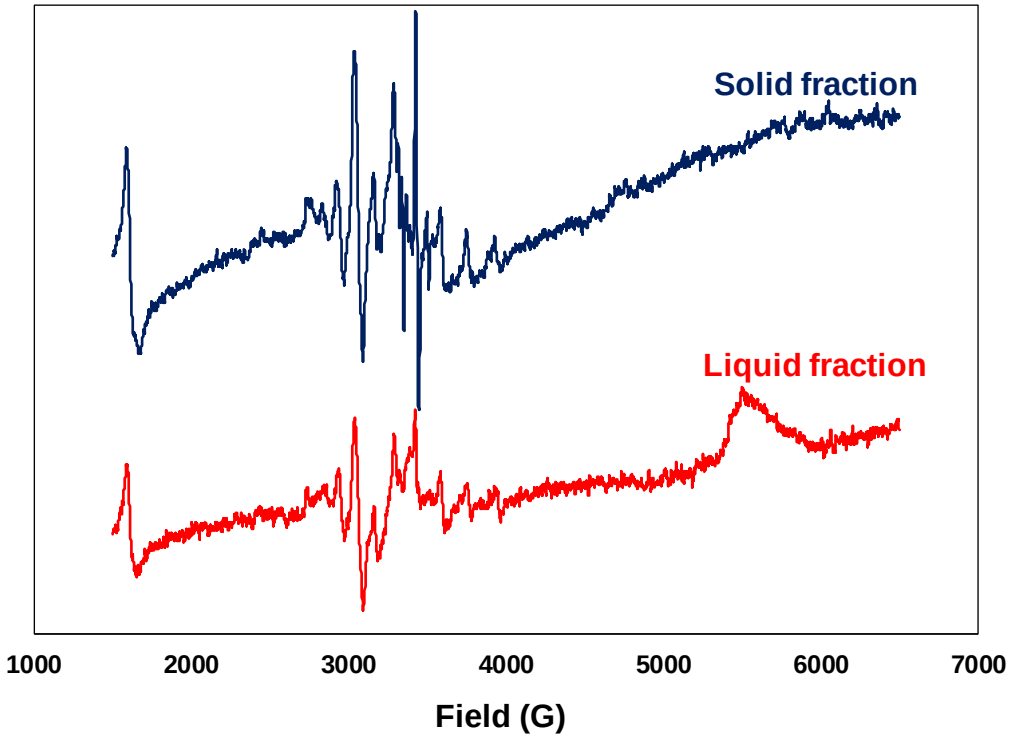


**Figure 25.** $^{99}$Tc EPR spectra measured at 125 K of the solid (blue trace) and liquid (red trace) **Parr Reaction 5** product fractions obtained using simulant prepared in FY 2016 containing 0.1 M gluconate and catalytic noble metals.

Even after lowering the temperature to 1.8 K, the spectra of both the solid and the liquid fractions of **Parr Reaction 5** bear a strong resemblance to those collected at 125 K, with the exception that the 6000 Gauss region of the liquid spectrum is observed to be resolved into a multiplet (Figure 26). The strong resemblance of the spectra at 125 K and 1.8 K characterized by narrow line widths, suggest that the oxidation state of Tc(IV) is less likely to be present. The main driver for this conclusion is the narrow line widths, which strongly suggest a system with an electronic spin of ½. EXAFS data (Lukens et al. 2002) suggests that Tc(IV) under similar conditions should have a coordination number of six. Due to the large d-orbital splitting commonly associated with second and third row transition metals, Tc in such a pseudo octahedral field should provide a system in which the electron spin is greater than ½ (Lukens et al. 2002). These $s > ½$ systems result in broad hyperfine signals due to interaction between the electron spins.

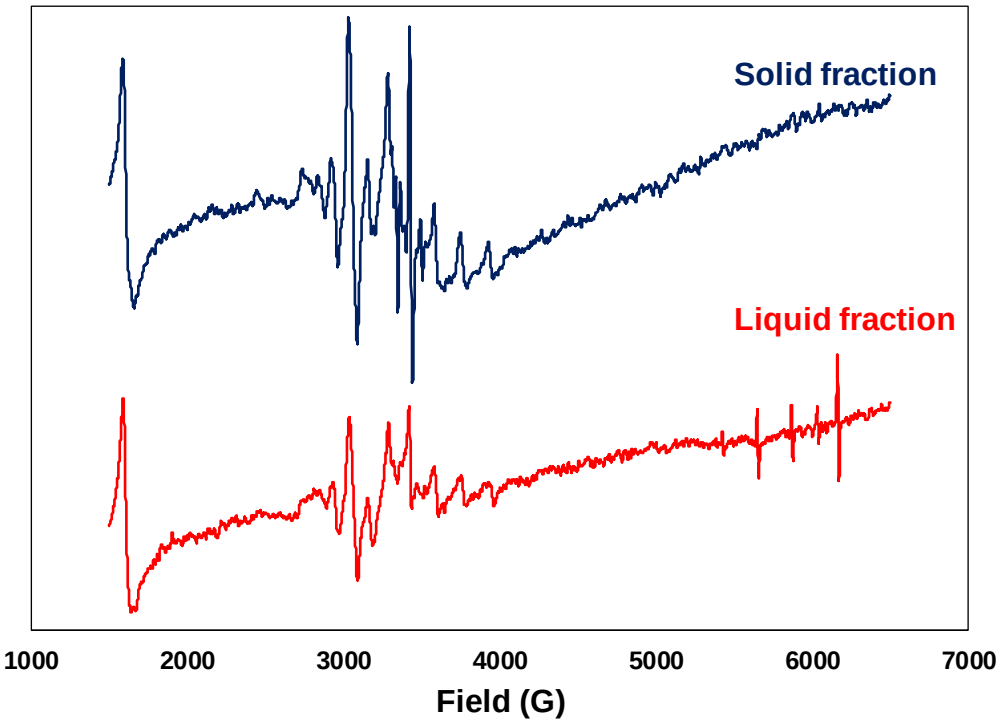


**Figure 26.** $^{99}$Tc EPR spectra of the **Parr Reaction 5** solid (blue trace) and liquid (red trace) product fractions measured at 1.8 K.

The XPS spectrum of the **Parr Reaction 5** liquid fraction was obtained by depositing a few drops on a carbon platform and allowing the liquid to evaporate off. The spectrum can be resolved into a single Tc chemical species with lower binding energy (assigned to Tc $3d_{3/2}$ lines) at 255.1 eV (Figure 27). Based on the Tc $3d_{5/2}$ electron binding energies reported in literature (Wester et al. 1987; Thompson et al. 1986) and our XPS measurements of the reference $[Tc(CO)_3]^+$ compounds (see section 4.1.1 of this report), it is assigned to Tc(I) oxidation state. The observed single shoulder with a lower binding energy of 261.6 eV cannot be attributed to Tc based on the binding energy gap between this and its nearest neighboring peak at 269.6 eV which is far greater than that expected between Tc $3d_{5/2}$ and $3d_{3/2}$ lines, and is presumably caused by some other elemental impurity such as Re. No Tc in oxidation states other than Tc(I) was observed by XPS. The absence of Tc(VI) in the XPS spectrum but appearance in the EPR signal mirrors the findings for the **Parr Reaction 1**. This again supports the fact that, since XPS spectra were recorded on dried samples, the procedure of drying may be responsible for decomposition or disproportionation of Tc(VI).

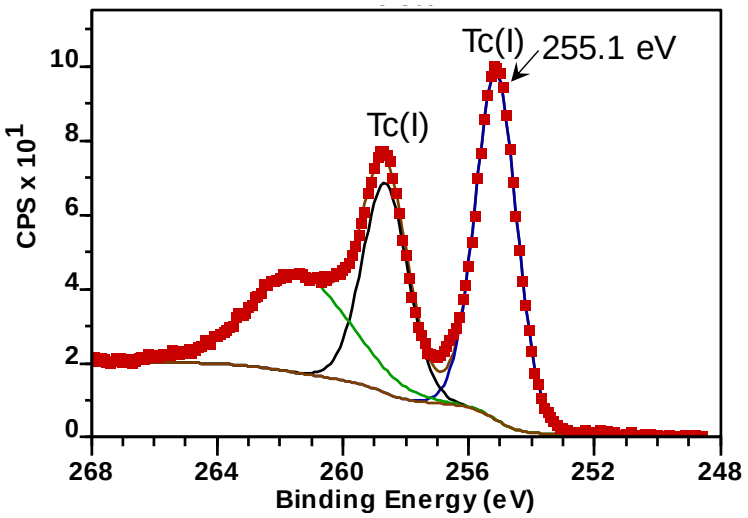


**Figure 27.** X-ray photoelectron spectrum of Tc $3d_{5/2}$ and $3d_{3/2}$ regions for the liquid fraction of **Parr Reaction 5** product. Red squares: experimental spectrum, blue trace: Tc(I) fit, green trace: Re impurity.

In order to optimize the time necessary for the formation of the $[Tc(CO)_3]^+$•gluconate product, a series of control experiments were performed where the reactions were monitored periodically. A reduction reaction using pseudo Hanford tank supernatant simulant containing gluconate and noble metals in presence of CO at temperature (80°C) and pressure (250 psi) was run for 3 days. LSC and $^{99}$Tc NMR demonstrated no change in solution $TcO_4^-$ concentration within the time period of 3 days. Therefore, a periodic monitoring of the reaction was done to see the length of time for the reaction to reach completion. It was observed that the reduction of $TcO_4^-$ intensity starts after day 4; however no immediate evolution of Tc(I) is observed. Monitoring of the reaction solution by EPR shows a signal similar to the one observed in **Parr Reaction 1** suggesting the formation of Tc(VI) species. The $^{99}$Tc NMR suggests that the generation of Tc(I) starts after 10 days.

## 4.4 Oxidative stabilities of *in-situ* non-pertechnetate species

The oxidative stabilities of the Parr reaction products were quantified using $^{99}$Tc NMR, either through monitoring the disappearance of the $[Tc(CO)_3]^+$ species, or by monitoring the appearance of the $TcO_4^-$ resonance. The measurements for **Parr Reactions 1 – 4** had been initiated in FY 2015 and were continued in FY 2016. For the **Parr Reactions 5 – 9**, the reactions were conducted over the course of FY 2016 including measurements of kinetic stabilities of non-pertechnetate species. These results are described below.

### 4.4.1 Parr Reaction 1

The 10-day reaction was conducted in FY 2014 and monitoring of oxidative stability of the product continued throughout FY 2015. The liquid fraction comprising primarily of $[Tc(CO)_3]^+$•gluconate, had shown steady oxidative decomposition to $TcO_4^-$ over the entire course of the year, as observed by $^{99}$Tc NMR. The $^{99}$Tc NMR of the isolated liquid fraction showed a decrease in $[Tc(CO)_3]^+$•gluconate

concentration from 63% immediately after the 10-day elevated temperature reaction was stopped, to 23% after another 365 days, with an increase in the amount of $TcO_4^-$. After about a month after the 10-day reaction, the build-up of $TcO_4^-$ in the liquid fraction was higher than that accounted for by the oxidation of $[Tc(CO)_3]^+$•gluconate from the liquid fraction alone. This suggested conversion of some NMR inactive Tc fraction in the liquid phase into $TcO_4^-$, and/or release and conversion of Tc from solid phase to $TcO_4^-$ in the liquid phase.

Monitoring of the liquid fraction was continued this year (Table 16) when the overall amount of Tc(I) reduced to 7%, while the total amount of $TcO_4^-$ in solution increased to 84%. It is worth mentioning that dynamic pseudo-equilibrium between liquid and solid fractions plays an important role for the total Tc(I) stability. As observed in Figure 28, the total Tc(I) concentration in the solution phase reduces to 7% over 887 days in the liquid $^{99}$Tc NMR sample removed from the contact with the reaction solids. However, it was found that the liquid Tc(I) is significantly more stable when kept in contact with the solid phase, and decreased only to 25% in the same time period of 887 days.

**Table 16.** Time monitoring of the liquid fraction of **Parr Reaction 1** product by $^{99}$Tc NMR spectroscopy. Each resonance area was determined by integration and normalized for the number of scans. The integrals of the resonances corresponding to the $[Tc(CO)_3]^+$•gluconate complex are shown as a sum of integrals of the individual -1094, -1232, and -1254 ppm resonances.

| **Time elapsed after the reaction was stopped (days)** | **NMR-active liquid fraction** | | | **Sum of solid fraction and NMR-inactive liquid fractions** |
|---|---|---|---|---|
| | **$[Tc(CO)_3]^+$** | **$TcO_4^-$** | **Tc (I) + Tc (VII)** | |
| Before reaction | N/A | 1 [a] | N/A | N/A |
| 0.04 | 0.63 | 0.06 | 0.69 | 0.31 |
| 0.17 | 0.55 | 0.06 | 0.61 | 0.39 |
| 0.79 | 0.49 | 0.06 | 0.55 | 0.45 |
| 3 | 0.45 | 0.06 | 0.50 | 0.50 |
| 5 | 0.39 | 0.09 | 0.48 | 0.52 |
| 8 | 0.38 | 0.09 | 0.47 | 0.53 |
| 19 | 0.34 | 0.14 | 0.48 | 0.52 |
| 49 | 0.31 | 0.22 | 0.54 | 0.46 |
| 99 | 0.32 | 0.28 | 0.60 | 0.40 |
| 150 | 0.32 | 0.35 | 0.67 | 0.33 |
| 224 | 0.29 | 0.45 | 0.74 | 0.26 |
| 298 | 0.26 | 0.54 | 0.80 | 0.20 |
| 365 | 0.23 | 0.62 | 0.85 | 0.15 |
| 467 | 0.18 | 0.69 | 0.87 | 0.13 |
| 569 | 0.14 | 0.74 | 0.88 | 0.12 |
| 671 | 0.09 | 0.81 | 0.90 | 0.10 |

| Time elapsed after the reaction was stopped (days) | NMR-active liquid fraction | | | Sum of solid fraction and NMR-inactive liquid fractions |
|---|---|---|---|---|
| | $[Tc(CO)_3]^+$ | $TcO_4^-$ | Tc (I) + Tc (VII) | |
| 729[b] | 0.08 | 0.82 | 0.90 | 0.10 |
| 773 | 0.08 | 0.83 | 0.91 | 0.09 |
| 887 | 0.07 | 0.84 | 0.91 | 0.09 |

[a] Corresponds to the total Tc in the sample, which was added to the simulant as $TcO_4^-$.
[b] XPS done on separated solid.

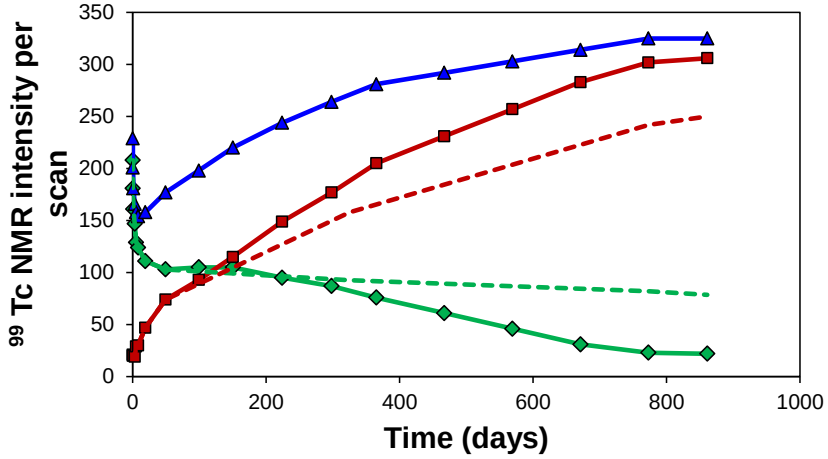


**Figure 28.** Time monitoring of $[Tc(CO)_3]^+$ and $TcO_4^-$ species in the solution fraction of **Parr Reaction 1** product. Red squares: $TcO_4^-$. Green diamonds: combined $[Tc(CO)_3]^+$ species corresponding to the resonances at -1094, -1232 and -1254 ppm. Blue triangles: total NMR-active $^{99}Tc$ species. The red and green dashed lines represent the $TcO_4^-$ and combined $[Tc(CO)_3]^+$ species respectively when the solution fraction of the product is kept in contact with the solid.

### 4.4.2 Parr Reaction 2

The reaction conducted in the presence of noble metals and absence of gluconate, exhibited conversion of 72% of Tc(VII) to $[Tc(CO)_3]^+$ in the liquid fraction. About 12% of the Tc remained unreacted as $TcO_4^-$ in solution, suggesting the rest 16% was present either as an NMR inactive liquid fraction, or was entrapped within the solids formed during the 10-day reaction. Over the course of next 330 days, all the $[Tc(CO)_3]^+$ in the liquid fraction was converted to Tc(VII) while 7% of the total Tc fraction was present either as a NMR inactive liquid fraction or was present in the solids, or had been released into the liquid fraction as Tc(VII). The detailed description of this experiment is reported elsewhere (Chatterjee et al. 2015).

Monitoring was continued in FY 2016 and FY 2017 (Table 17). At the beginning of FY 2017, 9% of the starting Tc was either present as NMR inactive Tc in the liquid fraction or was trapped within the

solid phase. It was observed that the release of this 9% of Tc into solution as $TcO_4^-$ is considerably slow. Thus, while within the first 330 days, the total amount of $TcO_4^-$ in the liquid fraction had risen to 91%, over the next 517 days only another 6% growth of $TcO_4^-$ was observed. This suggests that this Tc was present trapped in solid phase, which protected it from the atmospheric oxidative conditions and resisted its release into the solution for over two years.

XPS studies conducted on the solid phase from **Parr Reaction 2** have shown the presence of both Tc(I) and Tc(IV). While it was initially assumed that it would be unlikely for the highly mobile Tc(I) to remain in the solid phase, its detection through XPS confirms its entrapment in the solid. This entrapment is also presumably responsible for the unexpected stability of Tc(I) as well as the Tc(IV) that is observed in XPS as well. While both Tc(I) and Tc(IV) are susceptible to fast oxidation when air is present, and the fact that these species are observed by XPS several days post preparation suggest that their presumable entrapment within the solid phase resists their oxidation, and enhances their oxidative stability.

**Table 17.** $^{99}$Tc NMR time monitoring of the liquid fraction of **Parr Reaction 2 product** containing noble metals. The area of each resonance was determined by the integration of the energy peaks previously identified and normalized for the number of scans.

| **Time elapsed after the reaction was stopped (days)** | **NMR-active species in the liquid fraction** | | | **Sum of solid fraction and NMR-inactive liquid fractions** |
|---|---|---|---|---|
| | **$[Tc(CO)_3]^+$** | **$TcO_4^-$** | **Tc (I) + Tc (VII)** | |
| Before reaction | N/A | 1 [a] | N/A | N/A |
| 0.05 | 0.72 | 0.12 | 0.84 | 0.16 |
| 3 | 0.44 | 0.10 | 0.54 | 0.46 |
| 5 | 0.38 | 0.15 | 0.53 | 0.47 |
| 8 | 0.36 | 0.16 | 0.52 | 0.48 |
| 19 | 0.31 | 0.24 | 0.55 | 0.45 |
| 60 | 0.18 | 0.51 | 0.68 | 0.32 |
| 125 | 0.11 | 0.68 | 0.79 | 0.21 |
| 170 | 0 | 0.83 | 0.83 | 0.17 |
| 330 | 0 | 0.91 | 0.91 | 0.09 |
| 502 | 0 | 0.92 | 0.92 | 0.08 |
| 629 | 0 | 0.94 | 0.94 | 0.06 |
| 681 [b] | 0 | 0.95 | 0.95 | 0.05 |
| 781 | 0 | 0.96 | 0.96 | 0.04 |
| 847 | 0 | 0.97 | 0.97 | 0.03 |

[a] Corresponds to the total Tc in the sample, which was added to the simulant as $TcO_4^-$.
[b] XPS done on separated solid

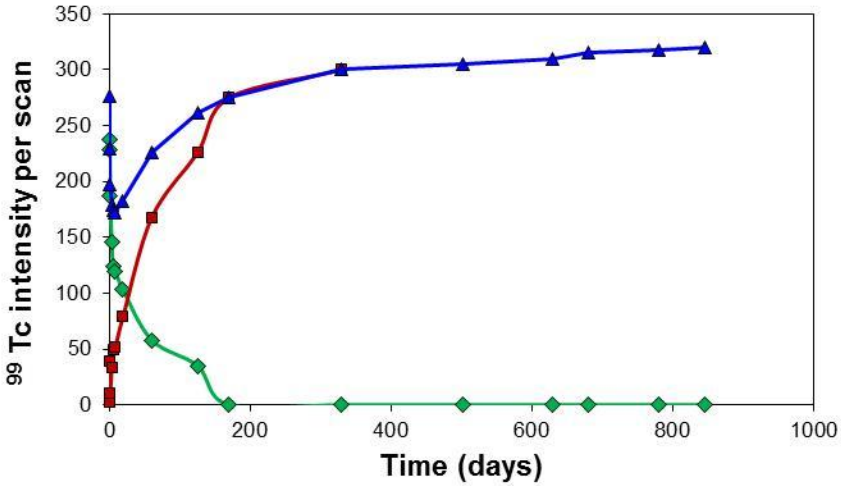


**Figure 29.** Time monitoring of $[Tc(CO)_3]^+$ and $TcO_4^-$ species in the solution fraction of **Parr Reaction 2**. Red squares: $TcO_4^-$. Green diamonds: $[Tc(CO)_3]^+$ species corresponding to the resonance at -1094 ppm. Blue triangles: total NMR-active $^{99}Tc$ species.

### 4.4.3 Parr Reaction 3

The reacted simulant containing gluconate but without noble metals has generated remarkably stable Tc(VI) non-pertechnetate species. This sample, prepared in 2014 and preserved under ambient laboratory conditions for a period of 12 months, displayed a strong EPR signal with an identical profile of the original (5-day) spectrum and only slightly reduced intensity suggesting that the chemical integrity of the reduced Tc species is preserved. The monitoring of the reaction product in 2016 (Table 18) showed the sustained stability of the species, with the EPR continuing to show the same profile (Figure 30).

The $^{99}Tc$ NMR trends with time were consistent with the EPR results. The initial reaction resulted in reduction of 75% of initial Tc to Tc(VI), as evidenced by the $TcO_4^-$ signal getting reduced to 25% of its original intensity. The remarkable stability of the Tc(VI) species is evidenced by only 13% of the reduced Tc converting back to $TcO_4^-$ over the course of the first year, and only another 6% getting oxidized over the next year and half.

**Table 18.** $^{99}Tc$ NMR Time Monitoring of **Parr Reaction 3**. The reported data correspond to the liquid reaction product as sample contained no solids.

| **Time elapsed after the reaction was stopped (days)** | **$TcO_4^-$** | **Fraction of NMR-inactive non-$TcO_4^-$** |
|---|---|---|
| Before reaction | 1[a] | N/A |
| 0.05 | 0.25 | 0.75 |
| 0.3 | 0.24 | 0.76 |
| 1 | 0.26 | 0.74 |

| Time elapsed after the reaction was stopped (days) | $TcO_4^-$ | Fraction of NMR-inactive non-$TcO_4^-$ |
|---|---|---|
| 3 | 0.27 | 0.73 |
| 6 | 0.27 | 0.73 |
| 10 | 0.27 | 0.73 |
| 21 | 0.27 | 0.73 |
| 72 | 0.30 | 0.70 |
| 130 | 0.32 | 0.68 |
| 200 | 0.35 | 0.65 |
| 381 | 0.38 | 0.62 |
| 493 | 0.39 | 0.61 |
| 630 | 0.40 | 0.60 |
| 756 | 0.42 | 0.58 |
| 879 | 0.44 | 0.56 |

[a] Corresponds to the total Tc in the sample, which was added to the simulant as $TcO_4^-$.

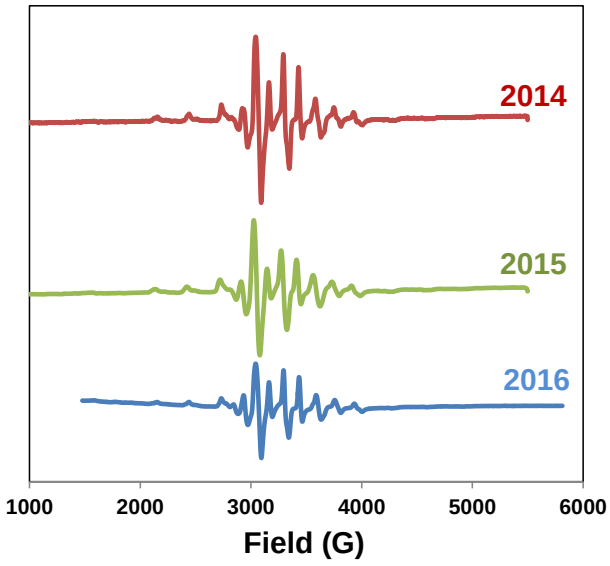


**Figure 30.** $^{99}$Tc EPR spectra of the liquid fraction of **Parr Reaction 3** product collected at Day 5 after (red trace), day 365 (green trace), and day 756 (blue trace) after generation of the sample.

### 4.4.4 Parr Reaction 4

The reacted simulant in the absence of gluconate and noble metals showed the formation of $[Tc(CO)_3(H_2O)_2(OH)]$ and Tc(IV). Immediately after the high pressure/high temperature reaction, the liquid fraction consisted of 11% $[Tc(CO)_3]^+$ while 7% of the starting Tc remained in $TcO_4^-$ form (Table 19). This suggested the conversion of 82% of starting Tc either to an NMR inactive fraction in the liquid state or that 82% of the starting Tc was entrapped in the solids formed. Over the next 200 days, the Tc(I) species present in the solution phase converted completely into $TcO_4^-$. Of the initial 82% present either as NMR inactive species or Tc trapped in the solids, 37% converted to solution phase $TcO_4^-$ over that period. Monitoring was continued in FY 2016, and over the next 1.5 years, 85% of the initial Tc converted to Tc(VII), and only 15% remained as NMR inactive fraction in the liquid state or entrapped in solids.

**Table 19.** $^{99}$Tc NMR Time Monitoring of the Liquid Fraction of **Parr Reaction 4** product. The area of each resonance was determined by the integration of previously identified peaks and normalized for the number of scans.

| Time elapsed after the reaction was stopped (days) | NMR-active species found in the liquid fraction | | | Sum of solid fraction and NMR-inactive liquid fractions |
|---|---|---|---|---|
| | $[Tc(CO)_3]^+$ | $TcO_4^-$ | Tc (I) + Tc (VII) | |
| Before reaction | N/A | 1 [a] | N/A | N/A |
| 0.04 | 0.11 | 0.07 | 0.18 | 0.82 |
| 1 | 0.10 | 0.08 | 0.18 | 0.82 |
| 2 | 0.09 | 0.08 | 0.18 | 0.82 |
| 6 | 0.08 | 0.10 | 0.18 | 0.82 |
| 10 | 0.08 | 0.11 | 0.19 | 0.81 |
| 15 | 0.07 | 0.13 | 0.20 | 0.80 |
| 23 | 0.05 | 0.15 | 0.20 | 0.80 |
| 29 | 0.04 | 0.17 | 0.21 | 0.79 |
| 37 | 0.01 | 0.22 | 0.23 | 0.77 |
| 45 | 0.01 | 0.22 | 0.23 | 0.77 |
| 49 | 0 | 0.23 | 0.23 | 0.77 |
| 70 | 0 | 0.26 | 0.26 | 0.74 |
| 110 | 0 | 0.30 | 0.30 | 0.70 |
| 200 | 0 | 0.45 | 0.45 | 0.55 |
| 300 | 0 | 0.52 | 0.52 | 0.48 |
| 402 | 0 | 0.58 | 0.58 | 0.42 |
| 509 | 0 | 0.65 | 0.65 | 0.35 |
| 623 [b] | 0 | 0.72 | 0.72 | 0.28 |
| 734 | 0 | 0.79 | 0.79 | 0.21 |
| 887 | 0 | 0.85 | 0.85 | 0.15 |

[a] Corresponds to the total Tc in the sample, which was added to the simulant as $TcO_4^-$.
[b] XPS done on separated solid

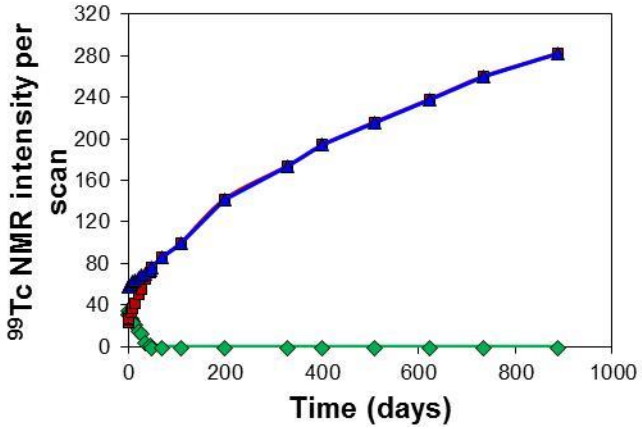


**Figure 31.** Time monitoring of $[Tc(CO)_3]^+$ and $TcO_4^-$ species in the solution fraction of **Parr Reaction 4**. Red squares: $TcO_4^-$. Green diamonds: $[Tc(CO)_3]^+$ species corresponding to the resonance at -1094 ppm. Blue triangles: total NMR-active $^{99}Tc$ species.

### 4.4.5 Parr Reaction 5

The products obtained from **Parr Reaction 5** were very similar to those obtained from **Parr Reaction 1** with the exception of the fact that it took much longer for the Tc(I) to form. This coupled with the fact that the conversion of Tc(VII) to Tc(I) only occurs after 14 days (based on **Parr Reactions 6** and **7**), we conclude that lowering the pressure from 1300 psi to 250 psi does not alter the nature of the products significantly, provided sufficient time is allowed for the Tc reduction reactions to go to completion.

The oxidative decomposition of the low-valent Tc products also follows a very similar pathway as for those generated by **Parr Reaction 1** (Table 20). Thus, immediately after the completion of the Parr reaction, 60% of $[Tc(CO)_3]^+$•Gluconate is observed to be present in the liquid phase. After 180 days of monitoring, that reduces to 25% of the total Tc.

On the other hand, the total $TcO_4^-$ left in the supernatant liquid immediately following the completion (21 days) of the reaction is 5% of the starting Tc, suggesting the rest 35% is either trapped within the solid precipitate or is present as a NMR inactive component in the liquid phase. EPR studies have provided evidence that NMR inactive components can arise from a Tc(VI) species. After 180 days of monitoring, the total amount of $TcO_4^-$ in the liquid fraction rises to 45%, suggesting a decrease of solid Tc and/or NMR inactive form of Tc by 5% (conversion of $[Tc(CO)_3]^+$•gluconate to $TcO_4^-$ in the liquid phase accounts for 25% of the increase in $TcO_4^-$).

**Table 20.** Time monitoring of the observed $^{99}$Tc NMR resonances in the liquid fraction of **Parr Reaction 5** product. Each resonance area was determined by integration and normalized for the number of scans. The integrals of the resonances corresponding to the $[Tc(CO)_3]^+$•gluconate complex are shown as a sum of integrals of the individual -1091, -1231, and -1253 ppm resonances.

| **Time elapsed after the reaction was stopped (days)** | **NMR-active liquid fraction** | | | **Sum of solid fraction and NMR-inactive liquid fractions** |
|---|---|---|---|---|
| | **$[Tc(CO)_3]^+$** | **$TcO_4^-$** | **Tc (I) + Tc (VII)** | |
| Before reaction | N/A | 1 [a] | N/A | N/A |
| 0.01 | 0.60 | 0.05 | 0.65 | 0.35 |
| 0.125 | 0.56 | 0.06 | 0.62 | 0.38 |
| 2 | 0.54 | 0.06 | 0.60 | 0.40 |
| 3 | 0.51 | 0.09 | 0.60 | 0.40 |
| 7 | 0.48 | 0.09 | 0.57 | 0.43 |
| 10 | 0.45 | 0.11 | 0.56 | 0.44 |
| 14 | 0.43 | 0.14 | 0.57 | 0.43 |
| 30 | 0.39 | 0.22 | 0.61 | 0.39 |
| 37 | 0.37 | 0.25 | 0.62 | 0.38 |
| 49 | 0.35 | 0.27 | 0.62 | 0.38 |
| 61 | 0.32 | 0.29 | 0.61 | 0.39 |
| 99 | 0.29 | 0.31 | 0.60 | 0.40 |
| 150 | 0.27 | 0.38 | 0.65 | 0.35 |
| 181 | 0.25 | 0.45 | 0.70 | 0.30 |

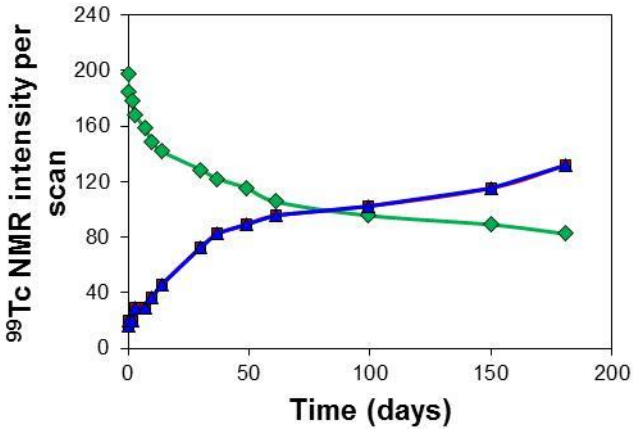


**Figure 32.** Monitoring of $[Tc(CO)_3]^+$ and $TcO_4^-$ species in the solution fraction of **Parr Reaction 5** product as a function of time. Blue squares: $TcO_4^-$. Green diamonds: combined $[Tc(CO)_3]^+$ species corresponding to the resonances at -1091, -1231 and -1253 ppm.

### 4.4.6 Parr Reaction 6

The Parr reaction product consisted of 25% NMR-inactive Tc presumably Tc(VI) while the rest 75% remained unconverted as $TcO_4^-$. The reaction product was found to be unstable, undergoing a complete oxidation to $TcO_4^-$ within 7 days (as shown in Table 21), indicating the high instability of this product. We speculate that the low $CO/H_2$ pressure and low temperature (25 °C vs. 80 °C in most other Parr Reaction tests) are the cause for little formation of $[Tc(CO)_3]^+$•gluconate species or their rapid re-oxidation to $TcO_4^-$.

**Table 21.** $^{99}$Tc NMR monitoring of **Parr Reaction 6** product as a function of time. The reported data correspond to the liquid fraction of reaction mixture as sample contained no solids.

| **Time elapsed after the reaction was stopped (days)** | **$TcO_4^-$** | **Percent NMR-inactive non-$TcO_4^-$** |
|---|---|---|
| Before reaction | 1[a] | N/A |
| 0.05 | 0.75 | 0.25 |
| 0.6 | 0.80 | 0.20 |
| 1 | 0.85 | 0.15 |
| 3 | 0.90 | 0.10 |
| 4 | 0.93 | 0.07 |
| 6 | 0.97 | 0.03 |
| 7 | 1 | 0 |

### 4.4.7 Parr Reaction 7

The Parr reaction product contained 80% of total Tc as unreacted $TcO_4^-$, while the rest was converted to Tc(IV). About 50% of the Tc(IV) product oxidized to $TcO_4^-$ within 7 days (Table 22); and the monitoring the reaction products is currently ongoing. This observation is consistent with previous studies, which reported fast decomposition of Tc(IV), as $TcO_2 \bullet nH_2O$, under aerated conditions (Lukens et al. 2002).

**Table 22.** $^{99}$Tc NMR monitoring of **Parr Reaction 7** product as a function of time. The reported data correspond to the liquid fraction of reaction mixture as sample contained no solids.

| **Time elapsed after the reaction was stopped (days)** | **$TcO_4^-$** | **Percent NMR-inactive non-$TcO_4^-$** |
|---|---|---|
| Before reaction | 1 [a] | N/A |
| 0.03 | 0.80 | 0.20 |
| 0.5 | 0.82 | 0.18 |
| 1 | 0.84 | 0.16 |
| 4 | 0.87 | 0.13 |
| 7 | 0.90 | 0.10 |

### 4.4.8 Parr Reactions 8 and 9

Monitoring of the Tc speciation of the reaction products generated in **Parr Reactions 8** and **9** as a function of time is currently ongoing. The preliminary observations indicate that the presence of Cr(VI) as an oxidant accelerates decomposition of the Tc(I) $[Tc(CO)_3]^+ \bullet$gluconate species (Figure 33, Table 23).

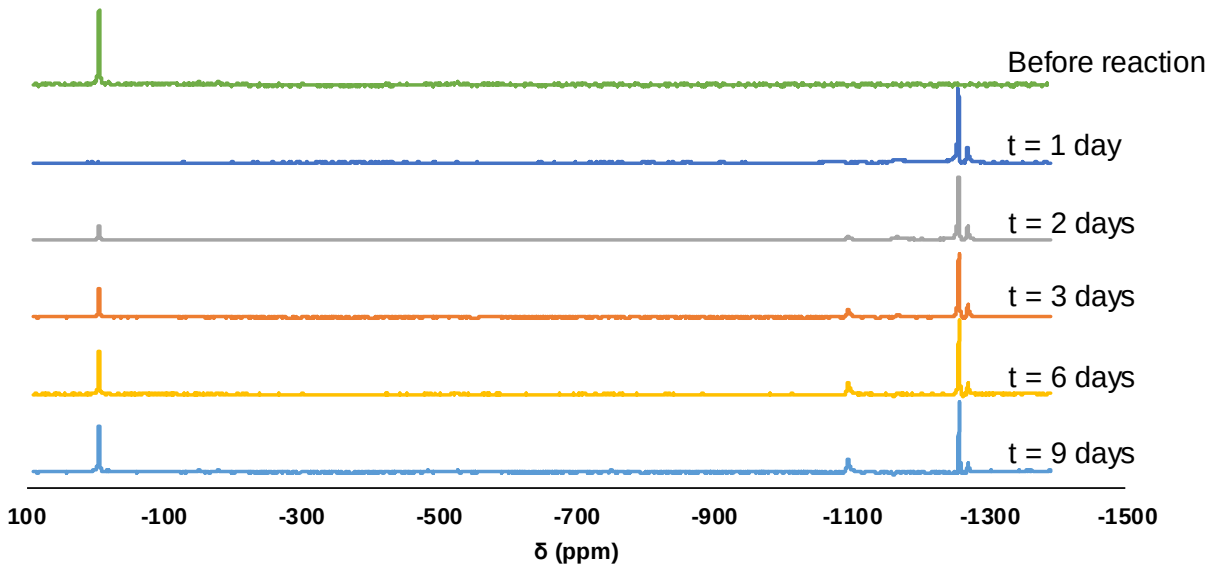


**Figure 33.** Monitoring the kinetics of decomposition of $[Tc(CO)_3]^+$•gluconate using solution $^{99}Tc$ NMR Spectroscopy

**Table 23.** Observed $^{99}Tc$ NMR resonances in the liquid fraction of **Parr Reaction 8** product as a function of time. Each resonance area was determined by the integration and normalization for the number of scans. The integrals of the resonances corresponding to the $[Tc(CO)_3]^+$•gluconate complex are shown as a sum of integrals of the individual -1094, -1162, -1256, and -1270 ppm resonances.

| **Time elapsed after the reaction was stopped (days)** | **NMR-active species found in the liquid fraction** | | | **Sum of solid fraction and NMR-inactive liquid fractions** |
|---|---|---|---|---|
| | **$[Tc(CO)_3]^+$** | **$TcO_4^-$** | **Tc (I) + Tc (VII)** | |
| Before reaction | N/A | 1 [a] | N/A | N/A |
| 0.01 | 0.60 | 0.05 | 0.65 | 0.35 |
| 0.5 | 0.51 | 0.13 | 0.64 | 0.36 |
| 2 | 0.45 | 0.20 | 0.65 | 0.35 |
| 3 | 0.42 | 0.25 | 0.67 | 0.33 |
| 6 | 0.38 | 0.29 | 0.67 | 0.33 |
| 9 | 0.35 | 0.33 | 0.68 | 0.32 |

## 4.5 Comments on mechanism of *in-situ* reduction of $TcO_4^-$ and formation of non-pertechnetate species

The series of the Parr reactions performed to date allows us to gain some mechanistic understanding regarding the *in situ* reduction of $TcO_4^-$ to non-pertechnetate species.

The fact that the formation of the suspected Tc(VI) species is observed only in the presence of gluconate (**Parr Reactions 1, 3, 5,** and **6**) suggests that the presence of a chelator is critical for the stabilization of the Tc(VI) oxidation state. The fact that the formation of the Tc(VI) species is not observed under ambient CO pressure (**Parr Reaction 7**) is suggestive that either CO also contributes to the stabilization of the Tc(VI), or that the increased pressure is necessary to overcome a high activation barrier. To our knowledge, the Tc(VI) species isolated in the Parr reactions are by far the most stable Tc(VI) species ever reported in aqueous solutions. This stability in aqueous solutions is pretty remarkable as previous studies suggest that the presence of water from moisture is sufficient to accelerate the oxidation of Tc(VI) species to $TcO_4^-$. Solids of Tc(VI) of the general formulae $[(CH_3)_4N]_2TcO_4$ have been isolated (Astheimer et al. 1975) only under moisture free conditions. Tc(VI) halides of the form $TcCl_6$ have been reported in the presence of a concentrated stream of $Cl_2$ gas, but undergo rapid disproportionation in air (Colton 1962). $TcF_6$ has also been reported to exist in solid, liquid and vapor states, but not in aqueous solutions (Rard et al. 2005; Osborne et al. 1977; Selig et al. 1962). Colton and Thomkins (1968) reacted thionyl chloride ($SO_2Cl_2$, an extremely strong Lewis acid) with $NH_4TcO_4$ to prepare the thionyl chloride adduct $(NH_4)_2[TcO_2Cl_4]$ $SO_2Cl_2$, which contains Tc(VI), but this was observed to rapidly disintegrate to Tc(VII). Majumdar et al. (1969) reported the formation of Tc(VI) by chemical reduction of $TcO_4^-$ with hydrazine. More recently, several Tc(VI) complexes have been isolated and characterized structurally, including $TcOF_4$ and $(TcOF_4)_3$ (Rard et al. 1999). However, their solution chemistry remains elusive owing to the instability of Tc(VI). While one electron electrochemical reductions of Tc(VII) to Tc(VI) had been observed in several aqueous media (Rard et al. 1999; Kissel and Feldberg, 1969; Rard 1999; Deutsch et al. 1978; Hurst 1980; Krychkov et al. 1979), the Tc(VI) species generated in these studies were extremely short-lived and underwent rapid disproportionation within minutes to Tc(VII) and Tc(V). It was only recently that we observed that at very high ionic strength matrices, the stability of the Tc(VI) species can be enhanced. However, the stability of our electrochemically generated complexes are nowhere near the stability of these chelator-Tc(VI) species generated under Parr reaction conditions. This is consistent with the observations of Takayama et al. (1995) who reported the formation of an EDTA coordinated Tc(VI) dimer in solution. The high ionic strength matrices and the presence of chelators can extend the half-life of Tc(VI) species for years, as observed in the Parr reaction products. This observation is incredibly important as it can have significant implications in the chemical and redox speciation of Tc in Hanford Site tank waste supernatants and interstitial water within saltcake.

The EPR spectra of the suspected Tc(VI) product generated in **Parr Reaction 1** and **Parr Reaction 3** are near identical, which is suggestive that they are presumably originating from the same chemical species. This suggests that reduction of $TcO_4^-$ to Tc(I) proceeds through a Tc(VI) intermediate, Tc(VI)•gluconate, for the reactions done in the presence of gluconate.

The fact that reduction stops at the Tc(VI) stage in **Parr Reactions 3** and **6**, indicates that a higher activation barrier needs to be overcome for the products to undergo further reductions. The catalyst for

this can either be the presence of noble metals to catalyze the further reduction in case of reaction **3**, or a higher temperature to overcome the activation barrier as in case of reaction **6**.

The identification of Tc(IV) species in **Parr Reactions 1, 2** and **4** suggest that the reduction pathway presumably goes through an intermediate Tc(IV) species. This hypothesis is consistent with observations by Alberto and coworkers (Alberto et al. 1998 and Alberto et al. 1995) for the generation of $[Tc(CO)_3]^+$ species from two step reduction of $TcO_4^-$ via a Tc(V) intermediate, $TcOCl_4^-$, which resulted in a Tc(IV) intermediate, $TcCl_6^{2-}$. The generation of Tc(IV) is more dominant for Parr Reactions 2 and 4, where gluconate was absent. This suggests that in the absence of gluconate, the Tc(VI) product is not stabilized and therefore the reaction proceeds to form Tc(IV) species. Whether Tc(IV) is formed upon a direct $3e^-$ reduction of $TcO_4^-$ via an alternate reduction pathway, or is formed from the decomposition of a Tc(VI) intermediate, is still under investigation. However, our preliminary results point towards a Tc(IV) formed by an alternate pathway. This is because, the Tc(IV) species observed in the reactions both in the presence and absence of gluconate, have the same photoelectron binding energy, suggesting their very similar chemical environment. This presumably would not have been the case if the Tc(IV) generated in reaction **1** would have been a Tc(IV)•gluconate product formed from the reduction of Tc(VI)•gluconate.

In addition to the high stability of some of the non-pertechnetate species in the solution state, particularly intriguing is their stability when associated with the solid state. As a representative example, XPS of the solid formed in **Parr Reaction 1** and **2** show significant fractions of Tc(I) being stabilized for significantly longer durations than their observed stability in the solution phase. Additionally, when the solution fraction is kept in physical contact with the solid fraction, the solid retains and stabilizes Tc(I) for much longer times. This has important implications for Hanford tank wastes which have layers of solids in their bottoms that are often suspended during gas bubble expulsion. The solids could be stabilizing the non-pertechnetate species in the tank waste for prolonged periods.

One significant finding is that the reduction of reaction gas pressure does not significantly impact the nature of the reaction products. A comparison between reactions **1** and **5** show that reduction of the pressure from 1300 psi to 250 psi slows down the reaction, but results in the same Tc-bearing products. While the reaction performed under ambient pressure (**Parr Reaction 7**) did not indicate any formation of Tc(I) species, we anticipate that allowing the reaction to run for longer periods will eventually lead to formation of Tc(I) species.

It should be noted that the presence of oxidants such as $CrO_4^{2-}$ do not prevent the formation of Tc(I) products. While the resultant chemical environments seem to be slightly different as are the reaction products generated in the absence of Cr(VI), the fact that Tc(I) species are still generated has significant implications in tank waste chemistry, as they are populated with significant quantities of Cr(VI).

It is observed that replacing gluconate with IDA results in the formation of the $[Tc(CO)_3]^+$•IDA complex. This is a significant finding as IDA is found in high-organics tank wastes containing significant non-pertechnetate concentrations (Serne et al. 2015) and therefore, based on the high stability of the $[Tc(CO)_3]^+$•IDA complex observed in our stability studies, this complex may result in significant contribution to the overall $[Tc(CO)_3]^+$ concentration in Hanford tank waste.

## 4.6 DFT modelling of $^{99}$Tc NMR chemical shifts

Further detail of the discussion below can be found in the journal article that was published on this work (Hall et al. 2016)

### 4.6.1 Validation of Computational Methods

In order to effectively model the $^{99}$Tc NMR chemical shifts, a computational method first needed to be developed. Since relativistic effects have been noted to be non-trivial for 4d transition metals, we have chosen to compare the chemical shielding with and without the zeroth order regular approximation (ZORA) for each exchange-correlation functional. In order to most accurately model the molecules of interest to this study, technetium carbonyl compounds, a compound of this general structure, $[Tc(CO)_3(OH_2)_3]^+$, is used as a reference compound. This decreased the overall absolute mean standard deviation for some functionals as compared to referencing against $TcO_4^-$.

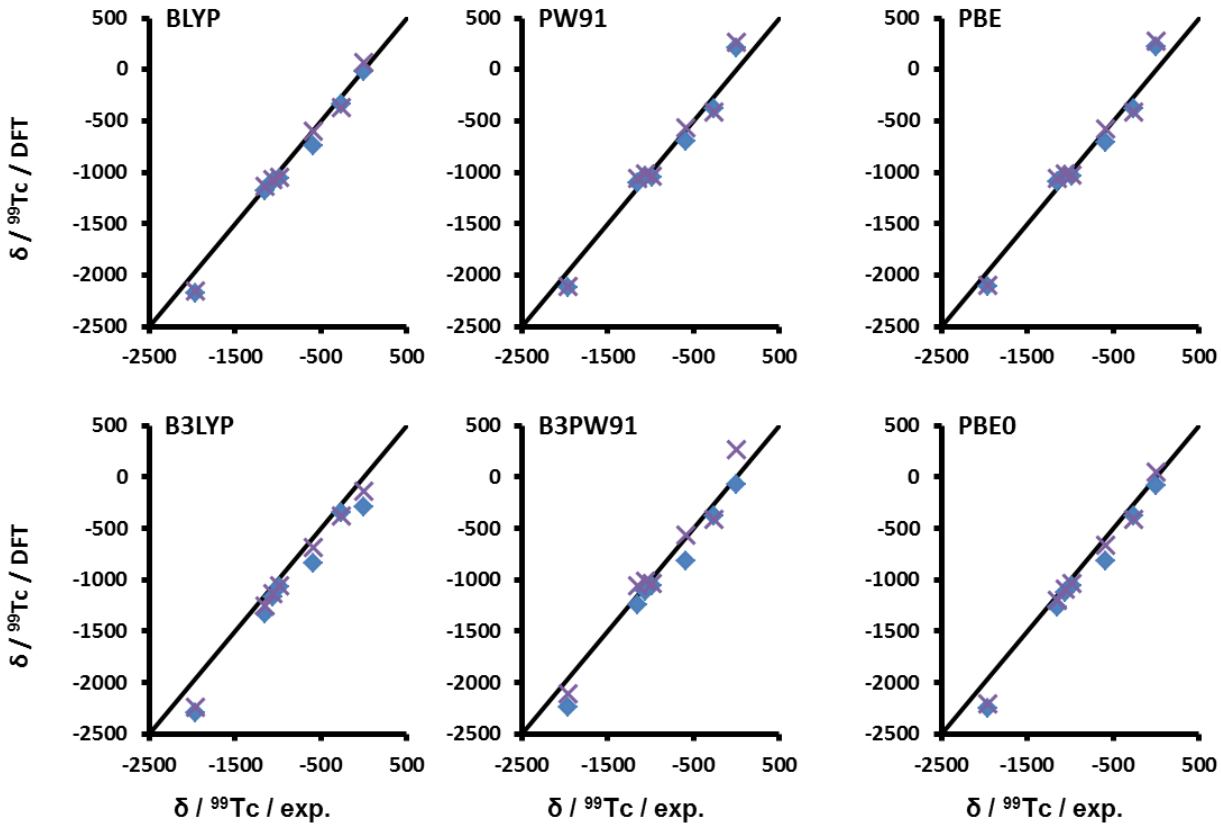


**Figure 34.** DFT computed $^{99}$Tc NMR chemical shifts plotted vs empirically measured values for the pure GGA exchange correlation BLYP and the hybrid B3LYP. An ideal line with a slope of 1 is shown for reference. Blue diamonds represent the SOMF calculations without ZORA, while purple X's represent calculations incorporating ZORA.

Figure 34 displays calculated chemical shifts for the BLYP and B3LYP functionals versus empirically measured values with an idealized line with a slope of 1 and intercept of 0 for comparison. Parameters relating to analysis by linear regression are found in Table 23. Figure 34 shows that the ZORA+SOMF calculation for BLYP is in good agreement between DFT computed and empirical values. The mean absolute deviation from experiment is 86 ppm (Table 23). Inclusion of ZORA into the BLYP functional shows less deviation than for other well performing functionals tested and does decrease the mean absolute deviation to 66 ppm. The drop in mean absolute deviation is attributable in large part to the more accurate prediction of the chemical shift for $[Tc(CO)_3(OH)]_4$. This is true for the other functionals tested as well and is easily visualized by examining Figure 34 where the data points corresponding to the tetranuclear species lie much closer to the idealized line in all cases. It should be noted that the aforementioned 66 ppm absolute mean deviation corresponds to only ~0.7% of the overall $^{99}$Tc NMR spectral window (9,000 ppm).

Importantly, the uncorrected accuracy of the chemical shift is the linear correlation between the computed values and the experimental values. A deviation from empirical values in an orderly fashion ($R^2 \approx 1$) can be corrected *ex post facto*. A linear regression analysis can be seen in Table 24; it should be noted that, when calculating the slope for each given data set, the value for $[Tc(CO)_3(OH_2)_3]^+$ was excluded, as it was artificially set to -869 ppm for all computational data. BLYP ZORA+SOMF calculations yield a favorable $R^2$ value of 0.994 for the line formed by plotting DFT computed values against experimental values, and 0.993 for BLYP/ZORA+SOMF level calculations.

**Table 24.** Linear regression analysis of the functionals used in this study. Due to the chemical shift of $[Tc(CO)_3(OH_2)_3]^+$ being set to -869 ppm as a reference compound it has been excluded from the below analysis.

| XC | Relativistic | Slope | $R^2$ | Mean Absolute Deviation |
|---|---|---|---|---|
| BLYP | SOMF | 1.06 | 0.994 | 86 |
| | ZORA + SOMF | 1.08 | 0.993 | 66 |
| B3LYP | SOMF | 1.03 | 0.978 | 190 |
| | ZORA + SOMF | 1.06 | 0.993 | 127 |
| PW91 | SOMF | 1.10 | 0.980 | 104 |
| | ZORA + SOMF | 1.11 | 0.974 | 108 |
| B3PW91 | SOMF | 1.06 | 0.990 | 131 |
| | ZORA + SOMF | 1.08 | 0.992 | 90 |
| PBE | SOMF | 1.10 | 0.978 | 106 |
| | ZORA + SOMF | 1.11 | 0.973 | 107 |
| PBE0 | SOMF | 1.07 | 0.990 | 139 |
| | ZORA + SOMF | 1.09 | 0.992 | 94 |

Overall, chemical shifts were better predicted for compounds which have a similar chemical shift to our chosen reference compound, and which possess a single Tc center. Inclusion of ZORA became most necessary for two molecules in particular, $TcO_4^-$ and $[Tc(CO)_3(OH)]_4$. Examination of Table 23 or Figure 34 shows that there are three functionals, BLYP, B3PW91, and PBE0 that are much better than the others at predicting the chemical shift of $TcO_4^-$. This is particularly interesting for $TcO_4^-$ as it is the standard reference for experimental $^{99}$Tc NMR spectra and highlights the need to wisely choose a reference compound for DFT NMR calculations.

### 4.6.2 $^{99}$Tc NMR of trihydroxo species

In order to test the ability of the best performing computational methods against a compound of unknown experimental shift, we attempted to obtain an experimental $^{99}$Tc NMR spectrum for $[Tc(CO)_3(OH)_3]^{2-}$ and compute its chemical shift. Exposure of $[Tc(CO)_3Cl_3]^{2-}$ to an alkaline solution will allow substitution of chlorides with aqua ligands and hydroxides, producing $[Tc(CO)_3(OH_2)_2(OH)]$ and $[Tc(CO)_3(OH_2)(OH)_2]^-$ depending on solution alkalinity. Going to more alkaline conditions $(Et_4N)_2[Tc(CO)_3Cl_3]$ was dissolved in a 10 M caustic solution and a new $^{99}$Tc NMR shift was found experimentally at -1204 ppm.

In order to investigate the structure responsible for this spectral signal, the calculated chemical shift from the four best performing functionals, BLYP, B3LYP, B3PW91, and PBE0, was analyzed for three possible structures seen in Figure 35. Due to the large improvement seen in calculated chemical shift with inclusion of ZORA for $[Tc(CO)_3(OH)]_4$, which contains more than one Tc center, only the ZORA + SOMF level of theory is being considered. The chemical shift of $[Tc(CO)_3(OH)_3]^{2-}$ has calculated values of -1261 ppm (BLYP), -1424 ppm (B3LYP), -1336 ppm (PBE0), and -1325 ppm (B3PW91). The magnitude of the chemical shift is overestimated in all instances. This is in agreement with the results for the other $[Tc(CO)_3(OH_2)_{3-x}(OH)_x]1^{-x}$ species which are generally overestimated for BLYP, B3LYP, and PBE0.

While the error in chemical shift is within the range of error seen during validation of the computational method, other possible reaction products, seen in Figure 35, were considered. Literature precedence exists for $[Tc_2\mu\text{-}(OH)_3(CO)_6]^-$ with the Re analog, $[Re_2\mu\text{-}(OH)_3(CO)_6]^-$, and halide derivatives, $[Tc_2\mu\text{-}Cl_3(CO)_3]^-$ and $[Tc_2\mu\text{-}Br_3(CO)_3]^-$ being known (Alberto et al. 1994, Alberto et al. 1997, Zobi et al. 2008).

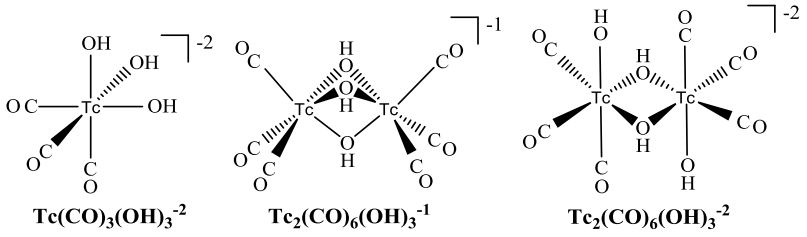


**Figure 35.** Possible reaction products of $(Et_4N)_2[Tc(CO)_3Cl_3]$ with 10 M NaOH / 5 M $NaNO_3$ caustic solution.

Technetium compounds with three strong $\pi$-backbonding ligands in a *fac* geometry with two bridging anionic ligands, [*trans*-$Tc_2\mu$-$Cl_2(CO)_4(NO)_2Cl_2$], also exist in the literature (Schibli et al. 2005) giving some precedence for [*trans*-$Tc_2\mu$-$(OH)_2(CO)_6(OH)_2]^{2-}$ as a possible structure. Calculations on these two structures were performed with unrestrained symmetry, and after averaging the chemical shift of the technetium centers, [$Tc_2\mu$-$(OH)_3(CO)_6$] gave chemical shifts of -1019 (BLYP), -1171 ppm (B3LYP), -1101 ppm (PBE0), and -1093 ppm (B3PW91). The chemical shifts for [$Tc_2\mu$-$(OH)_2(CO)_6(OH)_2]^{2-}$ were calculated as -1075 (BLYP), -1205 ppm (B3LYP), -1149 (PBE0), and -1146 (B3PW91). These values are summarized in Table 24. As expected, the $^{99}$Tc chemical shifts corresponding to the dimeric structures have a lower magnitude chemical shift than the mononuclear species. All values calculated for [*trans*-$Tc_2\mu$-$(OH)_2(CO)_6(OH)_2]^{2-}$ underestimate the experimentally observed value. While to a lesser degree [$Tc_2\mu$-$(OH)_3(CO)_6$] is also underestimated in all cases other than B3LYP which overestimates the value by a single ppm. This goes against the trend seen in Table 25 and Figure 23 in which BLYP, B3LYP, and PBE0 consistently overestimate the magnitude of chemical shift. While a definitive assignment is not possible due to the error displayed by the calculations, the trend of overestimation of $[Tc(CO)_3(OH_2)_{3-x}(OH)x]^{1-x}$ species by BLYP, B3LYP, and PBE0 suggest the mononuclear $[Tc(CO)_3(OH)_3]^{2-}$ as the most likely structure of the signal observed at -1204 ppm. Further empirical measurements will be necessary to unambiguously assign this species and are currently underway.

**Table 25.** Calculated chemical shift for possible products of the reaction of $[Tc(CO)_3Cl_3]^{2-}$ with 10 M caustic solution. For the purposes of this table, **1** = $[Tc(CO)_3(OH)_3]^{2-}$, **2** = [$Tc_2\mu$-$(OH)_3(CO)_6$], and **3** = [*trans*-$Tc_2\mu$-$(OH)_2(CO)_6(OH)_2]^{2-}$.

| XC | Relativistic | 1 | 2 | 3 |
|---|---|---|---|---|
| BLYP | ZORA+SOMF | -1261 | -1075 | -1019 |
| B3LYP | ZORA+SOMF | -1424 | -1205 | -1171 |
| B3PW91 | ZORA+SOMF | -1325 | -1146 | -1093 |
| PBE0 | ZORA+SOMF | -1336 | -1149 | -1101 |

# 5.0 References


Abram U and R Kirmse. 1993. "EPR Spectroscopy on Technetium Compounds. " *Radiochim. Acta* 63, pp. 139–143.

Alberto R, A Egli, U Abram, CK Hegetschweiler, V Gramlich, and PA Schubiger. 1994. "Synthesis and reactivity of $[NEt_4]_2[ReBr_3(CO)_3]$. Formation and structural characterization of the clusters $[NEt_4][Re_3(\mu_3\text{-}OH)(\mu\text{-}OH)_3(CO)_9]$ and $[NEt_4][Re_2(\mu\text{-}OH)_3(CO)_6]$ by alkaline titration. " *J. Chem. Soc., Dalton Trans.* pp. 2815−2820.

Alberto R, R Schibli, A Egli, PA Schubiger, WA Herrmann, G Artus, U Abram, and TA Kaden. 1995 "Metal-Carbonyl Syntheses .22. Low-Pressure Carbonylation of $[MOCl_4]^-$ and $[MO_4]^-$ - the Technetium(I) and Rhenium(I) Complexes $[NEt_4]_2[MCl_3(CO)_3]$" *J. Organomet. Chem.* 492, pp. 217-224.

Alberto R, R Schibli, D Angst, PA Schubiger, U Abram, and S Abram. 1997. "Application of technetium and rhenium carbonyl chemistry to nuclear medicine. Preparation of $[NEt_4]_2[TcCl_3(CO)_3]$ from $[NBu_4][TcO_4]$ and structure of [NEt4][$Tc_2$(μ-Cl)3(CO)6]; structures of the model complexes $[NEt_4][Re_2(\mu\text{-}OEt)_2(\mu\text{-}OAc)(CO)_6]$ and $[ReBr(\{\text{-}CH_2S(CH_2)_2Cl\}_2)(CO)_3]$." *Transition Met. Chem.* 22, pp. 597−601.

Alberto R, R Schibli, A Egli, U Abram, S Abram, TA Kaden, and PA Schubiger. 1998. "Steps towards $[(C_5Me_5)TcO_3]$: Novel synthesis of $[(C_5Me_5)Tc(CO)_3]$ from $[\{Tc(\mu^3\text{-}OH)(CO)_3\}_4]$ and oxidation of $[(C_5Me_5)M(CO)_3]$ (M = Tc, Re) with $Br_2$. " *Polyhedron* 17(7), pp. 1133-1140.

Astheimer L, J Hauck, HJ Schenk, and K Schwochau. 1975. "Tetraoxo Anions of Hexavalent Technetium and Rhenium." *J. Chem. Phys*. 63, pp. 1988-1991.

Chatterjee SD, Hall GB, TG Levitskaia, ED Walter and NM Washton. 2015. *Oxidative Stability of Tc() Tricarbonyl Species Relevant to Hanford Tank Waste: FY 2016 Status Report*. PNNL-25076, EMSP-RPT-033, Pacific Northwest National Laboratory, Richland, WA.

Cho H, WA de Jong, BK McNamara, BM Rapko, and IE Burgeson. 2004. "Temperature and Isotope Substitution Effects on the Structure and NMR Properties of the Pertechnetate Ion in Water. " *J. Am. Chem. Soc*. 126, 11583-11588.

Colton R. 1962. "Technetium Chloride." *Nature* 193, pp. 872-873.

Colton R and IB Tomkins. 1968. "Halides and Oxide Halides of Technetium. I. Technetium (V) Oxide Halides and the Reaction of Thionyl Chloride with Ammonium Pertechnetate." *Aust. J. Chem*. 21, pp. 1981-1985.

DeAngelis TP and WR Heineman, 1976 " An electrochemical experiment using an optically transparent thin layer electrode," *J. Chem. Educ.* 53, pp. 594-596.

Deutsch E, WR Heineman, R Hurst, JC Sullivan, WA Mulac, and S Gordon. 1978. "Production, Detection, and Characterization of Transient Hexavalent Technetium in Aqueous Alkaline Media by Pulse Radiolysis and Very Fast Scan Cyclic Voltammetry." *J. Chem. Soc. Chem. Comm*. pp. 1038-1040.

Duncan JB, SE Kelly, RA Robbins, RD Adams, MA Thorson, and CC Haass. 2011. *Technetium Sorption Media Review*. RPP-RPT-S0122, Rev. 0, Washington River Protection Solutions, LLC, Richland, WA.

Franklin KJ, CJL Lock, BG Sayer, and GJ Schrobilgen. 1982. "Chemical Applications of Technetium-99 NMR Spectroscopy: Preparation of Novel Technetium(VII) Species and Their Characterization by Multinuclear NMR Spectroscopy." *J. Am. Chem. Soc.* 104(20), pp. 5303-5306.

Gorshkov NI, AA Lumpov, AE Miroslavov, and DN Suglobov. 2000. "Synthesis of $[Tc(CO)_3^+ \bullet (H_2O)_3]^+$ ion and investigation of its reaction with hydroxyl ion in the aqueous solutions. " *Radiochemistry*, 45(2), pp. 116-119.

Hall GB, SD Chatterjee, TG Levitskaia, T Martin, NA Wall, and ED Walter. 2015. *Synthesis and Characterization of Tc(I) Carbonyl Nitrosyl Species Relevant to the Hanford Tank Waste: FY 2016 Status Report.* PNNL-24916, EMSP-RPT-030, Pacific Northwest National Laboratory, Richland, WA.

Hall GB, A Andersen, NM Washton, SD Chatterjee and TG Levitskaia. 2016. "Theoretical Modeling of 99Tc NMR Chemical Shifts. " *Inorg. Chem.* 55, pp. 8341-8347.

Hurst RW. "Part I. Carbon and Mercury-Carbon Optically Transparent Electrodes. Part II. Investigation of Redox Properties of Technetium by Cyclic Voltammetry and Thin Layer Spectroelectrochemistry." Ph.D. dissertation (University of Cincinnati, Cincinnati, Ohio, 1980), 198 pp.

Kissel G and SW Feldberg. 1969. "Disproportionate of the Technetate Ion in Aqueous Alkaline Media. An Electrochemical Study." *J. Phys. Chem.* 73, pp. 3082-3088.

Kissinger PT and WR Heineman, 1996 "Laboratory Techniques in Electroanalytical Chemistry," 2nd ed., *Dekker: New York*, pp. 73− 76.

Kramer DJ, A Davison, AG Jones. 2001. "Structural models for $[M(CO)_3(H_2O)_3]^+$ (M=Tc, Re): fully aqueous synthesis of technetium and rhenium tricarbonyl complexes of tripodal oxygen donor ligands." *Inorg. Chim. Acta* 312, pp. 215-220.

Krychkov SV, AK Pikaev, AF Kuzina, and VI Spitsyn. 1979. "Electrolytic Dissociation of Technetic Acid in Aqueous Solution by Pulsed Radiolysis." *Proc. Acad. Sci. USSR, Phys. Chem. Sect*. (Engl, trans.) 247, pp. 690-692.

Levitskaia TG, A Andersen, SD Chatterjee, GB Hall, ED Walter, and NM Washton. 2015. *Spectroscopic Properties of Tc(I) Tricarbonyl Species Relevant to the Hanford Tank Waste*. PNNL-25000, EMSP-RPT-032, Pacific Northwest National Laboratory, Richland, WA.

Levitskaia TG, A Andersen, SD Chatterjee, HM Cho, JM Peterson, BM Rapko, ED Walter, and NM Washton. 2014. *Speciation and Oxidative Stability of Alkaline Soluble, Non-Pertechnetate Technetium*. PNNL- 23654, EMSP-RPT-024, Pacific Northwest National Laboratory, Richland, WA.

Levitskaia TG, S Chatterjee, NK Pence, J Romero, T Varga, MH Engelhard, Y Du, L Kovarik, BW Arey, ME Bowden and ED Walter. 2016. "Inorganic Tin Aluminophosphate Nanocomposite for Reductive Separation of Pertechnetate." *Environ. Sci. Nano.* 3(5), pp.1003-1013

Lukens WW, JJ Bucher, NM Edelstein, and DK Shuh. 2002. "Products of Pertechnetate Radiolysis in Highly Alkaline Solutions: Structure of $TcO_2.xH_2O$." *Environ. Sci. Technol.* 36, pp. 1124-1129.

Lukens WW, DK Shuh, NC Schroeder, and KR Ashley. 2004. "Identification of the Non-Pertechnetate Species in Hanford Waste Tanks, Tc(I)-Carbonyl Complexes." *Environ. Sci. Technol.* 38(1), pp. 229-33.

Majumdar SK, RA Pacer and CL Rulfs. 1969. "Rhenium and Technetium (VI) and Meso (VII) Species." *J. Inorg. Nucl. Chem*. 31, pp. 33- 41.

Neese F. 2012. "The ORCA program system." *Wiley Interdiscip. Rev. Comput. Mol. Sci.* 2, pp. 73−78.

Osborne DW, F Schreiner, K Otto, JG Malm, and H. Selig. 1977. "Heat Capacity, Entropy, and Gibbs Energy of Technetium Hexafluoride Between 2.23 and 350 K; Magnetic Anomaly at 3.12 K; Mean β Energy of $^{99}$Tc." *J. Chem. Phys*. 68, pp. 1108-1118.

Pilbrow JR. 1996. "ESR Fundamentals." *Appl. Radiat. Isot.* 47, pp. 1465-1470.

Rapko BM, SA Bryan, JL Bryant, S Chatterjee, MK Edwards, JY Houchin, TJ Janik, TG Levitskaia, JM Peterson, RA Peterson, SI Sinkov, FN Smith, and RS Wittman. 2013a. *Development of a Chemistry-Based, Predictive Method for Determining the Amount of Non-Pertechnetate Technetium in the Hanford Tanks: FY 2012 Progress Report*. PNNL-22173, Pacific Northwest National Laboratory, Richland, WA.

Rapko BM, SA Bryan, S Chatterjee, TG Levitskaia, MK Edwards, JM Peterson, RA Peterson, and SI Sinkov. 2013b. *Investigations into the Nature of Alkaline Soluble, Non-Pertechnetate, Technetium*. PNNL-22957, EMSP-RPT-018, Pacific Northwest National Laboratory, Richland, WA.

Rard JA, MH Rand, G Anderegg, and H Wanner. 1999. *Chemical Thermodynamics of Technetium*, edited by M. C. A. Sandino and E. Östhols (North Holland/Elsevier, Amsterdam, 1999).

Rard JA. 1983. *Critical Review of the Chemistry and Thermodynamics of Technetium and Some of Its Inorganic Compounds and Aqueous Species*. Lawrence Livermore National Laboratory, Manuscript, UCRL-53440.

Rard JA. 2005. "Current Status of the Thermodynamic Data for Technetium and Its Compounds and Aqueous Species." *J. Nuc. Radiochem. Sci*. 6(3), pp. 197-204.

Rehr JJ, RC Albers and SI Zabinsky. 1992 “High-order multiple-scattering calculations of x-ray-absorption fine structure,” *Phys. Rev. Lett.* 69, pp. 3397-3400.

Scheele RD, DE Kurath, and GN Brown. 2009. *Scale-Up, Production, and Procurement of PEP Simulants*. PNNL-18678, WTP-RPT-204, Rev 0, Pacific Northwest National Laboratory, Richland WA.

Schibli R, N Marti, P Maurer, B Spingler, M-L Lehaire, V Gramlich, and CL Barnes. 2005. "Syntheses and characterization of dicarbonyl-nitrosyl complexes of technetium(I) and rhenium(I) in aqueous media: spectroscopic, structural, and DFT analyses." *Inorg. Chem.* 44 (3), pp. 683-690.

Schroeder NC, SD Radzinski, KR Ashley, AP Truong, and PA Sczcepaniak. 1998. "Science and Technology for Disposal of Radioactive Tank Wastes." Schulz WW and Lombardo NJ, Eds.; Plenum Press: New York; pp. 301-320.

Schroll CA, S Chatterjee, WR Heineman and SA Bryan. 2012. "Thin Layer Spectroelectrochemistry on an Aqueous micro-Drop." *Electroanalysis* 24(5), pp. 1065 – 1070.

Selig K and JG Malm. 1962. "The Vapor-Pressure and Transition Points of $TcCl_6$." *J. Inorg. Nucl. Chem*. 24, pp. 641-644.

Serne RJ, BM Rapko, and IL Pegg. 2015. *Technetium Inventory, Distribution, and Speciation in Hanford Tanks*. PNNL-23319, Rev. 1; EMSP-RPT-022, Rev. 1, Pacific Northwest National Laboratory, Richland, WA.

Takayama T, Y Kani, T Sekine, H Kudo, and K Yoshihara. 1995. "Formation of nitridotechnetium(VI) u-oxo dimer complexes with EDTA and EDDA." *J. Radioanal. Nucl. Chem.* 199, pp. 217-227.

Thompson M, AD Nunn and EN Treher. 1986. "X-ray Photoelectron Spectroscopy of Potential Technetium-Based Organ Imaging Agents." *Anal. Chem.* 58, pp. 3100-3103.

Wester DW, DH White, FW Miller, RT Dean, JA Schreifels, and JE Hunt. 1987. "Synthesis and Characterization of Technetium Complexes with Phosphorus containing Ligands. The Homoleptic Trimethylphosphite, Dimethylmethylphosphonite and Methyldiethylphosphinite Technetium(I) Cations. " *Inorg. Chim. Acta* 131, pp. 163-169.

Zobi F, B Spingler, and R Alberto, 2008. "Syntheses, Structures and Reactivities of $[CpTc(CO)_3X]^+$ and $[CpRe(CO)_3X]^+$." *Eur. J. Inorg. Chem.* pp. 4205−4214.

# Appendix A

The detailed assignments of the products obtained in **Parr Reactions 1** and **5** are included in the main body. The assignments for the rest of the Parr reactions are included here.

## Parr Reaction 2

*Reaction conditions: 10 mM $TcO_4^-$ in simulant containing noble metals pressurized to 1300 psi with CO containing 75 ppm $H_2$ at 80C for 10 days*

The chemical reduction of $TcO_4^-$ in the simulant solution *in presence of noble metals in the absence of gluconate* was conducted in FY 2015. Upon completion of the 10-day reaction, the product was observed to contain a greenish-brown precipitate and a brown solution. Based on $^{99}$Tc NMR of the resultant solution and assuming no or very little partitioning of $TcO_4^-$ into the solid fraction, it was determined that ~88% of the total $TcO_4^-$ had been reduced. Initial NMR analysis of the liquid fraction revealed a single new resonance at -1092 ppm, in addition to the $TcO_4^-$ resonance at 0 ppm. The former resonance was attributed to a $[Tc(CO)_3]^+$ species, and initially contributed 72% of the total Tc in the liquid fraction. The overall NMR active Tc in the liquid fraction was 84% of the starting Tc (combination of $TcO_4^-$ and $Tc(CO)_3^+$), while the rest was present either in the solid or as a NMR inactive species in the liquid fraction. Over the course of 330 days, the entire $[Tc(CO)_3]^+$ species in the liquid fraction decomposed to $TcO_4^-$ as observed by NMR. Further, a total amount of 7% of the non-NMR active Tc was also decomposed to Tc(VII) within that period. EPR spectra were inconclusive in determining the nature of the non-NMR active species both in the solution as well as in the solid fraction.

Therefore, complementary XAS and XPS measurements were attempted in FY 2016 to gain insight into the different species present in the solid fraction. The XAS spectrum of the solid fraction can be represented by a combination of the individual spectra of pure Tc(VII), Tc(IV) and Tc(I) compounds. It is observed that using $TcO_2 \cdot xH_2O$ as the dominating Tc(IV) component with 58% contribution, and $[Tc(CO)_3(H_2O)_2(OH)]$ and $TcO_4^-$ as the Tc(I) and Tc(VII) components with 13 and 29% contributions results in an excellent fit to both the XANES and the EXAFS regions as shown in Figure 36, and the fit parameters are given in Table 26.

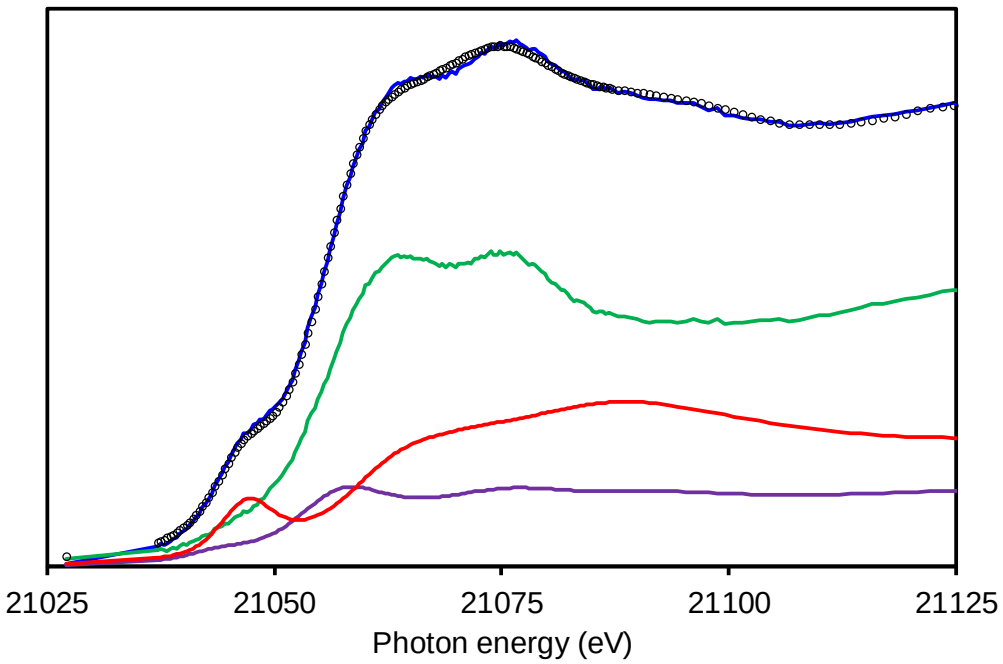


**Figure 36.** Tc K-edge XANES spectrum and fit for the solid fraction of **Parr Reaction 2** product. Circles: experimental data; blue trace: calculated fit obtained using $[Tc(CO)_3(H_2O)_3]^+$ as the Tc(I) species, $TcO_2 \bullet xH_2O$ as the Tc(IV) species, $TcO_4^-$ as the Tc(VII) species; violet trace: contribution from $[Tc(CO)_3(H_2O)_3]^+$; green trace: contribution from $TcO_2 \bullet xH_2O$; red trace: contribution from $TcO_4^-$.

**Table 26.** Tc K-edge XANES results for the solid fraction of **Parr Reaction 2** product.[a]

| Tc(I) | σ | p | $TcO_2 \bullet xH_2O$ | σ | p | $TcO_4^-$ | σ | p |
|---|---|---|---|---|---|---|---|---|
| 0.13 | 0.03 | 0.023 | 0.58 | 0.03 | 0.0 | 0.29 | 0.02 | 0.0 |

a) Standard deviation of the fit is given as σ. The value of p is the probability that the improvement to the fit from including this spectrum is due to noise. Components with $p < 0.05$ are significant at the two-sigma level and those with $p < 0.01$ are significant at the 3 sigma level.

The photoelectron spectrum of the solid product can be resolved into three different Tc chemical species with lower binding energies (assigned to Tc $3d_{3/2}$ lines) at 254.7 eV, 256.4 eV and 259.1 eV. Based on the Technetium $3d_{5/2}$ binding energies reported in literature, these are assigned to Tc(I), Tc(IV) and Tc(VII) oxidation states respectively. It is important to note that the mobile Tc(I) and Tc(VII) are retained in the solid fraction, similar to that observed in **Parr Reaction 1**. Their presence can presumably be explained by the presence of some interstitial liquid that gets trapped within the solids. The presence of Tc(I) species is particularly worth noting as it suggests that while the species in solution is susceptible to oxidation, it being present within the solid phase enhances its stability. Presumably, some of the components of the solid are responsible for stabilizing Tc in the reduced oxidation states for long lengths of time when there is physical contact.

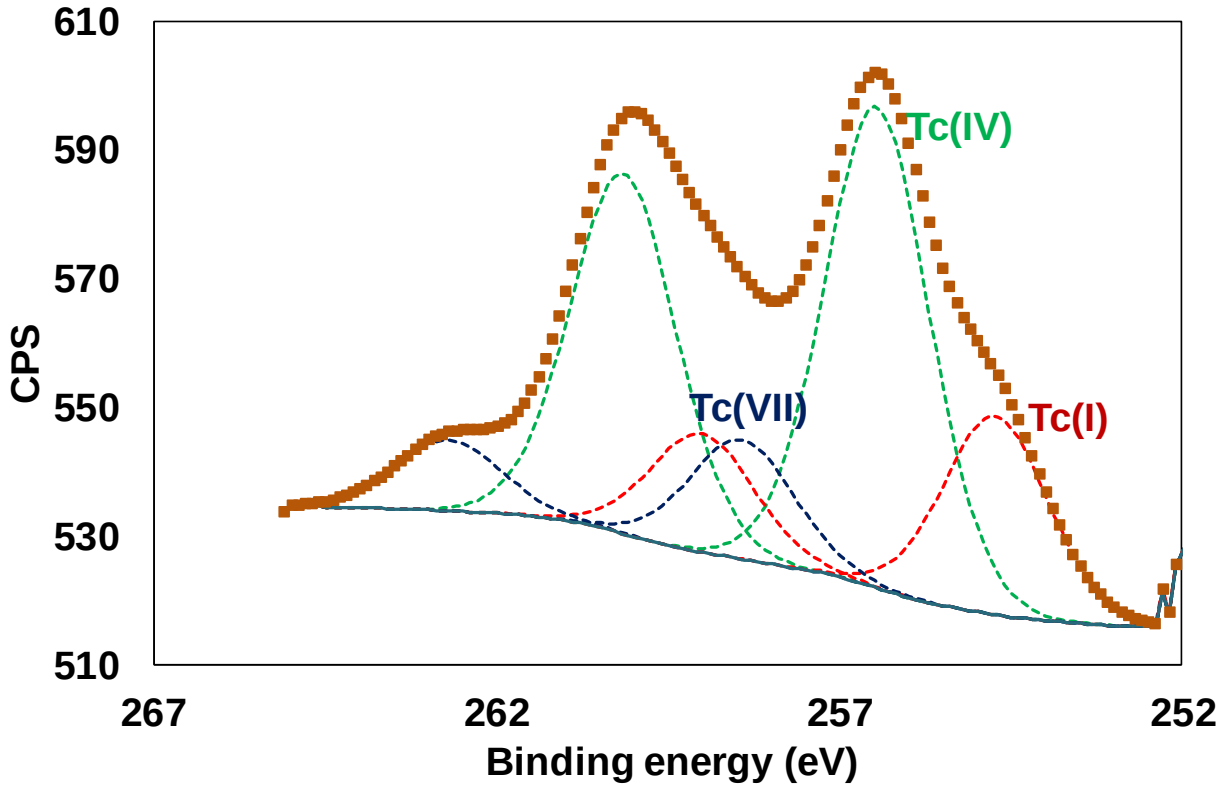


**Figure 37.** X-ray photoelectron spectrum of Tc $3d_{5/2}$ and $3d_{3/2}$ regions for the solid fraction of **Parr Reaction 2** product. Brown squares: experimental spectrum, red trace: Tc(I) fit, green trace: Tc(IV) fit, dark blue trace: Tc(VII) fit.

## Parr Reaction 3

*Reaction conditions: 10 mM $TcO_4^-$ in simulant containing 100 mM gluconate pressurized to 1300 psi with CO containing 75 ppm $H_2$ at 80°C for 10 days.*

The product obtained from the chemical reduction of $TcO_4^-$ in the simulant solution in the presence of CO and gluconate and in the absence of noble metals was observed to consist of a liquid-only phase with a wine-red color. LSC results indicated 100% retention of Tc in the liquid fraction, while $^{99}$Tc NMR revealed that 25% of the initial $TcO_4^-$ remained non-reduced after termination of the 10-day reaction. NMR measurement showed a single resonance attributed to $TcO_4^-$. Absence of any other Tc resonances suggested the formation of paramagnetic Tc reduction products Tc(IV and/or VI). The EPR spectrum of the reaction solution showed a 10-line resonance that was assigned to a highly symmetric Tc(VI) or Tc(II) species based on its g-value, line-width and hyperfine splittings. Based on similarity of the hyperfine splittings with the product obtained from **Parr Reaction 1**, as well as from the electrochemically generated Tc(VI) species, this is assigned to be a Tc(VI) product. The oxidation state such as Tc(IV) was considered less likely due to narrow line widths, which strongly suggest a system with an electronic spin of ½. Based on EXAFS data collected by Lukens and coworkers on a series of Tc(IV) complexes (Lukens et al. 2002), Tc(IV) under similar conditions should have a coordination number of six. Due to the large d-orbital splitting commonly associated with second and third row transition metals, Tc in such a

pseudo octahedral field should provide a system in which the electron spin is greater than ½ (Lukens et al. 2002). Such S > ½ systems result in broad hyperfine signals due to interaction between the electron spins, and Tc(IV) complexes were therefore regarded unlikely to be present in this solution.

The non-pertechnetate species exhibited remarkable stability when the solution was unprotected from exposure to air and light, undergoing only 13% further decomposition over the next 12 months. The monitoring was continued throughout FY 2016, where the non-pertechnetate species retained its stability, undergoing only a ~6% additional decomposition to $TcO_4^-$. This result strongly supports our hypothesis based on observations from FY 2015 that the stable non-pertechnetate species in the intermediate oxidation states could exist in Hanford tank waste supernatants.

In order to gain further insight into the nature of the species present in the **Parr Reaction 3** liquid phase, XAS analysis of the sample was performed. For recording the X-ray absorbance spectra, the liquid was allowed to evaporate, and a spectrum of the dried solid was collected. Although XAS of Tc(VI) is rarely observed, the obtained spectra contained no component that can be attributed to any species other than a combination of Tc(VII) and Tc(IV) species and very minor contributions from Tc(I). While this is surprising based on the strong presence of paramagnetic non-Tc(IV) species as detected by EPR spectroscopy, this is in keeping with the observation that Tc(VI) species is hard to observe in dried state as observed in **Parr Reaction 1**. This is presumably suggestive of the reduction/disproportionation of the observed Tc(VI) in the reaction solution to Tc(IV) either upon drying or in the presence of the X-ray beam.

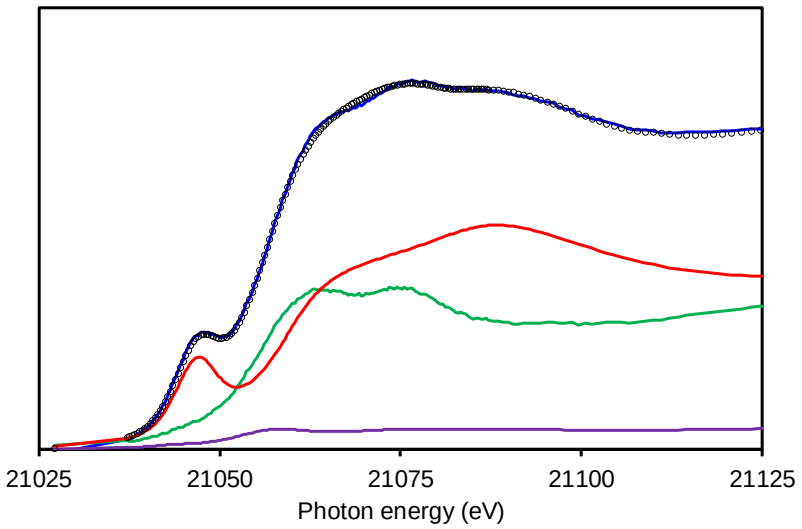


**Figure 38.** Tc K-edge XANES spectrum and fit for the solid fraction of **Parr Reaction 3** product. Circles: experimental data; blue trace: calculated fit obtained using $[Tc(CO)_3(H_2O)_3]^+$ as the Tc(I) species, $TcO_2 \bullet nH_2O$ as the Tc(IV) species, and $TcO_4^-$ as the Tc(VII) species; violet trace: contribution from $[Tc(CO)_3(H_2O)_3]^+$; green trace: contribution from $TcO_2 \bullet nH_2O$; red trace: contribution from $TcO_4^-$.

**Table 27.** Tc K-edge XANES results for the solid fraction of **Parr Reaction 3** product.[a)]

| Tc(I) | σ | p | $TcO_2$•x$H_2O$ | Σ | p | $TcO_4^-$ | σ | p |
|---|---|---|---|---|---|---|---|---|
| 0.06 | 0.03 | 0.046 | 0.44 | 0.02 | 0.0 | 0.59 | 0.02 | 0.0 |

a) Standard deviation of the fit is given as σ. The value of p is the probability that the improvement to the fit from including this spectrum is due to noise. Components with $p < 0.05$ are significant at the two-sigma level and those with $p < 0.01$ are significant at the 3 sigma level.

The photoelectron spectrum was obtained on a sample that was deposited on a carbon tape and allowed to dry out. The spectrum can be resolved into three different Tc chemical species with lower binding energies (assigned to Tc $3d_{3/2}$ lines) at 256.3 eV, 257.6 eV and 259.0 eV respectively. Based on the Tc $3d_{5/2}$ binding energies reported in literature, these are tentatively assigned to Tc(IV), Tc(VI) and Tc(VII) oxidation states respectively. The resulting fit parameters are given in Table 27. As observed in previous cases, there is very little contribution from the Tc(VI) fraction in both the XAS and XPS spectra. This is even more significant here, as EPR spectra reveals that the Tc(VI) not only is the dominant Tc species in this solution only product, but EPR also shows the Tc(VI) species is remarkably stabile with almost no decomposition even after two years of monitoring. This in fact provides strong support suggesting that the Tc(VI) species indeed undergoes decomposition to other Tc valence species upon evaporation.

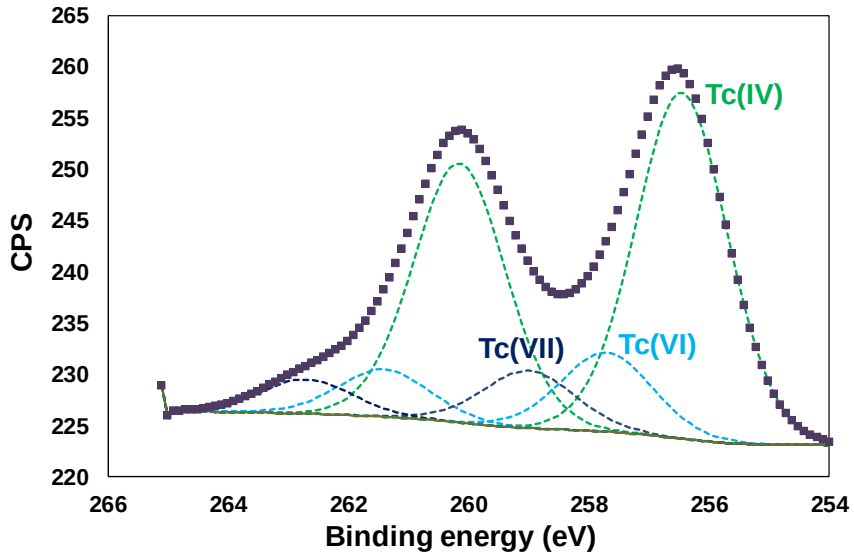


**Figure 39.** X-ray photoelectron spectrum of Tc $3d_{5/2}$ and $3d_{3/2}$ regions for the solid fraction of **Parr Reaction 3** product. Black squares: experimental spectrum, green trace: Tc(IV) fit, light blue trace: Tc(VI) fit, dark blue trace: Tc(VII) fit.

## Parr Reaction 4

*Reaction conditions: 10 mM $TcO_4^-$ in simulant pressurized to 1350 psi with CO containing 75 ppm $H_2$ at 80°C for 10 days*

The product obtained from this chemical reduction of $TcO_4^-$ in tank supernatant simulant solution in presence of CO and *the absence of gluconate and noble metals* was observed to consist of a mixture of phases having a greenish-brown precipitate and brown supernatant. LSC counting results suggested about 18% of the total Tc to be present in the liquid fraction while the rest (82%) was present in the solid phase. Of the 18% present in the liquid phase, 11% was observed to be converted to the $[Tc(CO)_3]^+$ species $[Tc(CO)_3(H_2O)_2(OH)]$ characterized by a resonance in the $^{99}Tc$ NMR spectrum observed at -1075 ppm. Monitoring of kinetic stability of this liquid sample indicated a complete oxidation of solution Tc to $TcO_4^-$ within 50 days. Additionally, over a period of 200 days, 27% of the Tc present in the solid fraction was converted to solution phase $TcO_4^-$ as indicated by the enhancement of Tc intensity. The EPR spectra were inconclusive in determining the nature of the NMR inactive species both in solution as well as in the solid fraction.

The photoelectron spectrum of the solid fraction of the product was obtained on a sample that was deposited on a carbon tape and allowed to dry out. It can be resolved into two different Tc chemical species with lower binding energies (assigned to Tc $3d_{3/2}$ lines) at 256.4 eV and 259.1 eV, respectively. Based on the Technetium $3d_{5/2}$ binding energies reported in literature, these are tentatively assigned to Tc(IV) and Tc(VII) oxidation states, respectively.

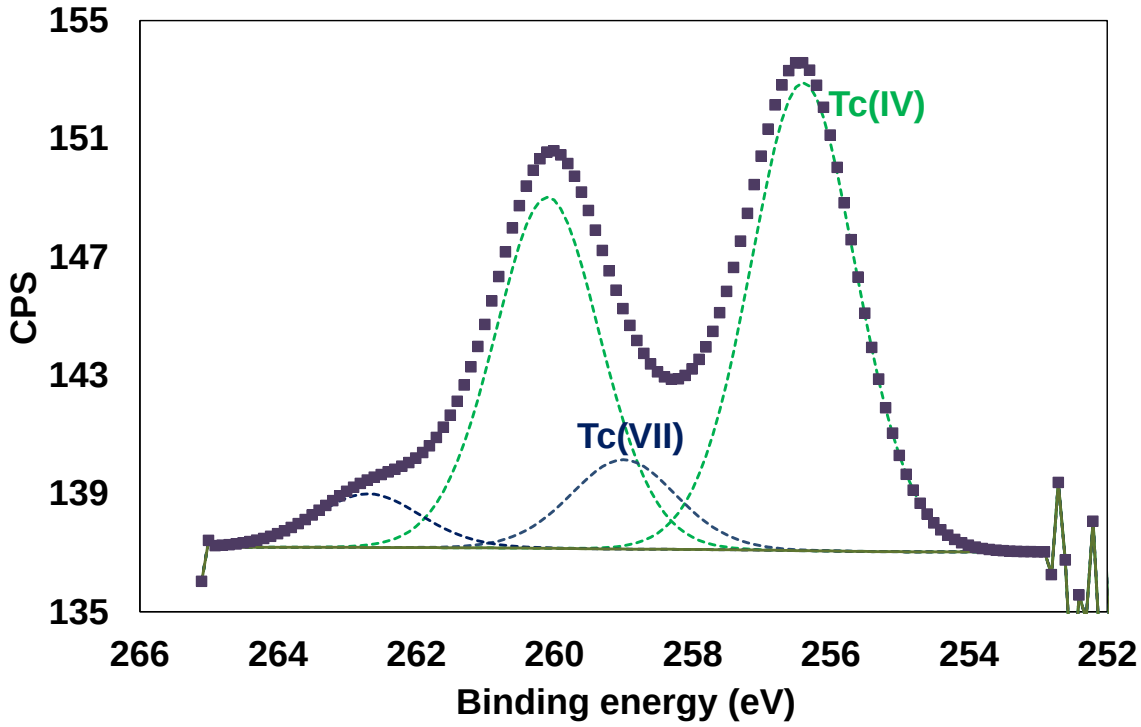


**Figure 40.** X-ray photoelectron spectrum of Tc $3d_{5/2}$ and $3d_{3/2}$ regions for the solid fraction of **Parr Reaction 4** product. Black squares: experimental spectrum, green trace: Tc(IV) fit, dark blue trace: Tc(VII) fit.

## Parr Reaction 6

*Reaction conditions: 10 mM $TcO_4^-$ in simulant containing 100 mM gluconate and noble metals pressurized to 250 psi with CO containing 75 ppm $H_2$ at room temperature for 14 days*

To determine the effect of temperature on the nature of the Parr reaction product, a control reaction was performed where the $TcO_4^-$ solution was subjected to a pressure of 250 psi under CO for 14 days in tank supernatant waste simulant in presence of noble metals at room temperature. The reaction generated a liquid only product having a pink-red color. $^{99}$Tc NMR showed that the 14-d reaction solution contained 75% $TcO_4^-$, indicating reduction of only 25% of the starting Tc. The EPR spectrum of the liquid collected at 125 K exhibits two distinct regions. The low field end of the spectrum has a single signal around 1,600 Gauss and based on its g-value and similarity with the EPR observed for the Parr product formed under similar conditions at 80C, is attributed to Fe clusters. The high-field portion of the spectrum shows a single spectral signature at approximately 3100 Gauss, displaying a 10-line $^{99}$Tc signal. Lowering the temperature to 4K has no discernible effect on the spectra. Based on the fact that the spectra is observed at a high temperature of 125 K, coupled with the narrow line width, suggests that this pattern is unlikely to be caused by a Tc(IV) species and is more likely to originate from a s=1/2 species such as Tc(II) or Tc(VI). Based on the similarity of the EPR spectra with that from the Tc(VI) product obtained in either of **Parr Reactions 1, 3** or **5**, this is assigned to be originating from a Tc(VI) species. It is worth mentioning that the species is highly unstable and decomposes completely to $TcO_4^-$ within a period of 7 days.

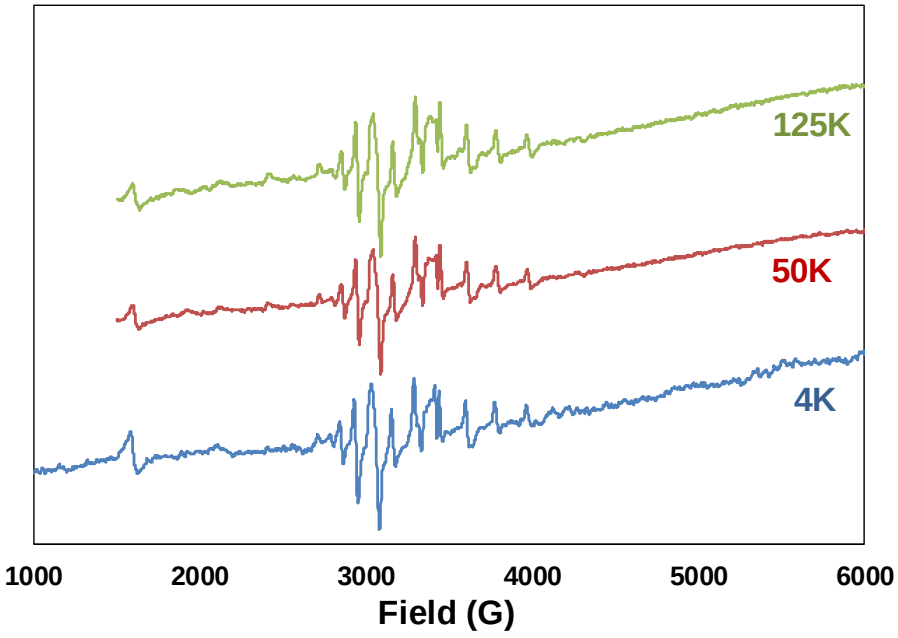


**Figure 41.** $^{99}$Tc EPR spectra of the liquid fractions of the CO/$H_2$-reacted pseudo-Hanford tank supernatant simulant (composition of the simulant is given in Table 1) containing 0.1 M gluconate and catalytic noble metals measured at (green trace) 125 K, (red trace) 50 K and (blue trace) 4 K.

## Parr Reaction 7

*Reaction conditions: 10 mM $TcO_4^-$ in simulant containing 100 mM gluconate and noble metals under ambient pressure of CO containing 75 ppm $H_2$ at 80°C for 21 days*

To determine the effect of pressure on the nature of the Parr reaction products, a control reaction was performed where the $TcO_4^-$ solution was exposed to a positive pressure of CO for 30 minutes. Subsequently, the reaction was conducted under ambient pressure for 21 days in tank-waste simulant in presence of noble metals at 80°C. The reaction resulted in a dirty brown solid and brown solution. $^{99}$Tc NMR of the liquid fraction showed 80% of reactant Tc remained in the form of $TcO_4^-$, which was the starting Tc species. This suggests that 20% of the starting Tc was converted to an NMR inactive fraction in the liquid fraction, or was entrapped in the solid phase EPR of either the liquid or the solid fractions did not provide any conclusive information on the Tc speciation in either phase.

The photoelectron spectrum of the liquid fraction showed a broad band that can be resolved into multiple peaks (Figure 42). The band could tentatively be assigned to a Tc chemical species with a lower binding energy of 256.3 eV, which can be tentatively assigned to a Tc(IV) species based on literature values. It should be noted that this assignment is speculative, and more characterizations are required for an accurate assignment of the non-pertechnetate species generated in this reaction.

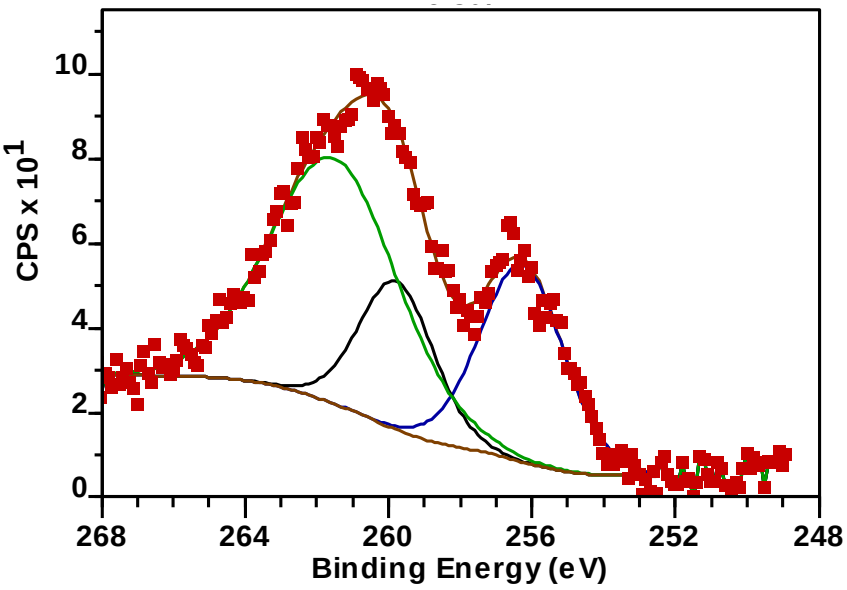


**Figure 42.** X-ray photoelectron spectrum of Tc $3d_{5/2}$ and $3d_{3/2}$ regions for the liquid fraction of **Parr Reaction 7** product. Red squares: experimental spectrum, blue trace: Tc(IV) fit, green trace: Re impurity, dark brown trace: baseline for the fit, light brown trace: best fit combination of Tc valence state reference compounds.

## Parr Reaction 8

*Reaction conditions: 10 mM $TcO_4^-$ in Hanford tank supernatant simulant containing 100 mM gluconate, noble metals and 30 mM $CrO_4^{2-}$ pressurized to 1350 psi with CO containing 75 ppm $H_2$ at 80 °C for 21 days*

To study the effect of an oxidant that is common in Hanford tank supernatants, such as $CrO_4^{2-}$, the chemical reduction step consisted of subjecting the $TcO_4^-$ solution to a temperature of 80°C and pressure of 250 psi under CO for 21 days in the tank-supernatant waste simulant in presence of noble metals and $CrO_4^{2-}$. The reaction generated a brownish-green liquid and minute quantities of a black solid. The LSC counting of the reaction mixture revealed 95% of the starting Tc was in the liquid phase, suggesting that the rest (5%) was present in the solid phase. The solution was analyzed using NMR and EPR spectroscopies. $^{99}$Tc NMR spectrum of the liquid fraction revealed complete reduction of starting $TcO_4^-$, indicated by the complete absence of the $TcO_4^-$ resonance at about 0 ppm. The NMR signal is dominated by resonances characteristic of a $[Tc(CO)_3]^+$ species, showing four resonances at -1094, -1162, -1256 and -1270 ppm, as shown in Figure 43. While the resonance at -1094 ppm was observed in the **Parr Reaction 5** product obtained under the same reaction conditions in the absence of $CrO_4^{2-}$, the resonance at -1162 was not observed in Parr reaction 5. Also, the resonances at -1256 and -1270 ppm are slightly shifted from that observed in the reaction in absence of $CrO_4^{2-}$. This is suggestive that introduction of Cr(VI) results in changes in the chemical environment. It should be noted that the changes in observed chemical shifts can be a consequence of generation a paramagnetic species in Cr(III) through the reduction of Cr(VI) under the reducing reaction environment.

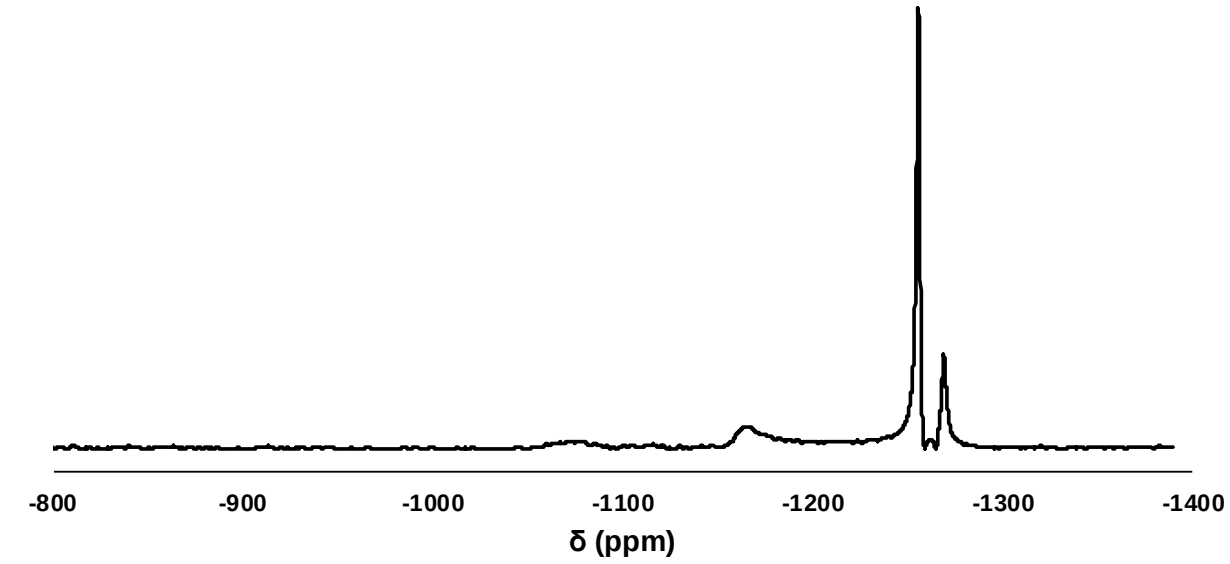


**Figure 43.** $^{99}$Tc NMR spectrum of the liquid fraction of **Parr Reaction 8** product showing the resonances corresponding to $[Tc(CO)_3]^+$•gluconate species

The EPR spectrum on the liquid fraction does not provide any conclusive results. On the other hand, the EPR spectrum of the solid fraction, shown in Figure 44, collected at 3.8 K shows a broad band centered around ~3300 G, that can be approximately resolved into a 10-line spectrum. Based on the

broadness and the hyperfine splittings, this can be tentatively assigned to a Tc(IV) species. The g-value and hyperfine splitting of this spectrum matches closely to that previously reported for $TcO_2$ prepared in a variety of ways (Lukens et al. 2002).

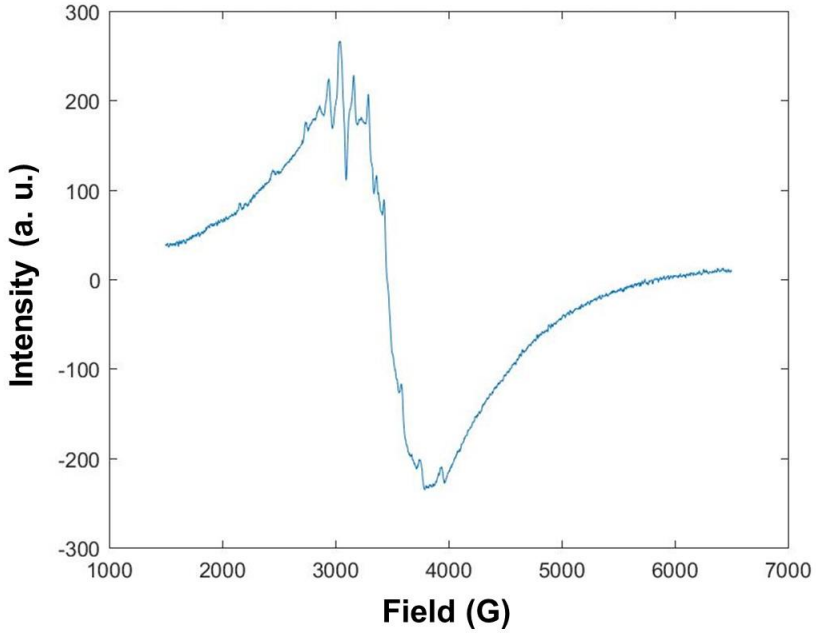


**Figure 44.** $^{99}$Tc EPR spectra of the solid fraction of **Parr Reaction 8** product containing 0.1 M gluconate, catalytic noble metals and 30 mM $CrO_4^{2-}$ measured at 3.8 K.

The photoelectron spectrum of the liquid fraction of **Parr Reaction 8** was obtained by depositing a few drops on a carbon platform and allowing the liquid to evaporate off. The spectrum can be resolved into a single Tc chemical species with lower binding energy (assigned to Tc $3d_{3/2}$ lines) at 255.6 eV (Figure 45). Its binding energy is slightly greater than the spectra of the solid generated in the absence of $CrO_4^{2-}$ (**Parr Reaction 5)**, suggesting a slightly different, more electron deficient chemical environment for the Tc(I) center than observed in the **Parr Reaction 5** solid. Based on the Technetium $3d_{5/2}$ binding energies reported in literature, this again is tentatively assigned to a Tc(I) oxidation state. A shoulder with a lower binding energy at 261.6 eV is also observed. However, the binding energy gap between this and its nearest neighboring peak at 269.6 eV is far greater than that expected between Tc $3d_{5/2}$ and $3d_{3/2}$ lines. Therefore, it is presumably attributed to be caused by some other elemental impurities such as Re. No Tc(VI) or other oxidation states are observed in the XPS spectra. This absence of Tc(VI) in the XPS seemingly contradicts the results obtained from EPR, and mirrors the observations in the reaction done under similar conditions at 1300 psi. This again supports the fact that, since XPS spectra were recorded on dried samples, the procedure of drying may be responsible for decomposition or disproportionation of Tc(VI).

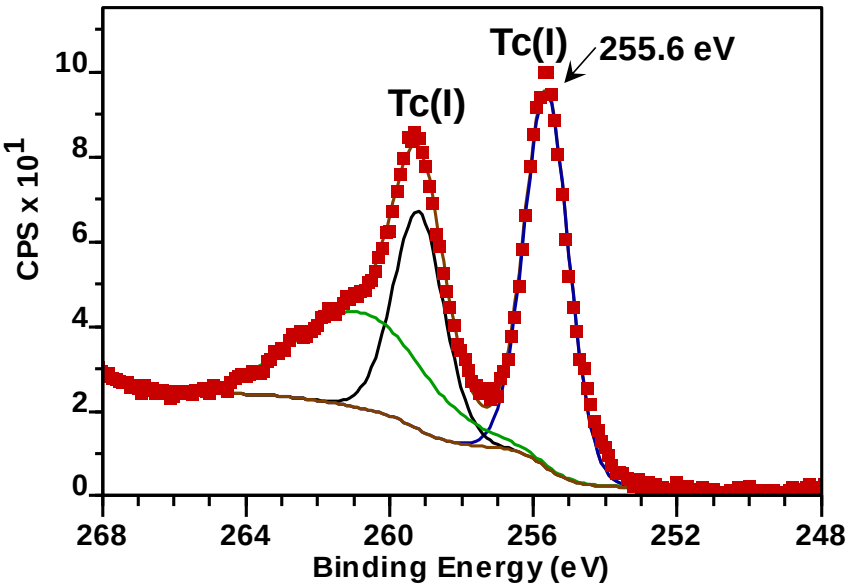


**Figure 45.** X-ray photoelectron spectrum of Tc $3d_{5/2}$ and $3d_{3/2}$ regions for the liquid fraction of **Parr Reaction 8** product. Red squares: experimental spectrum, blue trace: Tc(I) fit, green trace: Re impurity, dark brown trace: baseline for the fit.

## Parr Reaction 9

*Reaction conditions: 10 mM $TcO_4^-$ in simulant containing 100 mM IDA and noble metals pressurized to 250 psi with CO containing 75 ppm $H_2$ at 80°C for 14 days*

To determine the effect of changing chelating ligands on the nature of the Parr reaction product, a reaction was performed where the $TcO_4^-$ solution was subjected to a pressure of 250 psi under CO for 14 days in tank-waste simulant in the presence of noble metals at 80°C. The chelating ligand gluconate was replaced by IDA in this Parr test. The reaction product obtained after 14 days of reaction, consisted of a light straw colored liquid and a dark brown-black precipitate. The $^{99}$Tc NMR of the product showed a sharp resonance at -1006 ppm, which can be attributed to a $[Tc(CO)_3]^+$•IDA species based on our previous observations (Levitskaia et al. 2015). It is worth mentioning the line-width of the $[Tc(CO)_3]^+$•IDA resonance here is significantly narrower compared to that observed for a pure $[Tc(CO)_3]^+$•IDA product.

The $^{99}$Tc NMR of the $[Tc(CO)_3]^+$•IDA product (Figure 46) could account for only 20% of the starting Tc concentration; therefore the reaction is presently being allowed to continue for longer.

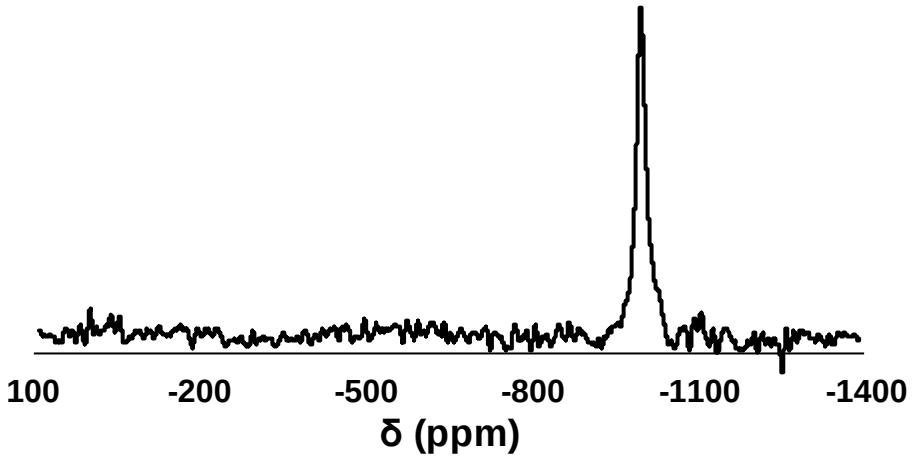


**Figure 46.** $^{99}$Tc NMR spectrum of the liquid fraction of **Parr Reaction 9** product showing the resonances corresponding to $[Tc(CO)_3]^+$•IDA species.

# Distribution*

**U.S. Department of Energy**

**Office of Environmental Management**
G Chamberlain
K Gerdes
NP Machara
JA Poppiti
R Rimando

**ORP**
BJ Harp
AA Kruger
BM Mauss

**RL**
MW Cline

**Lawrence Berkeley National Laboratory**
WW Lukens

**Savanah River National Laboratory**
DJ McCabe
WR Wilmarth

**Pacific Northwest National Laboratory**
SD Chatterjee
Y Du
MH Engelhard
VL Freedman
GB Hall
TG Levitskaia
RA Peterson
V Shutthanandan
ED Walter
NM Washton
DM Wellman
Information Release (PDF)

*All distribution will be made electronically.

Pacific Northwest
NATIONAL LABORATORY

*Proudly Operated by* **Battelle** *Since 1965*

U.S. DEPARTMENT OF
ENERGY

902 Battelle Boulevard
P.O. Box 999
Richland, WA 99352
**1-888-375-PNNL** (7665)

***www.pnnl.gov***